

University College London

Phosphoregulation of KCC2 function

Yvonne Elizabeth Frances Moore

Thesis submitted for the degree of Doctor of Philosophy

2018

I, Yvonne Moore, confirm that the work presented in this thesis is my own. Where information has been derived from other sources, I confirm that this has been indicated in the thesis.

In memory of my Mum

Abstract

The function of neuronal networks relies on a well-maintained balance between excitation and inhibition, disruption of which can have dramatic pathological impacts on brain function. Insights into mechanisms that can enhance neuronal inhibition are therefore highly sought as these may lead to the identification of novel strategies to treat various neurological disorders. Here, I present work exploring a novel mechanism of enhancing GABA_A receptor-mediated inhibition, the major source of fast synaptic inhibition in the brain. This was achieved by potentiating the function of the major chloride transporter in the brain, KCC2. Through genetic mutation of KCC2 threonine sites 906 and 1007 to alanine residues *in vivo* (KCC2-T906A/T1007A knock-in mouse model), I demonstrate the powerful impact that phospho-modulation of these sites has on KCC2 function. Not only did preventing KCC2-T906/T1007 phosphorylation enhance E_{GABA} hyperpolarization in mature neurons, it accelerated the developmental excitatory-to-inhibitory GABAergic shift, seemingly by enhancing the rate of chloride extrusion. This is evident when neurons were challenged with increased [Cl⁻]_i, as KCC2-T906A/T1007A neurons were able to more effectively remove this excess Cl⁻. This is of particular interest for epilepsy-associated disorders as neurons load with chloride during seizures, a process hypothesized to contribute to seizure initiation. Indeed, loss-of-function mutations in KCC2 are a genetic cause of epilepsy, and deficits in KCC2 function are seen in patients with idiopathic and acquired epilepsy, highlighting a potential for KCC2 as a novel

target for treating seizures; the KCC2-T906A/T1007A mice provided the first opportunity to assess this potential. Using several chemoconvulsant models, I have demonstrated that KCC2-T906A/T1007A mutations limit the onset and severity of seizures. Therefore, this thesis highlights KCC2 as a novel therapeutic target for seizures and suggests phospho-modulation of KCC2 may be a potential strategy for increasing KCC2 function in patients with epilepsy.

Acknowledgements

It has been a privilege to complete my PhD under the supervision of Prof. Stephen Moss. I am so grateful for all the encouragement, guidance and opportunities which he has given me. I cannot thank him enough for accepting me into his lab.

The Moss lab has been a wonderful environment to spend the past several years, and I have been fortunate to be surrounded by many intelligent and enthusiastic people. Firstly, I am very thankful to Tarek Deeb for teaching me much of what I know about KCC2 and electrophysiology. His enthusiasm and dedication for his work is infectious, and all our KCC2 discussions developed my ability to think critically and establish my own ideas. I am also grateful to Paul Davies for all his mentorship, kind support and positivity; his advice has always been invaluable. Thank you to all the Moss lab postdoctoral scientists and graduate students, past and present; most of what I have learned is due to the generosity of the numerous people who took the time to teach me. Particular thanks go to “Team KCC2” members; being part of such a supportive and encouraging group has aided in my confidence as a scientist. Thank you also to the many technicians that we have had in the Moss lab, whose efforts in looking after the mouse colony and the general maintenance of the lab are really appreciated. I am also grateful to the admin staff at UCL and Tufts University for all the help I have received from them. Tufts University and the Moss lab has been a great and supportive environment, but also a very fun place to complete my PhD and our many nights out will always be fondly remembered.

Outside of the lab, there are many people who helped me achieve this goal. My husband Tarek has been a source of unwavering support during my PhD and I am so lucky to have met such a wonderful and encouraging partner. My Dad, David, as well as my two brothers, Karl and Mark, have been there at my most difficult times, and I could not have made it this far without their love and support.

Table of Contents

Title Page.....	1
Dedication.....	3
Abstract.....	4
Acknowledgements.....	6
Table of Contents.....	8
Abbreviations.....	18
Chapter 1 : Introduction.....	23
Part I: KCC2 function in neuronal physiology.....	23
Identification and characterization of synaptic inhibition.....	23
Discovery and characterization of K^+/Cl^- transport by KCCs.....	27
Depolarizing GABA in the immature nervous system.....	28
The dynamic nature of neuronal Cl^-	29
Part II: Structure function of KCC2.....	32
Structure of KCC2a and KCC2b.....	32
Pharmacology of KCC2.....	33
Cellular regulation of KCC2 expression and function.....	34
KCC2 protein interactions.....	40

Part III: KCC2 dysfunction in seizure-related disorders.....	46
GABAergic interneurons control neuronal excitation and synchronization...	46
Seizures and epilepsy.....	50
KCC2 mutations underlie epilepsy in humans	52
Genetic susceptibility to seizures in animal models.....	56
Idiopathic epilepsy in humans	57
Acquired epilepsy in humans.....	58
Acquired epilepsy in animal models	59
KCC2 dysfunction increases Cl ⁻ loading and seizure severity.....	61
Restoring Cl ⁻ homeostasis as a treatment for seizures	64
Thesis Aims.....	67
Hypothesis	67
Chapter 2 : Materials and Methods	68
Knock-in mouse Generation and Colony Maintenance	68
Generation of T906A/T1007A knock-in mice	68
Animal care	69
Genotyping.....	69
Tissue Preparation.....	72
P1 mouse pup dissection and culturing.....	72

Hippocampal dissection from adult mice	72
Brain slicing for electrophysiology and biochemistry experiments	73
Cardiac Perfusion	74
Brain slicing for Nissl Staining	74
Biochemistry	75
Antibodies	75
Protein assay	76
Immunoprecipitation	77
Slice Biotinylation	77
Sodium dodecyl sulphate polyacrylamide gel electrophoresis (SDS-PAGE)....	79
Western blotting	80
Histology	82
Nissl Staining	82
Patch clamp electrophysiology.....	83
Solutions and Set Up.....	83
E _{GABA} Measurements.....	84
Resting Membrane Potential (RMP) Measurements	86
Input Resistance Measurements	86
Glutamate Challenge Assay	86
Cl ⁻ loading Assay	87

Extracellular Field Recordings	87
<i>In vitro</i> seizure assays	
Field EPSPs	90
Behavior.....	90
Open Field	91
Rotarod	91
Elevated Plus.....	91
EEGs	92
Surgery.....	92
Recordings	92
Chapter 3 : KCC2-T906A/T1007A mutations increase KCC2 function	94
Summary.....	94
Introduction.....	96
Identification of phosphorylation as a critical regulator of KCC2 function	96
A role for KCC2-T906/T1007 phosphorylation in the modulation of KCC2 function.....	97
Results	101
Generation and behavioral characterization of KCC2-T906A/T1007A knock-in mice.....	101

KCC2-T906A/T1007A mutations increase KCC2 function at all stages of neuronal development	103
Gross brain morphology and neuronal network excitability is normal in KCC2-T906A/T1007A mice	107
Discussion	115
Chapter 4 : Increasing KCC2 function limits seizure onset and severity.....	121
Summary.....	121
Introduction.....	123
KCC2 dysfunction in epilepsy.....	123
Modelling seizures in mice	125
Results	127
KCC2-T906A/T1007A mice have reduced seizure-like activity <i>in vitro</i>	127
KCC2-T906A/T1007A mice have reduced seizure-like activity in the <i>in vivo</i> kainate model	132
Discussion	138
KCC2 function impacts seizure initiation	138
A role for KCC2 in seizure termination	140
Increasing KCC2 function limits high frequency neuronal synchronization during seizures.....	141
Chapter 5 : Mechanisms underlying enhanced KCC2 function and reduced seizure activity in KCC2-T906A/T1007A mice.....	144

Summary.....	144
Introduction.....	146
Impact of KCC2-T906A/T1007A mutations on the kinetic properties of KCC2	146
Activity-dependent Cl ⁻ loading occurs under hyperexcitable conditions	147
A pathological relevance of KCC2 phosphorylation for seizures.....	148
Results	149
KCC2-T906A/T1007A mutations enhance rate of Cl ⁻ transport.....	149
KCC2-T906A/T1007A mutations confer resistance to E _{GABA} depolarization under hyperexcitable conditions	150
Kainate-induced seizures increase KCC2-T1007 phosphorylation	154
Discussion	156
KCC2-T906A/T1007A mutations impact the kinetic properties of KCC2.....	156
KCC2-T906A/T1007A mutations limit activity-dependent deficits in GABAergic inhibition	157
Pathological relevance of KCC2-T1007 phosphorylation	158
Chapter 6 : General Discussion	161
A novel mechanism of potentiating GABAergic inhibition	161
A potential therapeutic strategy for seizure-associated disorders.....	162
Physiological mechanisms underlying KCC2-T906/T1007 (de)phosphorylation	164

Therapeutic perspective of targeting KCC2-T906/T1007 phosphorylation ..165

References.....167

List of Figures

Figure 1:1: GABA _A signaling shifts from depolarizing to hyperpolarizing responses during development.....	30
Figure 1:2: KCC2-mediated Cl ⁻ efflux copes with the dynamic GABA _A -mediated Cl ⁻ loads	31
Figure 1:3: Mouse KCC2b sequence.....	35
Figure 1:4: GABAergic interneurons are highly diverse	48
Figure 1:5: Feedforward vs feedback inhibition	49
Figure 1:6: KCC2-loss of function mutations cause epilepsy	54
Figure 1:7: Tonic versus clonic seizure activity	62
Figure 2:1: Creation and sequencing of KCC2-T906A/T1007A knock-in mice.	70
Figure 2:2: Threshold analysis for quantifying seizure-like activity in <i>in vitro</i> seizure models.....	89
Figure 3:1: Structure of threonine, phosphothreonine and alanine	97
Figure 3:2: Motor and anxiety-like behaviors are normal in KCC2-T906A/T1006A mice.....	102
Figure 3:3: KCC2 function is increased in KCC2-T906A/T1007A hippocampal neurons	104
Figure 3:4: Assessing the ideal conditions required to visualize total and surface expression of KCC2 from brain slices by western blot.....	106
Figure 3:5: KCC2 total and surface expression is unaffected by KCC2-T906A/T1007A mutations	108

Figure 3:6: Assessing gross brain structure in WT and KCC2-T906A/T1007A mice	111
Figure 3:7: Assessing synaptic protein expression in WT and KCC2-T906A/T1007A mice.....	112
Figure 3:8: Excitatory synaptic function is normal in the hippocampus of KCC2- T906A/T1007A mice.....	113
Figure 3:9: Resting state relative EEG power is comparable between WT and KCC2-T906A/T1007A mice	114
Figure 4:1: KCC2-T906A/T1007A mutations were protective against 4-AP-induced epileptiform activity.....	128
Figure 4:2: KCC2-T906A/T1007A mutations reduced high frequency neuronal synchronization during 4-AP-induced SLEs.....	130
Figure 4:3: KCC2-T906A/T1007A mutations conferred resistance to 4-AP induced status-like activity.	131
Figure 4:4: Seizure-like activity induced by 0-Mg ²⁺ was reduced in the KCC2- T906A/T1007A mice compared to WT mice.....	133
Figure 4:5: KCC2-T906A/T1007A mutations reduced high frequency neuronal synchronization during 0-Mg ²⁺ -induced SLEs.	135
Figure 4:6: Kainate induces epileptiform activity and tonic seizures.....	136
Figure 4:7: The development and severity of kainate-induced seizures was reduced in KCC2-T906A/T1007A mice.....	137
Figure 5:1: KCC2-T906A/T1007A mutations enhance the rate of KCC2-mediated Cl ⁻ extrusion	151

Figure 5:2: KCC2-T906A/T1007A mutations limited E_{GABA} depolarization under hyperexcitable conditions153

Figure 5:3: Kainate-induced seizures increase KCC2-T1007 phosphorylation in WT mice.....155

Abbreviations

$[\text{Cl}^-]_i$	Intracellular chloride concentration
$[\text{Cl}^-]_o$	External Cl^- concentration
$[\text{K}^+]_i$	Intracellular potassium concentration
$[\text{K}^+]_o$	Extracellular potassium concentration
0-Mg ²⁺	No magnesium
4-AP	4-aminopyridine
⁸⁶ Rb ⁺	Rubidium ion
AAALAC	Association for Assessment and Accreditation of Laboratory Animal Care
ACSF	Artificial cerebrospinal fluid
AEBSF	4-(2-aminoethyl)benzenesulfonyl fluoride hydrochloride
AP2	Adapter protein 2
APS	Ammonium persulphate
ATP	Adenosine triphosphate
BDNF	Brain-derived neurotrophic factor
Ca ²⁺	Calcium ion
CaCl ₂	Calcium chloride
Cl ⁻	Chloride ion
CNS	Central nervous system
DIV	Days <i>in vitro</i>

DMSO	Dimethyl sulphoxide
DNA	Deoxyribonucleic acid
E_{Cl^-}	Equilibrium potential for Cl^-
EDTA	Ethylenediaminetetraacetic acid
EEG	Electroencephalogram
E_{GABA}	Equilibrium potential for $GABA_A$ currents
Egr4	Early growth factor 4
EGTA	Ethylene glycol-bis(β -aminoethyl ether)-N,N,N',N'-tetraacetic acid
EIMFS	Epilepsy of infancy with migrating focal seizures
EPSP	Excitatory post-synaptic potential
fEPSP	Field excitatory post-synaptic potential
FFT	Fast-fourier transform
GABA	γ -aminobutyric acid
$GABA_A$	Type-A γ -aminobutyric acid
GluA1	Glutamate receptor subunit 1
G Ω	Gigaohm
HBSS	HEPES buffered saline solution
HCO_3^-	Bicarbonate
HEK-293	Human embryonic kidney cells 293
HEPES	4-(2-hydroxyethyl)-1-piperazineethanesulfonic acid
HRP	Horseradish peroxidase
Hz	Hertz

IC ₅₀	Half of maximal inhibitory concentration
IgG	Immunoglobulin G
IPSP	Inhibitory post-synaptic potential
K ⁺	Potassium ion
KCC	K ⁺ /Cl ⁻ cotransporter
KCC2	K ⁺ /Cl ⁻ cotransporter type 2
KCC2-S940	KCC2 serine 940
KCC2-S940A	KCC2 serine 940 alanine substitution
KCC2-T007	KCC2 threonine 1007
KCC2-T906	KCC2 threonine 906
KCC2-T906A/T1007A	KCC2 threonine 906/threonine 1007 alanine substitution
KCl	Potassium chloride
KMeSO ₄	Potassium methyl sulfate
LDS	Lithium dodecyl sulfate
MgCl ₂	Magnesium chloride
mL	Milliliter
mM	Millimolar
mRNA	Messenger ribonucleic acid
mV	Millivolts
MΩ	Megaohm
Na ⁺ /K ⁺ -ATPase	Sodium-potassium adenosine triphosphatase
Na ₃ VO ₄	Sodium pervanadate

NaCl	Sodium chloride
Na-GTP	Sodium guanosine 5'-triphosphate
NaH ₂ PO ₄	Sodium phosphate monobasic
NaHCO ₃	Sodium bicarbonate
NaPO ₄	Sodium phosphate
NEM	N-ethylmaleimide
NKCC1	Sodium potassium co-transporter type 1
NMDA	N-methyl-D-aspartate receptor
OCT	Optimal cutting temperature
OSR1	Oxidative stress-responsive 1 protein
pA	Picoamps
PAGE	Polyacrylamide gel electrophoresis
PBS	Phosphate-buffered saline
PBS-T	Phosphate buffered saline with Tween-20
PCR	Polymerase chain reaction
PFA	Paraformaldehyde
PI3K	Phosphatidylinositol-4,5-bisphosphate 3-kinase
PKC	Protein kinase C
PP1	Protein phosphatase 1
PSD-95	Postsynaptic density protein 95
RCF	Relative centrifugal force
RMP	Resting membrane potential
SDS	Sodium dodecyl sulfate

SE	Status epilepticus
SEM	Standard error of the mean
SLE	Seizure-like event
SPAK kinase	STE20/SPS1-related proline-alanine-rich protein
TBI	Traumatic brain injury
TEMED	N, N, N', N'-tetramethylethylenediamine
TLE	Temporal lobe epilepsy
TrkB	Tyrosine receptor kinase B
TTX	Tetrodotoxin
VGAT	Vesicular GABA transporter
WNK1	With no lysine kinase isoform 1
WT	Wild-type

Chapter 1 : Introduction

Part I: KCC2 function in neuronal physiology

Identification and characterization of synaptic inhibition

The observation that membrane hyperpolarization can occur upon presynaptic neuronal stimulation identified the unitary events underlying fast synaptic inhibition in the brain: inhibitory post-synaptic potentials (IPSPs). By transiently moving the membrane potential to more negative values (hyperpolarizing response), IPSPs reduce the likelihood of overlapping excitatory post-synaptic potentials (EPSPs) to induce action potentials, the electrical impulses that enable communication with post-synaptic neurons. Action potentials are transmitted to the pre-synaptic button, which triggers Ca^{2+} influx. This initiates the release of neurotransmitters – the chemical messengers that physically bind to and activate/inhibit the post-synaptic neurons. Such electrochemical communication

between neurons, as opposed to solely electrical communication that had previously been proposed (Fulton 1939), was a seminal discovery in neuroscience that initiated the search for the underlying neurotransmitters responsible for this neuronal signaling as well as the mechanisms through which they exert their depolarizing/hyperpolarizing actions (Brock et al 1952).

γ -aminobutyric acid (GABA) was identified as the neurotransmitter responsible for mediating the majority of the inhibitory synaptic signaling in the brain. GABA was first discovered in the mammalian brain in 1950 (Awapara et al 1950, Roberts & Frankel 1950), and much of the initial studies on GABA stemmed from the identification of an inhibitory control mechanism in crustacean stretch receptor neurons (Florey 1954, Kuffler 1954). GABA was able to recapitulate the action of inhibitory neurons in crustacea (Kuffler & Edwards 1958). The observation that extracts of mammalian brain could also inhibit these neurons confirmed the presence of a similar inhibitory factor in the mammalian central nervous system, termed 'factor I' at the time (Florey & Mc 1959). Detection of GABA within factor I led to the proposal that GABA may be an inhibitory neurotransmitter in the mammalian central nervous system, although this idea was met with resistance. It was thought that the large quantities of GABA in the brain would likely impede rapid uptake into neurons, a requirement to terminate neurotransmitter signaling (Elliott & Van Gelder 1958). However, this doubt was eliminated when further testing of GABA, this time on cortical and cerebellar neurons, reproduced the powerful inhibitory actions of GABA that had been demonstrated in crustaceans (Krnjevic & Schwartz 1967). The rapid actions of GABA, coupled with confirmation

that it was indeed efficiently taken up into neurons (Krnjevic & Phillis 1963), led to the conclusion that this was probably the major inhibitory synaptic transmitter in the central nervous system. Large quantities of GABA in inhibitory synaptic terminals supported this idea (Kravitz et al 1963). The observation that both IPSPs and GABA induce similar changes in membrane potential and conductance, both resulting from an increase in Cl^- conductance (Boistel & Fatt 1958), cemented this notion. Based on the accumulated evidence, there was widespread agreement by the early 1970s that GABA was indeed the major inhibitory neurotransmitter in the mammalian brain.

In subsequent years, considerable attention was given to defining the nature of the receptor on which GABA exerts its fast synaptic actions, leading to the identification of Type-A γ -aminobutyric acid receptors (GABA_A receptors). Hydropathy analysis revealed that they are transmembrane channels and members of the cysteine-loop ligand gated ion channel superfamily (Schofield et al 1987). GABA_A receptors are comprised of five subunits that form a pentameric arrangement around a central anion-selective pore (Bormann et al 1987). In mammals, there are 19 subunit isoforms: six α subunits, three β subunits, three γ subunits, three ρ subunits, and one each of the ϵ , δ , θ , and π subunits. Assembly of α and β subunits is sufficient to form a functional receptor, however 2 α , 2 β and an auxiliary (γ , ϵ , δ , θ or ρ) subunit is the most common receptor composition (Rudolph & Knoflach 2011). The diversity of potential subunit combinations confers a complex array of differential neuronal expression, subcellular targeting, as well as divergent functional and pharmacological properties.

GABA_A receptors are permeable to both Cl⁻ and HCO₃⁻, thus the intracellular concentrations of both of these ions impacts the reversal potential (E_{GABA}) of GABA_A currents. The binding of two molecules of GABA between the interface of α and β subunits in the extracellular domain triggers the opening of the anion-selective pore which initiates the passive diffusion of Cl⁻ and HCO₃⁻ across the membrane, the direction of which is dictated by the concentration gradients of these ions across the neuronal membrane. HCO₃⁻ currents are always depolarizing due to an outward driving force for HCO₃⁻. However, GABA_A receptors are approximately four times more permeable to Cl⁻ than to HCO₃⁻ (Kaila & Voipio 1987), thus, in most neurons, E_{GABA} lies closer to the Cl⁻ reversal potential (E_{Cl^-}) rather than the more positive $E_{HCO_3^-}$ (Kaila 1994). This typically places E_{GABA} at more negative values than the resting membrane potential (RMP) due to low intracellular Cl⁻ concentrations; this results in rapid hyperpolarizing GABA_A receptor currents upon GABA_A receptor activation.

Due to this differential permeability of Cl⁻ and HCO₃⁻, hyperpolarizing GABA_A receptor currents are exclusively caused by inward Cl⁻ flux (as HCO₃⁻ currents are depolarizing). A loss of hyperpolarizing inhibition therefore indicates a disruption in Cl⁻ homeostasis, placing $[Cl^-]_i$ as a critical determinant of the strength of fast-synaptic inhibition. $[Cl^-]_i$ therefore requires tight maintenance to ensure appropriate levels of fast synaptic inhibition are maintained in the brain. This indicated that mechanisms must exist to maintain low $[Cl^-]_i$ levels in neurons, initiating a search for these putative Cl⁻ extruders.

Discovery and characterization of K^+/Cl^- transport by KCCs

Investigations into Cl^- transport mechanisms began on non-neuronal cells, particularly exploring mechanisms underlying reflexive cell volume regulation resulting from osmotic changes. Increased membrane permeability to K^+ and Cl^- occurs under osmotic challenges, and Dunham et al in 1980 determined that Cl^- was necessary for passive influx of K^+ into human red blood cells during this process (Dunham et al 1980). This was achieved by demonstrating that either replacement of extracellular Cl^- with other anions, or varying the amount of Cl^- outside the cell, reduced K^+ influx. Further work demonstrated that increases in cell volume in sheep red blood cells were accompanied by passive (ouabain-insensitive) K^+ influx, which again was dependent on Cl^- (Dunham & Ellory 1981). The electroneutral property of this K^+/Cl^- transport suggested Cl^- movement occurs in the same direction as K^+ . This was subsequently termed K^+/Cl^- cotransport. Four K^+/Cl^- cotransporters (KCCs) have been identified (KCC1, 2, 3 and 4), each of which has differential tissue expression. KCC2 is unique to the other KCCs in that it is exclusively expressed in the nervous system, and it can extrude Cl^- under isotonic conditions (Payne 1997), a characteristic attributed to a 15-residue amino acid sequence in the C-terminal domain of KCC2 that is absent in the other KCCs (Mercado et al 2006). This function enables KCC2 to maintain low $[Cl^-]_i$ in mature neurons, which is a distinct property of neuronal cells.

KCC2 uses the outwardly directed K^+ gradient, generated by the Na^+/K^+ -ATPase, to drive Cl^- out of neurons against its electrochemical equilibrium. This process is

essential for maintaining low $[Cl^-]_i$, which is necessary for establishing and maintaining hyperpolarizing GABA_A receptor mediated inhibition.

Depolarizing GABA in the immature nervous system

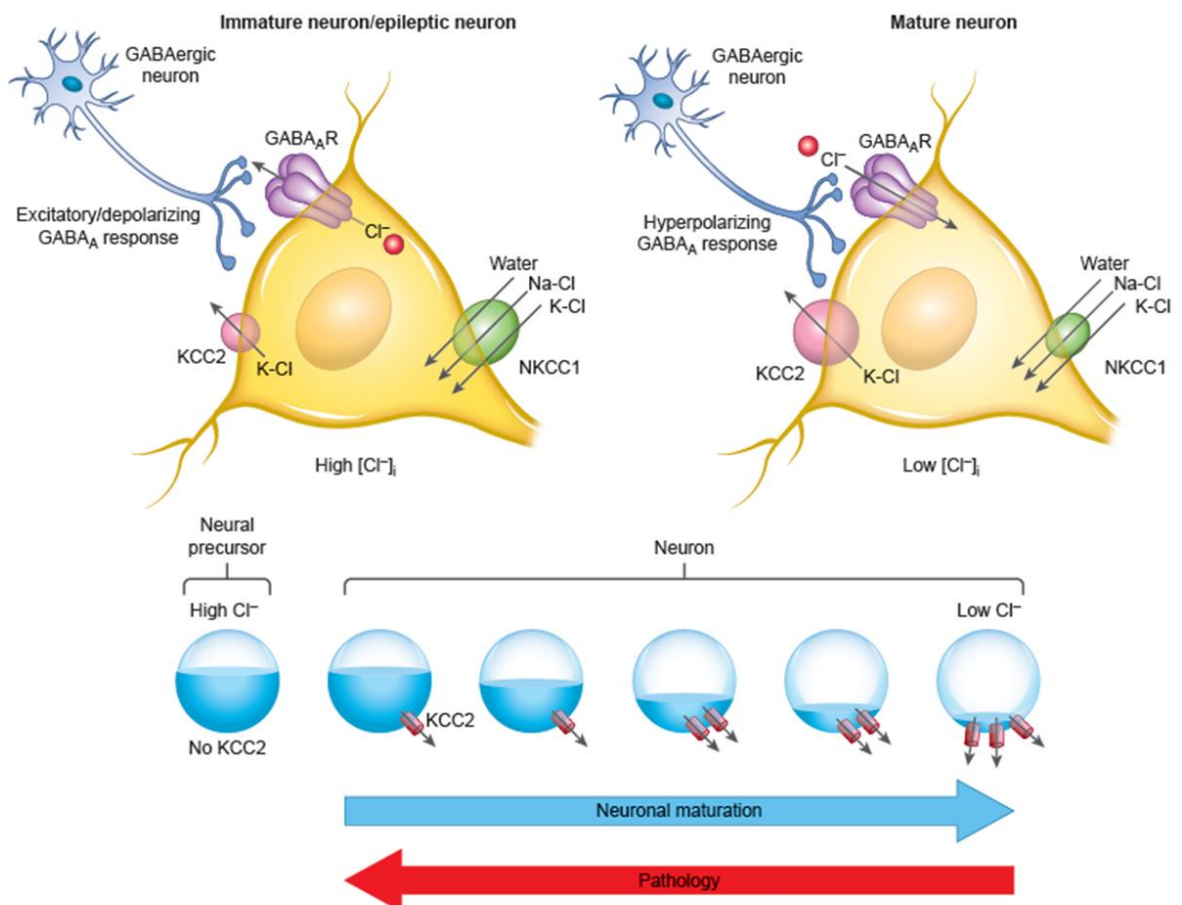
While the vast majority of GABA_A receptor currents are hyperpolarizing in the adult brain, this is not true in the earliest stages of brain development. Experiments performed by Ben-Ari et al. in 1989 revealed the basis for the depolarizing action of GABA in immature neurons to be elevated levels of intracellular Cl^- , reversing the driving force for Cl^- , causing efflux of Cl^- upon GABA_A receptor activation (Ben-Ari et al 1989). This difference in $[Cl^-]_i$ between the mature and immature nervous system occurs primarily due to alterations in the expression levels and activity of KCC2 and an additional Cl^- transporter, Na⁺-K⁺- Cl^- cotransporter 1 (NKCC1). NKCC1 is also present within neurons, but unlike KCC2, NKCC1 facilitates Cl^- uptake using the inward Na⁺ concentration gradient to drive K⁺ and Cl^- into neurons. NKCC1 is highly expressed in neural precursor cells and during early brain development (Plotkin et al 1997, Yamada et al 2004). In contrast, KCC2 is absent from neural precursor cells and newly developed neurons (Li et al 2002) (Stein et al 2004), but is strongly upregulated as neurons mature. This upregulation, during the course of development, coinciding with a downregulation of NKCC1, causes a progressive depolarizing to hyperpolarizing shift in E_{GABA} (Rivera et al 1999) (**Fig. 1.1**). However, the functional significance of

this excitatory-to-inhibitory shift remains unclear, although roles for this process in neuronal maturation have been proposed (Cancedda et al 2007).

The dynamic nature of neuronal Cl^-

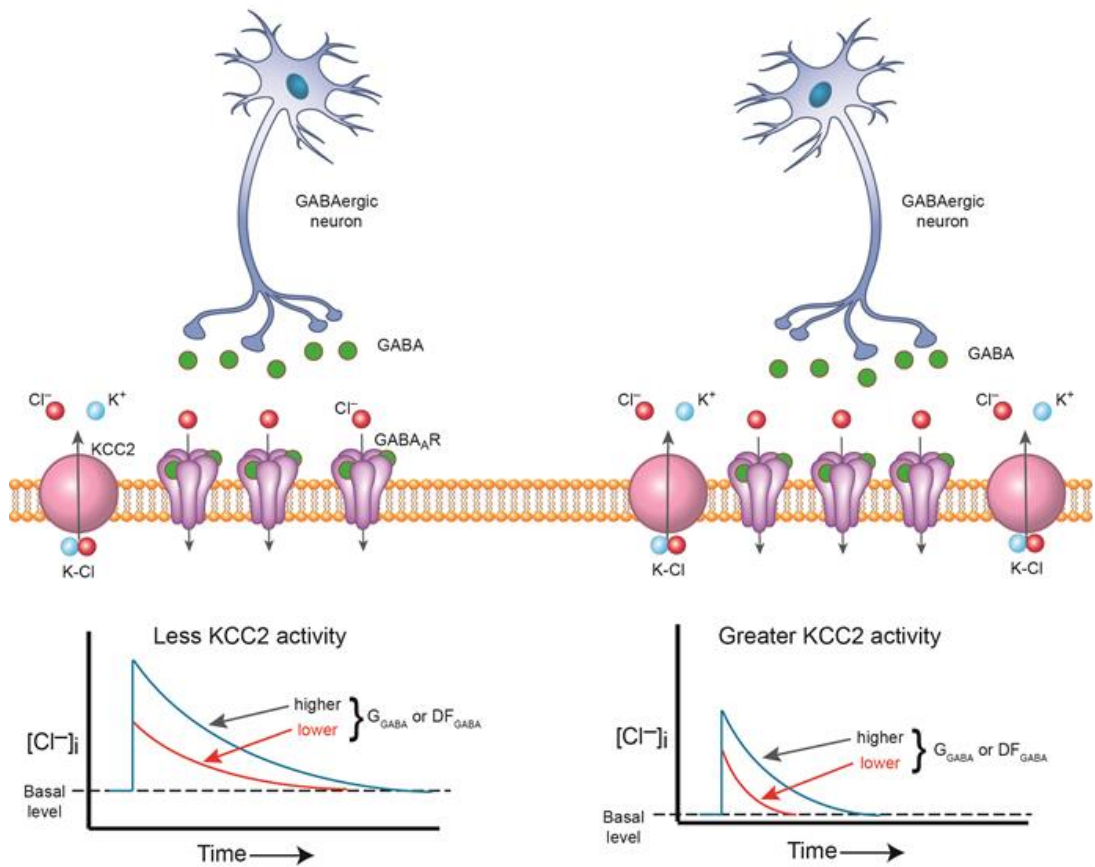
Despite the presence of KCC2 function to extrude Cl^- , neuronal intracellular Cl^- levels are not static. Regular influx of Cl^- through GABA_A receptor activation/other Cl^- channels transiently raises $[\text{Cl}^-]_i$ and depolarizes E_{GABA} (**Fig. 1.2**). The amount of Cl^- moving into the cell will vary depending on the number of Cl^- channels open (more channels open will allow for greater Cl^- flux), the kinetics of the subunits composing the Cl^- channels (i.e. how quickly they close once opened; channels that stay open longer will enable more Cl^- influx), and the duration of GABA stimulus (a longer presence of GABA will enable more Cl^- channel openings, causing more Cl^- influx). Moreover, the timing of an increase in GABA conductance can drastically impact the amount of Cl^- that enters the cell; if enhanced GABA conductance overlaps in space and time with an event that raises the membrane potential of the cell (e.g. an EPSP, a back-propagating action potential, or a pathologically sustained membrane depolarization) the driving force for Cl^- will increase and more Cl^- will enter the cell causing greater Cl^- loads (Buzsaki et al 2007). Despite these Cl^- loads, KCC2 is usually able to rapidly remove this excess Cl^- and maintain hyperpolarizing GABA_A currents (Doyon et al 2016, Kaila et al 2014).

Figure 1:1: GABA_A signaling shifts from depolarizing to hyperpolarizing responses during development



Neural precursor cells do not express KCC2 and consequently contain high levels of intracellular Cl⁻. In immature pyramidal neurons, GABA_A receptor mediated Cl⁻ currents are depolarizing due to a low level of KCC2 function and high levels of NKCC1 activity. GABA_A-receptor currents become hyperpolarizing as neurons mature due to a reduction in $[Cl^-]_i$ caused by an increase in KCC2-mediated Cl⁻ extrusion and a decrease in NKCC1 function. As neurons mature, they begin to express KCC2 protein which lowers the intracellular level of Cl⁻. In several neuropathies, the amount of KCC2 is reduced and the level of intracellular Cl⁻ rises.

Figure 1:2: KCC2-mediated Cl^- efflux copes with the dynamic GABA_A -mediated Cl^- loads



When KCC2 is active on the cell surface, it will transfer Cl^- out of the cell in a K^+ -dependent process. GABA released from presynaptic GABAergic interneurons will bind and activate postsynaptic GABA_A receptors, which allows Cl^- to passively flow back into the cell. This GABA_A conductance raises intracellular Cl^- , and the rate of recovery back to basal Cl^- values will depend on the amount of KCC2 activity, with more activity accelerating the return to basal values. Furthermore, the GABA_A -mediated Cl^- influx will vary depending on the conductance ($G_{\text{GABA}} = \text{single channel conductance } (\gamma) \times \text{number of channels open } (N)$) and the driving force on Cl^- ($DF_{\text{GABA}} = E_{\text{GABA}} - E_M$ (membrane potential)), with rapid increases in channel openings and membrane potential values exacerbating the intracellular Cl^- load.

Part II: Structure function of KCC2

Structure of KCC2a and KCC2b

Based on hydropathy analysis, KCC2 is thought to have 12 transmembrane domains flanked by intracellular N and C terminal regions (Payne et al 1996) (**Fig. 1.3**). The KCC2 gene, SLC12A5, codes for two isoforms: KCC2a and KCC2b. The human KCC2b isoform is composed of 1116 (1115 in mouse) amino acids, compared to 1156 (1155 in mouse) in KCC2a. The additional 40 amino acids of KCC2a are removed from the end of the N terminal of KCC2b (Uvarov et al 2007). While the role of KCC2b in mediating Cl^- transport is clear, the functional role of KCC2a has remained elusive. It is clear that this isoform has an essential role in brain function, as knock-out studies of both KCC2 isoforms result in death immediately after birth due to impaired GABAergic inhibition and subsequent respiratory failure (Hubner et al 2001), while knock-out of only KCC2b delays this lethality until the second postnatal week (Woo et al 2002). This is likely due to a dominance of KCC2a in the immature nervous system, particularly in the spinal cord, compared to a developmental upregulation of KCC2b over the first few postnatal weeks of life; by maturity, KCC2b accounts for approximately 95% of KCC2 protein (Uvarov et al 2007). KCC2a does exhibit similar levels of Cl^- transport function compared to KCC2b, as KCC2a is able to mediate rubidium (a radioactive isotope that can be transported by KCC2) uptake when expressed in HEK-293 cells at levels comparable to those exhibited by KCC2b (Uvarov et al 2007). This

suggests that the additional 40 amino acids present on KCC2a do not impact its Cl^- transport function. In support of this, KCC2a is also active when overexpressed in cultured neurons (Markkanen et al 2017). Aside from their different developmental expression, these two isoforms also exhibit distinct subcellular expression patterns; low levels of co-localization occur, with both isoforms expressed in non-overlapping dendritic compartments (Markkanen et al 2014). This suggests there may be different pools of KCC2 that exhibit distinct functions, although this has not yet been elucidated.

Pharmacology of KCC2

Little information is currently available about the molecular regions of KCC2 responsible for K^+/Cl^- transport, although deletion of its N-terminus results in functional inactivation of KCC2, indicating a crucial role for this region for ion translocation (Li et al 2007). The discovery of direct pharmacological inhibitors of KCC2 and NKCC1 has aided in our understanding of K^+/Cl^- transport. Bumetanide, a loop diuretic, binds and inhibits NKCC1; however, high extracellular levels of Cl^- prevents this inhibition, while increased Na^+ and K^+ concentrations have no impact on the actions of bumetanide (Haas & McManus 1983). This suggests that bumetanide and Cl^- compete for the same binding site, and that Na^+ , K^+ and Cl^- are required to bind for NKCC1 to translocate any ions. This explains the reliably electroneutral property of NKCC1. Similarly, the specific KCC2 inhibitor, VU0463271, appears to inhibit KCC2 by competing for the K^+ binding site (Delpire

et al 2009), supporting the necessity for dual binding of K^+ and Cl^- for the translocation of these ions to occur.

Cellular regulation of KCC2 expression and function

Neuronal specific expression

Tightly regulated transcriptional control ensures the restriction of KCC2 mRNA expression to the central nervous system. Binding of the RE-1 silencing transcription factor (REST) to two repressor elements (RE-1) within the 5' regulatory region of KCC2 prevents KCC2 mRNA expression in non-neuronal cells (Uvarov et al 2005, Yeo et al 2009). REST inhibition accelerates the developmental Cl^- shift in neurons, and is slowed by REST overexpression. These findings provide a mechanistic explanation for the developmental upregulation of KCC2 expression. Moreover, the neuron-enriched transcription factor, early growth response 4 (Egr4), is developmentally upregulated in neurons which binds to the promoter region of KCC2, causing an increase in KCC2 gene expression over development (Uvarov et al 2006). The developmental regulation of these transcription factors can be potentiated by the brain-specific growth factor (BDNF) (Ludwig et al 2011), providing insight into the potential signaling pathways that regulate this upregulation of KCC2. Furthermore, KCC2b upregulation is dependent on the expression of upstream stimulatory factor 1 and 2 (USF1 and

Figure 1:3: Mouse KCC2b sequence

MLNNLTDCEDGDGGANPGDGNPKESSPFINSTDEKGGKEYDGKNMALFEEEMDTSPMVS
SLLSGLANYTNLPQGSREHEEAENNEGGKKKPVQAPRMGTFMGVYLPCLQNIQVILFLRLT
WVVGIAGIMESFCMVFICCSCTMLTAISM**SAIATNGVVPAGGSY**MISRSLGPEFGGAVGLC
FYLGTTFAGAMYILGTIEILLAYLFPAMAIFKAEDASGEAAAMLNNMRVYGTCVLTCMATVVF
VGV**KYVNKF**ALVFLGCVILSILAIYAGVIKSAFDPPNFPI**CLLGN**RTLRHRGFDV**CAK**LAWEGN
ETVTRLWGLF**CSSR**FLNAT**CDEY**FTRNNVTEIQGIPGAASGLIKENLWSSYLTKGVIVERSG
MTSVGLADGTPIDMDHPYVFSDMTSYFLLVGIYFPSVTGIMAGSNR**SGDLRDAQKSIPTGT**
ILAIATTSAVYISSVVLFACIEGVVLRDKFGEAVNGNLVVGTLAWPSPWVIVIGSFFSTCGAGL
QSLT**GAPRLLQAISR**DGIVPFLQVFGHGKANG**PTW**ALLTACICEIGILIASLDEVAPILSMFFL
MCYMFVNLACAVQ**TLLRTPNWRPRF**RYHWTLSFLGMSLCLALMFICSWYYALVAMLIAG
LIYKYIEY**RGA**KEWGDGIRGLSLAARY**ALLR**LEEGPPHTKNWRPQL**LVLVRVDQDQNVV**
HPQLLSLTSQLKAGKGLTIVGSVLEGTFLFNHPQAQRAE**SIRRL**MEAEKVKGFQVVISNL
RDGVSHLIQSGGLGGLQHNTVLVWPRNWRQKEDHQTWRNFIELVRETTAGHLALLVTK
NVSMFPGNPERFSEGSIDVWWIVHDGGMLMLLPFLRRHHKVWRKCKMRIFTVAQMDDN
SIQMKKDLTTFYHLRITAEVEVEMHESDISAY**Y**E**KTL**VMEQRSQILQMHCLKNEREREI
Q**SI**T**DeSRG**SIRRNKPNANTRLRLNVPEETAGDSEEKPEEEVQLIHDQSAPSCSPSSSPGEEP
EGEGETDPEKVHL**T**WTKDKSVAEKNKGSPVSSSEGIKDFFSMKPEWENLNQSNVRRM**H**T
AVRLNEVIVKSRDAKLVLLNMPGPPRNRNGDEN**Y**MEFLEVLTEHLDRVMLVRGGG**RE**VITI
YS

The amino acid sequence for KCC2b. Red letters indicate putative intracellular domains, underlined letters indicate putative transmembrane domains, and bold letters are known regulatory sites on KCC2, including sites of phosphorylation (S, T and Y), and sites that when mutated reduce KCC2 surface expression (L) and function (C) through unknown mechanisms.

USF2) (Markkanen et al 2008). KCC2b contains an E-box binding complex on the KCC2b promoter, and interaction of USF1 and USF2 at the site contributes to the activation of KCC2b gene expression in cultured cortical neurons. Thus, multiple mechanisms regulate KCC2 gene transcription and translation, promoting KCC2 upregulation during development.

Phosphorylation

The C-terminus of KCC2 contains many phosphorylation sites (**Fig. 1.3; table 1**), regulation of which has drastic impacts on KCC2 function (Moore et al 2017). Phosphorylation is a reversible post-translational modification that is tightly associated with protein activity, and is therefore a key mechanism through which cells can rapidly respond to different conditions or signals. Phosphorylation only occurs at the side chains of three amino acids: serine, threonine and tyrosine. This is due to the presence of a nucleophilic (—OH) group on these amino acid side chains that attacks the terminal phosphate group ($\gamma\text{—PO}_3^-$) on adenosine triphosphate (ATP), resulting in the transfer of the phosphate to the amino acid side chain. Phosphorylation of a protein can drastically regulate protein function through several means, such as altering the conformation state of the protein to activate/inhibit its function. Phosphorylation can also impact the binding partners of that protein, subsequently altering its localization and/or function. Phosphorylation is therefore a critical control mechanism of cell function.

Discovery of phosphorylation sites on KCC2 has furthered our understanding of its cellular control, including the developmental excitatory-to-inhibitory GABAergic shift. KCC2 protein expression is lower in the immature brain compared to the mature brain (Friedel et al 2015); increases in KCC2 protein expression alone was therefore originally thought to dictate the level of KCC2 function. However, several phosphorylation sites on KCC2 have now been identified (**see table 1**), characterization of which suggests no simple linear relationship exists between KCC2 protein levels and the degree of KCC2 function. Indeed, it is emerging that both the residence time of KCC2 protein at the neuronal membrane, as well as its activity levels, are strongly regulated by phosphorylation.

The majority of the currently identified phosphorylation sites exist within KCC2's large carboxy-terminal domain, the most characterized of which is serine 940. This site is a target for protein kinase C (PKC), the identification of which resulted from *in vitro* kinase assays (Lee et al 2007). Radioactive metabolic labeling in HEK-293 cells established KCC2 as a substrate for PKC, and peptide mapping identified S940 as the major target for this kinase. The development of an antibody against phosphorylated S940 confirmed this finding, and S940 phosphorylation was determined to stabilize KCC2 at the plasma membrane by decreasing its internalization, enabling greater Cl⁻ extrusion.

Mutation of this site to alanine (S940A) removes the hydroxyl group needed for phosphorylation to occur. However, the S940A mutation does not impact the surface expression of KCC2, which suggests the phosphorylation acts to prevent access to the serine by other regulatory proteins, an effect that the alanine

mutation mimics (Silayeva et al 2015). Despite this, the S940A mutation reduces KCC2 function, suggesting the mutation alters the kinetic properties of KCC2. This could be due to a reduction in the velocity of Cl^- extrusion or a reduction in the affinity of the transporter for Cl^- or K^+ . Differentiation between these two aspects will be difficult as changes in either of these factors will influence the other. However, the demonstration that the S940A mutation can impact the kinetic properties of KCC2 supports a role for phosphorylation in the regulation of KCC2-mediated Cl^- extrusion and thus the strength of synaptic inhibition.

Two additional sites located near S940, threonine 934 (T934) and serine 937 (S937) increase Ti^+ (which can be transported by KCC2) influx in HEK-293 cells when mutated to aspartate residues (negatively charged amino acid that mimics phosphorylation) (Weber et al 2014). This suggests that phosphorylation of these residues may also upregulate KCC2 transport activity. The mutations do not impact KCC2 surface expression, indicating a kinetic regulation of KCC2 activity by these residues. In contrast, activity-dependent phosphorylation of two tyrosine residues, Y903 and Y1087, leads to reduced membrane stability of KCC2 by enhancing its lysosomal degradation (Lee et al 2010). A additional study on Y1087 revealed a similar reduction in KCC2 function when Y1087 is mutated to the negatively charged aspartate yet no impact on KCC2 surface expression was detected (Strange et al 2000). The reasons for these discrepancies is unclear, but likely involves the differences in cell types used (HEK-293 versus oocytes, respectively).

Two additional sites of phosphorylation within the C-terminus of KCC2, threonine 906 (T906) and threonine 1007 (T1007), have been identified in the immature brain (Rinehart et al 2009). KCC2-T906/T1007 phosphorylation is high in the immature nervous system, followed by a developmental decrease in the phosphorylation of these sites (Friedel et al 2015, Rinehart et al 2009). This observation suggested that these sites may play a role in maintaining KCC2 in an inhibited state in immature neurons, although this has never been directly confirmed. However, assessment of KCC2-T906A/T1007A point mutant constructs in HEK cells increases $^{86}\text{Rb}^+$ flux (a radioactive isotope that can be transported by KCC2) revealed a much greater level of KCC2 activity compared to WT KCC2 (Rinehart et al 2009). Many additional studies have supported this finding, demonstrating a role for T906/T1007 phosphorylation in inhibiting KCC2 (de Los Heros et al 2014, Friedel et al 2015, Inoue et al 2012, Titz et al 2015).

Additional sites involved in KCC2 regulation

Mutation of leucine 675 within the C-terminal domain reduces KCC2 transport activity (Doding et al 2012). Mutation of two further leucine residues, L657 and L658, prevents KCC2 from binding to the clathrin binding adaptor protein 2 complex (AP-2) subsequently reducing KCC2 internalization (Zhao et al 2008). Changes in the availability of these leucine residues for AP-2 binding through either conformational changes within KCC2 or occlusion by additional KCC2

binding partners likely regulates KCC2 endocytosis through this mechanism, although this is yet to be explored.

There are also several asparagine residues (N) in the third extracellular loop of KCC2 which are sites of glycosylation, specifically N283, N291, N310, N328, N338 and N339 (Agez et al 2017). However, little is known about the function of these post-translational modifications. Loss-of-function mutations in KCC2 (L311H, L426P and G551D) exhibit reduced glycosylation and reduced surface expression of KCC2 (Stodberg et al 2015); however, a role for glycosylation in modulating the membrane stability of KCC2 remains unknown.

Additionally, there are four cysteine residues located in the third extracellular loop of KCC2. Mutation of these residues (C287S, C302L, C322S, and C331L) impacts KCC2 transport activity. While these mutations do not impact KCC2 surface expression, they exhibit reduced $^{86}\text{Rb}^+$ uptake when expressed in HEK-293 cells (Hartmann et al 2010). However, the precise mechanism through which these cysteine residues modify KCC2 function is unknown.

KCC2 protein interactions

KCC2 interacting proteins regulate KCC2 protein expression and synaptic inhibition

Several protein binding partners of KCC2 have recently been identified and accumulating evidence suggests that these interactions are critically involved in regulating total KCC2 surface expression, as well as KCC2 stability at the plasma

membrane; corresponding changes in KCC2 function and the polarity of fast synaptic inhibition have also been detected.

Co-immunoprecipitation experiments revealed that with-no-lysine 1 (WNK1) and SPS1-related proline/alanine-rich kinase (SPAK) form a complex with KCC2 (Friedel et al 2015), an interesting finding given that these kinases are known to regulate the phosphorylation state of KCC2-T1007 and subsequently KCC2 function (Conway et al 2017, de Los Heros et al 2014, Friedel et al 2015, Rinehart et al 2009). WNK1 lies upstream of SPAK, thus it is thought that WNK1 may act a scaffold to bridge SPAK to KCC2 for phosphorylation of T1007.

The use of mass spectrometry led to the identification of the transmembrane protein neuropilin and tolloid like-2 (Neto2) as a KCC2 interacting protein (Ivakine et al 2013). Neto2 knockout mice have reduced KCC2 protein expression and depolarized E_{GABA} values, demonstrating Neto2 is critical protein involved in the regulation of KCC2 expression (Mahadevan et al 2015). Neto2 is an axillary subunit of kainate receptors, which together form a protein complex with KCC2 to positively regulate KCC2 expression levels (Mahadevan et al 2014). Overexpression of either Neto2 or the GluK2 kainate receptor subunit in hippocampal neurons increases the amount of KCC2 recycled to the plasma membrane, resulting in more hyperpolarized E_{GABA} values relative to control neurons (Pressey et al 2017).

KCC2 can also interact with the neuronal endocytic regulatory protein PACSIN1, but unlike Neto2 and GluK2, PACSIN1 is a negative regulator of KCC2 expression: knockdown of PACSIN1 in hippocampal neurons increases KCC2 expression and

hyperpolarizes E_{GABA} values (Mahadevan et al 2017). Identification of PACSIN1 as a binding partner and regulator of KCC2 came from a comprehensive investigation into the KCC2 “interactome” through the use of mass spectrometry. This study categorized these proteins into those that are enriched at either excitatory or inhibitory synapses, and determined most of these to regulate ion homeostasis, the dendritic cytoskeleton or receptor trafficking. The large majority of these interactions have not been further investigated, thus the importance of these interactions for KCC2 stability and neuronal functioning is unknown.

KCC2 protein interactions regulate excitatory synaptic function

Interestingly, a large number of KCC2 binding partners are located at excitatory synapses, an unexpected finding given KCC2’s canonical role in regulating synaptic inhibition (Gulyas et al 2001, Mahadevan et al 2017). This localization of KCC2 within spines places KCC2 in a position to regulate excitatory synaptic signaling, and indeed such a “moonlighting” action of KCC2 has now been demonstrated (Blaesse & Schmidt 2015). This function of KCC2 was first discovered by Li et al. who reported the presence of immature, highly motile filipodia-like dendritic spines and a reduction in functional synapses in KCC2-deficient neurons (Li et al 2007). Introduction of N-terminal-deleted KCC2, which lacks any Cl^- transport function, back into these neurons rescues these spine deficits, indicating this structural role for KCC2 is independent from its canonical Cl^- transport function. Consistent with a role of KCC2 in spine formation, overexpression of KCC2 via *in*

vivo electroporation of KCC2 cortical neurons, increases spine number; electroporation of N-terminal-deleted KCC2 was again sufficient to induce these effects further demonstrating the transport independence of this effect on spine morphology (Fiumelli et al 2013).

Gaining insight into the protein binding partners of KCC2 has elucidated several mechanisms that underlie this critical role for KCC2 in spine morphology. KCC2 directly interacts with the cytoskeleton-associated protein 4.1N via its C-terminal domain (Li et al 2007) and *in utero* electroporation of KCC2 increases dendritic spine density, yet the KCC2 C568A mutant, which cannot interact with 4.1N, does not recapitulate this effect (Fiumelli et al 2013). 4.1N also binds the AMPA receptor subunit GluA1 (Shen et al 2000), which may be responsible for an increase in the lateral diffusion of GluA1-containing AMPA receptors detected in KCC2 KO neurons (Gauvain et al 2011). 4.1N may therefore act as an intermediate between KCC2 surface expression and AMPA receptor clustering.

A further mechanism through which KCC2 impacts the actin cytoskeleton has been demonstrated: KCC2 interacts with and inhibits a guanine nucleotide exchange factor called β -pix, a protein that regulates cofilin-1, a major actin-regulating protein (Llano et al 2015). Ablating KCC2 from neurons results in increased cofilin-1 phosphorylation, large pools of stable actin, reduced spine motility, and diminished density of functional synapses. Overexpression of KCC2 C568A, which cannot bind 4.1N, rescues these deficits, suggesting that this mechanism is independent of 4.1N (Llano et al 2015); this indicates that KCC2 regulates actin dynamics and dendritic spines through multiple mechanisms. KCC2

mediated regulation of cofilin phosphorylation is also necessary for activity-driven membrane insertion of AMPA receptors and subsequently long-term potentiation (Chevy et al 2015).

The diversity of these interacting proteins indicates roles for KCC2 that go far beyond the canonical role of regulating Cl^- homeostasis and future investigations into additional binding partners would provide valuable information to further our understanding of this interesting non-transport function of KCC2.

Table 1: Phosphorylation sites on KCC2

Residue	+ve or -ve Impact on KCC2 Function	Initial Evidence	Kinase	Phosphatase	First identified by:
S728	-ve	Alanine mutations and ⁸⁶ Rb+ flux	?	?	Lee et al., JBC, 2007
Y903	-ve	Alanine mutations; phospho-tyrosine antibody	?	?	Lee et al. Mol Cell Neurosci., 2010
T906	-ve	Liquid chromatography – Mass spectrometry; alanine mutations and ⁸⁶ Rb+ flux	Conflicting data	?	Rinehart et al., Cell, 2009
T934	+ve	Alanine/Aspartate mutations and TI+ flux	?	?	Weber et al., JBC, 2014
S937	+ve	Alanine/Aspartate mutations and TI+ flux	?	?	Weber et al., JBC, 2014
S940	+ve	³² P; phospho-specific antibody; alanine mutations	PKC	PP1	Lee et al., JBC, 2007
T1007	-ve	Liquid chromatography – Mass spectrometry; alanine mutations and ⁸⁶ Rb+ flux	SPAK/OSR1	?	Rinehart et al., Cell, 2009
T1052	-ve	Electrophysiological and NH ₄ ⁺ flux characterization of alanine mutations	?	?	Titz et al., Neuropharmacology, 2015
Y1087	-ve	Aspartate substitution decrease ⁸⁶ Rb+ flux	?	?	Strange et al., Am J Physiol., 2000

Part III: KCC2 dysfunction in seizure-related disorders

GABAergic interneurons control neuronal excitation and synchronization

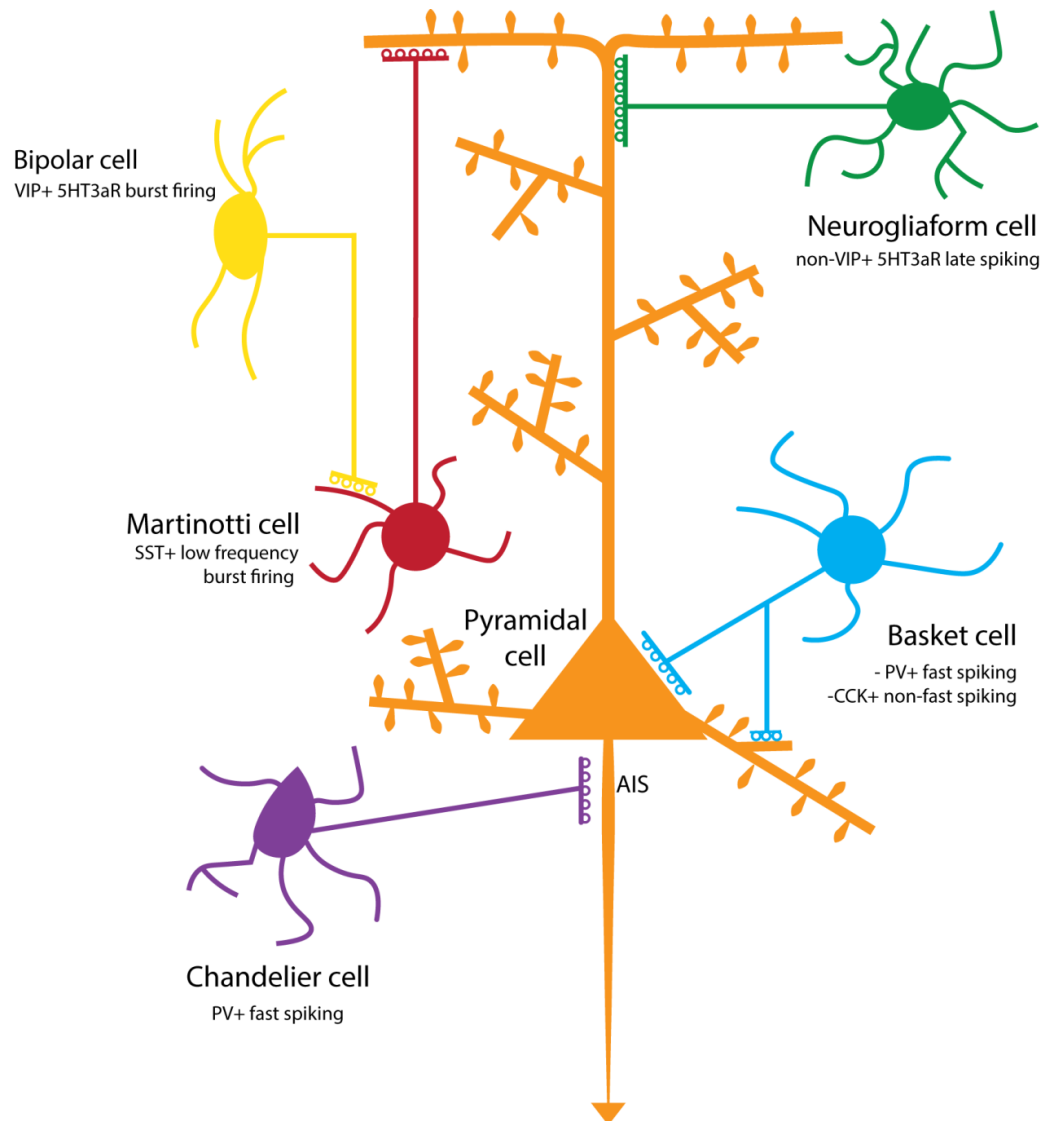
Inhibition in the nervous system is regulated through a small population of neurons that release GABA upon activation. The large majority of these GABA-positive neurons have short axons that project locally, and are appropriately termed GABAergic interneurons. Although these neurons are a minority population in the brain, accounting for approximately 20% of the neuronal population in rodents, they exert powerful control over neuronal activity by dictating neuronal firing patterns, synchronization and subsequently brain oscillation frequencies (Klausberger & Somogyi 2008, Tremblay et al 2016).

The ability of these neurons to effectively regulate network activity is amplified by their striking diversity, differing in their morphology, subcellular targeting and electrophysiological properties (**see fig. 1**) (Klausberger & Somogyi 2008, Marin 2012, Wamsley & Fishell 2017). Parvalbumin (PV), somatostatin (SST) and 5HT3aR are the major markers of GABAergic interneurons, which are further subdivided according to their morphology and electrophysiological properties (Petilla Interneuron Nomenclature et al 2008). PV cells are categorized as basket or chandelier cells, both of which are fast spiking but differ in their subcellular targeting: basket cells target the cell soma and proximal dendrites, while chandelier cells target the axon-initial segment (AIS). SST neurons are categorized as Martinotti or non-Martinotti cells, both of which target dendrites but differ in their firing properties: Martinotti cells exhibit bursting behavior, while non-

Martinotti cells are quasi fast-spiking. 5HT3aR cells are subdivided into vasoactive intestinal peptide (VIP) positive or negative neurons. VIP neurons are mostly bipolar and exhibit many firing properties including bursting and irregular spiking. Non-VIP 5HT3aR cells include neurogliaform cells, which target dendrites and have late spiking properties, as well as cholecystinin (CCK) positive neurons that target the soma and proximal dendrites, and are non-fast spiking (Wamsley & Fishell 2017). This striking interneuron diversity likely evolved to increase the repertoire of neuronal computations that can be performed, ultimately supporting more complex brain functions.

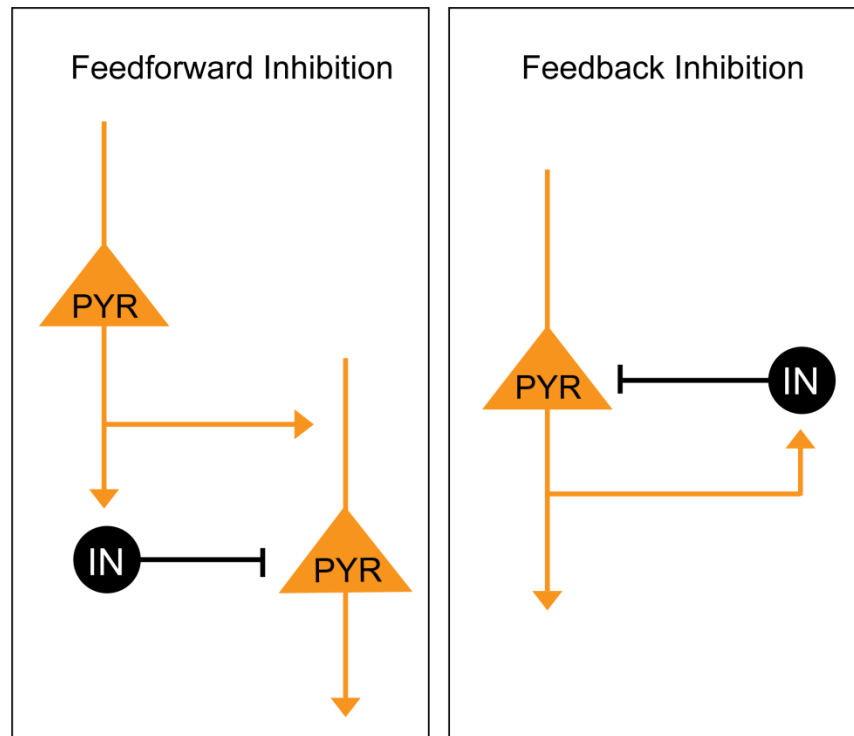
Local inhibitory circuits commonly comprise of simple feedforward or feedback systems. Feedforward inhibition limits the time window in which summation of excitatory inputs can occur, thus reducing the likelihood of action potential generation. This is achieved through excitatory inputs diverging onto both principle cells and interneurons; this interneuron activation provides inhibition to the downstream principle cell limiting the impact of the upstream excitatory drive onto the cell. Additionally, there is feedback inhibition which represents the simplest circuit for generating neuronal oscillations. These oscillations are caused by a pyramidal cell activating an interneuron which feeds back onto the same pyramidal cell to inhibit its activity. This in turn reduces the interneuron activity, releasing the break on the pyramidal cell, which initiates a further cycle of inhibition and facilitates an oscillatory pattern of activity (Isaacson & Scanziani 2011).

Figure 1:4: GABAergic interneurons are highly diverse



Interneurons subtypes can be categorized according to their morphology, subcellular targeting and electrophysiology properties. This high diversity of GABAergic interneurons facilitates more complex control of neuronal activity.

Figure 1:5: Feedforward vs feedback inhibition



Feedforward inhibition: Co-activation of a pyramidal cell (PYR) and an interneuron (IN) by an upstream excitatory input. The interneuron projects to the same downstream pyramidal cell, thus restricting the excitation induced by the upstream pyramidal cell. This can control action potential frequency.

Feedback inhibition: A pyramidal cell (PYR) activates an interneuron, which subsequently inhibits the same pyramidal cell. This negative feedback loop results in oscillatory activity as the neurons cycle through periods of activity/inactivity.

These simple inhibitory circuits form the core building blocks of the brain which ensure a well maintained balance between excitation and inhibition which ultimately restrains neuronal activity. It has been postulated that KCC2 and hyperpolarizing feed forward inhibition dictate coincident firing modes, and without hyperpolarizing inhibition the neurons switch to integrate and fire modes, thus increasing cell excitability (Pathak et al 2007). Moreover, without KCC2 function it is thought that feedback inhibition switches to feedback or recurrent excitation that further drives network excitability (Banerjee et al 2016, Ellender et al 2014, Fujiwara-Tsukamoto et al 2010). Therefore, disruption of KCC2 within these circuits may result in runaway excitation and neuronal synchronization that is characteristic of disorders of hyperexcitation such as epilepsy.

Seizures and epilepsy

The epilepsies are a class of chronic neurological disorders with diverse clinical presentations. These disorders are generally defined as the occurrence of two or more seizures more than 24 hours apart, with no immediately identifiable cause (Fisher et al 2014). Currently available pharmacological treatments are effective for many patients, but approximately one third of patients remain drug resistant. There is therefore great need for the identification of novel therapeutic targets to alleviate seizures in patients with epilepsy.

Seizures occur due to excessive neuronal activation and synchronization. It is therefore unsurprising that a large number of anti-convulsant drugs act to enhance GABAergic inhibition. GABA_A receptors are the site of action of many clinically-used drugs, including benzodiazepines, barbiturates, the IV anesthetic propofol, and neuroactive steroids, all of which act to potentiate GABA_A receptors and increase GABAergic inhibition. Benzodiazepines such as diazepam have been used as anticonvulsant therapies since 1965, when Henry Gastaut successfully treated status epilepticus (more than 5 minutes of continuous seizure activity) using these compounds (Gastaut et al 1965). However, the efficacy of benzodiazepines decreases with increasing seizure duration, which is clearly evident during the early stages of status epilepticus (SE) (Mayer et al 2002, Treiman et al 1998). If a patient develops resistance to benzodiazepines, then aggressive management with anesthetics is required, which is not ideal due to the complications associated with anesthesia. The majority of research on the development of diazepam resistance has focused on a reduction of GABA_A receptors on the cell surface under hyperexcitable conditions (Peng et al 2004, Terunuma et al 2008), although more recently it has been proposed that a reversal in the direction of Cl⁻ flow through GABA_A receptors is responsible (Deeb et al 2013, Staley 1992). Due to such a critical role for KCC2 in regulating the direction of Cl⁻ flow through GABA_A receptors, interest has grown in the potential for KCC2 as a therapeutic target for seizures. Indeed, KCC2 downregulation and depolarizing GABA_A currents have now been identified in patients with epilepsy (see below).

KCC2 mutations underlie epilepsy in humans

Risk factor mutations

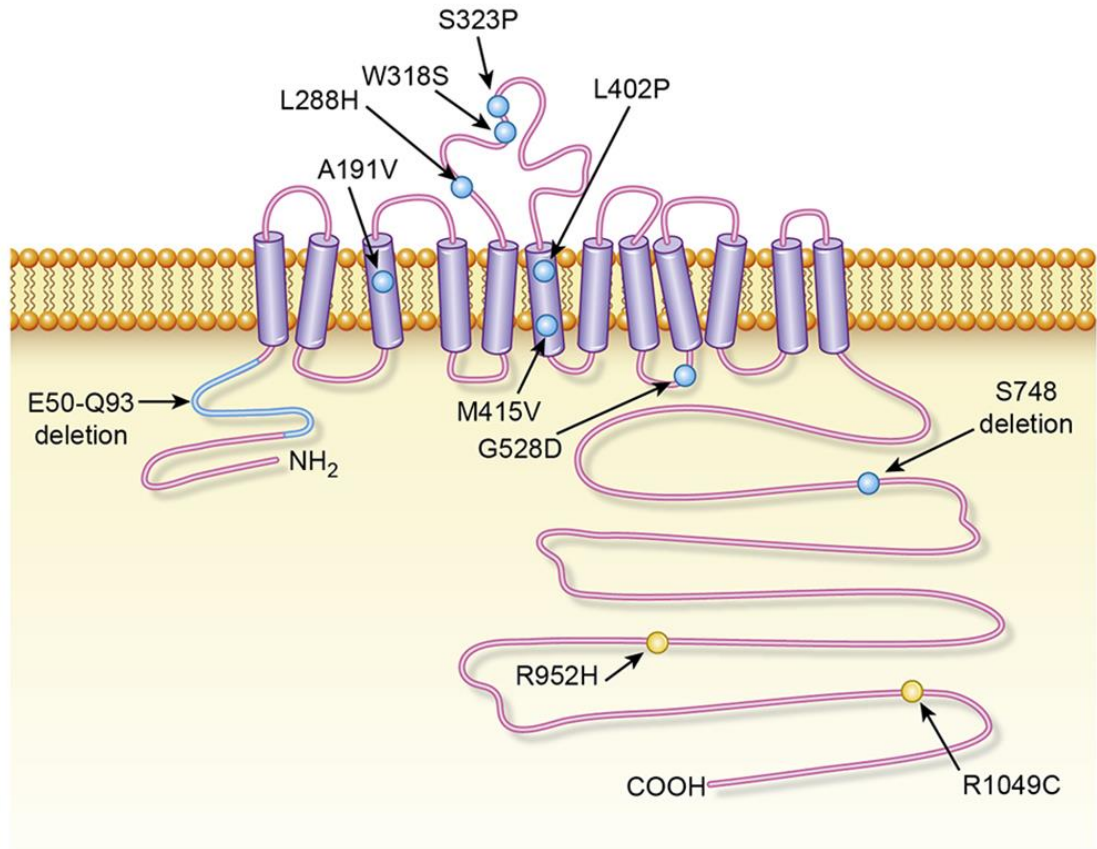
Two independent studies provided the initial evidence that mutations in KCC2 affect transporter function and predispose humans to epilepsy (**Fig. 1.4**). SLC12A5 variants, R952H and R1049C, were discovered in an Australian family with febrile seizures as well as in Canadian patients suffering from idiopathic generalized epilepsy (Kahle et al 2014, Puskarjov et al 2012). Co-expression of both variants in N2A cells causes a depolarizing E_{GLY} shift relative to WT KCC2. Additionally, *in utero* electroporation of KCC2-R952H reduces Cl^- extrusion at P6 in somatosensory layer 2/3 cortical pyramidal neurons relative to WT KCC2 electroporation (Puskarjov et al 2014b). Interestingly, these neurons also have decreased dendritic spine density in culture, highlighting a potential role for KCC2 function in mediating spine formation. Both mutation sites are within close proximity to the KCC2-S940 phosphorylation site, which is accompanied by decreased KCC2-S940 phosphorylation and surface expression compared to WT KCC2 when transfected into HEK-293 cells (Kahle et al 2014). Given the importance of KCC2-S940 phosphorylation for maintaining KCC2 function (Silayeva et al 2015), this work identifies a potential underlying mechanism responsible for the impaired KCC2 function of these variants. Identification of these risk factor mutations were informative about the potential role of KCC2 dysfunction in human patients in the initiation of epilepsy but were insufficient to conclusively demonstrate a causal role.

Causal mutations

Discovery of the first monogenic KCC2 mutations that cause epilepsy were identified through exome sequencing of two unrelated families, several individuals of which were affected by a severe infantile onset epilepsy syndrome, epilepsy of infancy with migrating focal seizures (EIMFS) (Stodberg et al 2015) (**Fig. 1.4**). These patients carry recessive SLC12A5 loss-of-function mutations, with the presence of compound het mutations necessary for developing the disorder. In one family, KCC2-L426P and G551D mutations were found in 2 children (these residues denote the positions within the human KCC2a sequence and are L403P and G528D in human KCC2b). L403P and G528D are located within transmembrane domain 6, and within the intracellular loop between transmembrane domain 8 and 9. In another family, homozygosity of a L311H variant (L228H in human KCC2b), located within the extracellular loop between transmembrane domain 5 and 6, was discovered in two children with EIMFS.

In vitro functional experiments revealed that these mutations do indeed reduce KCC2 function. A reduction in KCC2 surface expression as well as reduced glycosylation was also detected, highlighting a potential mechanism underlying their reduced Cl⁻ transport (Stodberg et al 2015). However, the impact of glycosylation on KCC2 function remains unclear.

Figure 1:6: KCC2-loss of function mutations cause epilepsy



Membrane topology diagram of KCC2 with a cytoplasmic N-terminal region, 12 transmembrane domains, a large extracellular loop, and a large cytoplasmic C-terminal domain. The mutations known to cause epilepsy are indicated in blue. KCC2 variants that are risk factors for the development of epilepsy are indicated in yellow.

4 additional KCC2 mutations have since been identified as a cause of EIMFS: 1 in the N-terminus, causing deletion of exon 3 and subsequent loss of residues E50-Q93; 1 in the large extracellular loop between transmembrane domains 5 and 6 (S323P); and 2 further mutations within transmembrane domains 3 (A191V) and 6 (M415V). The presence of both the A191V mutation and the E50-Q93 deletion was discovered in 2 siblings with EIMFS; a brother carrying only the E50-Q93 deletion was unaffected demonstrating the necessity of both mutations for the appearance of the disease. 2 additional patients carry the compound heterozygous mutations S323P and M415V (Saito et al 2016). Analyses of several of these mutations show they indeed impair KCC2 function, although do retain function relative to cells lacking KCC2, indicating that some KCC2 function is retained. The mutations do not alter the surface expression of KCC2, thus must be reducing KCC2-mediated Cl^- transport through alterations in the intrinsic transport function of KCC2 (Saito et al 2016). The mechanisms through which these mutations impact this Cl^- transport are unknown, but studies into the phosphorylation state of these mutants may provide some insight given the critical role of phosphorylation in mediating KCC2 function (Moore et al 2017).

Further, an additional patient with unclassified intractable epilepsy carries a W318S mutation within the large extracellular loop as well as deletion of S748 in the C-terminus, but no functional studies on these mutations have yet been performed, so their impact on KCC2 activity remains to be determined (Saito et al 2016).

Collectively, these studies confirm that adequate KCC2 function is absolutely critical for maintaining a healthy nervous system in humans, particularly in preventing seizures.

Genetic susceptibility to seizures in animal models

Further evidence that KCC2 dysfunction results in seizures has come from several studies on animals. Loss of KCC2a within the spinal cord in complete genetic Slc12a5 knock-out mice (KCC2a and KCC2b) abolishes synaptic inhibition, causing respiratory failure and death immediately after birth (Hubner et al 2001). Similarly, loss of only KCC2b is sufficient to cause spontaneous seizures and complete mortality in the early postnatal period, the time course of which corresponds to the normal developmental upregulation of KCC2 activity (Woo et al 2002). Moreover, retention of just 15-20% of KCC2 protein in mice prevents mortality but does enhance sensitivity to the convulsant pentylenetetrazol (PTZ) (Tornberg et al 2005). Interestingly, the importance of KCC2 for preventing seizures and death in animals is not specific to mice, as disruption of the *Kcc* gene in drosophila also leads to seizures and lethality (Hekmat-Safe et al 2006), demonstrating the ability to extrude neuronal Cl⁻ via KCCs is a mechanism conserved through evolution.

Altering the phosphorylation state of KCC2 is also sufficient to enhance the sensitivity of mice to chemoconvulsants. Preventing KCC2-S940 phosphorylation in mice (KCC2-S940A mutants) enhances kainate-induced seizure severity, leading

to rapid SE onset and a high incidence of SE-induced lethality (Silayeva et al 2015). This confirms the importance of maintaining the appropriate phosphorylation state of KCC2 for efficient Cl^- extrusion and prevention of runaway excitation that underlies seizures.

The potential pathological consequences of impaired KCC2 function in the mature nervous system has recently been explored, which is an important investigation given that loss of KCC2 function is detected in patients that develop epilepsy in adulthood (see below). Ablation of KCC2 in principal neurons in the adult mouse hippocampus leads to recurrent spontaneous seizures as well as hippocampal sclerosis, demonstrating that loss of KCC2 in the mature nervous system is sufficient to recapitulate epilepsy (Kelley et al 2018). Additional work has shown that pharmacological inhibition of KCC2 in the hippocampus of adult mice leads to epileptiform activity but not full convulsive seizures (Sivakumaran et al 2015), although this may be due to an insufficient degree of KCC2 inhibition under these conditions.

Idiopathic epilepsy in humans

KCC2 mutations do not underlie the majority of epilepsies. However, deficits in KCC2 expression and function are present in resected tissue from patients with idiopathic temporal lobe epilepsy (TLE). In tissue exhibiting severe hippocampal sclerosis, a subset of pyramidal neurons in the subiculum display depolarizing and even excitatory GABAergic responses during field discharges resembling inter-

ictal events (Cohen et al 2002). This correlates with a decrease in KCC2 mRNA and protein expression (Huberfeld et al 2007, Munoz et al 2007). Also in the subiculum, KCC2 mRNA levels are reduced with a coinciding upregulation of NKCC1 mRNA (Palma et al 2006). However, an increase in KCC2 expression in tissue from TLE patients has been described in one study (Karlocai et al 2016). Unfortunately, no functional studies were performed, and KCC2 phosphorylation was not examined, so it is difficult to interpret the impact of enhanced KCC2 protein expression on the degree of Cl^- extrusion in these patients.

Acquired epilepsy in humans

In contrast to patients with genetic forms of epilepsies, an initial brain insult can initiate the development of epilepsy, the most common being TLE. These insults include traumatic brain injury (TBI), gliomas, and status epilepticus, among others. KCC2 surface expression is decreased, and NKCC1 expression increased, in peritumoral neurons in patients with gliomas (Campbell et al 2015, Pallud et al 2014). Depolarizing and even excitatory responses have also been detected in these regions. Given the crucial role for KCC2 in maintaining effective synaptic inhibition, these changes in Cl^- homeostasis likely renders these peritumoral regions vulnerable to hyperexcitation and seizures. However, hyperexcitation itself can downregulate KCC2 (Lee et al 2011) (Lee et al 2010), so it is challenging to assess the timing of this downregulation. In other words, KCC2 downregulation could be either a cause or a consequence of seizures. This is difficult to assess in

humans as brain tissue is only collected from patients with advanced and refractory epilepsy when surgery is performed as a last therapeutic option. Due to these limitations, animal models of acquired epilepsies have been instrumental in assessing the impact of brain insults on KCC2 expression and function before onset of behavioral seizures.

Acquired epilepsy in animal models

Several rodent models of TLE exist, primarily induced using chemoconvulsants such as kainate or pilocarpine to generate a period of status epilepticus (SE) (Buckmaster 2004, Sharma et al 2007). SE induction depolarizes E_{GABA} (Kapur & Coulter 1995) and subsequent studies have identified a rapid reduction in KCC2 protein expression after SE. Kainate reduces KCC2-S940 phosphorylation and downregulates the surface expression of KCC2 30 minutes post-SE (Silayeva et al 2015) possibly due to excessive NMDA receptor activation (Lee et al 2011). Similarly, a reduction in KCC2 protein expression occurs 1 hour after pilocarpine induced SE (Lee et al 2010).

The induction of SE by these compounds is followed by a latent period, after which spontaneous seizures occur (Reddy & Kuruba 2013). Epileptogenesis is the period during which the brain becomes epileptic, occurring during the latent period between the initial insult and seizure onset. A deficit in neuronal Cl^- extrusion is present in the hippocampus and surrounding structures during this latent period, and reductions in KCC2 is present at 24 hours (Li et al 2008, Pathak

et al 2007), 7 days (Barmashenko et al 2011, Pathak et al 2007, Yu et al 2013), and 14 days (Barmashenko et al 2011, Bragin et al 2009, Li et al 2008) following pilocarpine-induced SE. This downregulation occurs in several neuronal subtypes within the hippocampal formation and entorhinal cortex, including CA1 neurons, dentate granule cells and fast spiking basket cells. Within this latent period, dentate granule cells exhibit depolarizing GABA_A currents, as well as increased spiking frequency and an overall enhancement of network excitability (Pathak et al 2007).

A further method of inducing TLE in mice is traumatic brain injury (TBI) caused by fluid percussion or controlled cortical impact (Buckmaster 2004). KCC2 deficits are also observed in these models. Reduced KCC2 protein and mRNA expression in the dentate gyrus results from fluid percussion-induced TBI 7 days post-injury, and depolarization of E_{GABA} occurs (Bonislowski et al 2007). Similar changes occur in the controlled cortical impact model, with downregulation of KCC2 expression occurring within 12 hours post injury in the parietal cortex, which remains downregulated at 7 days (Wu et al 2016).

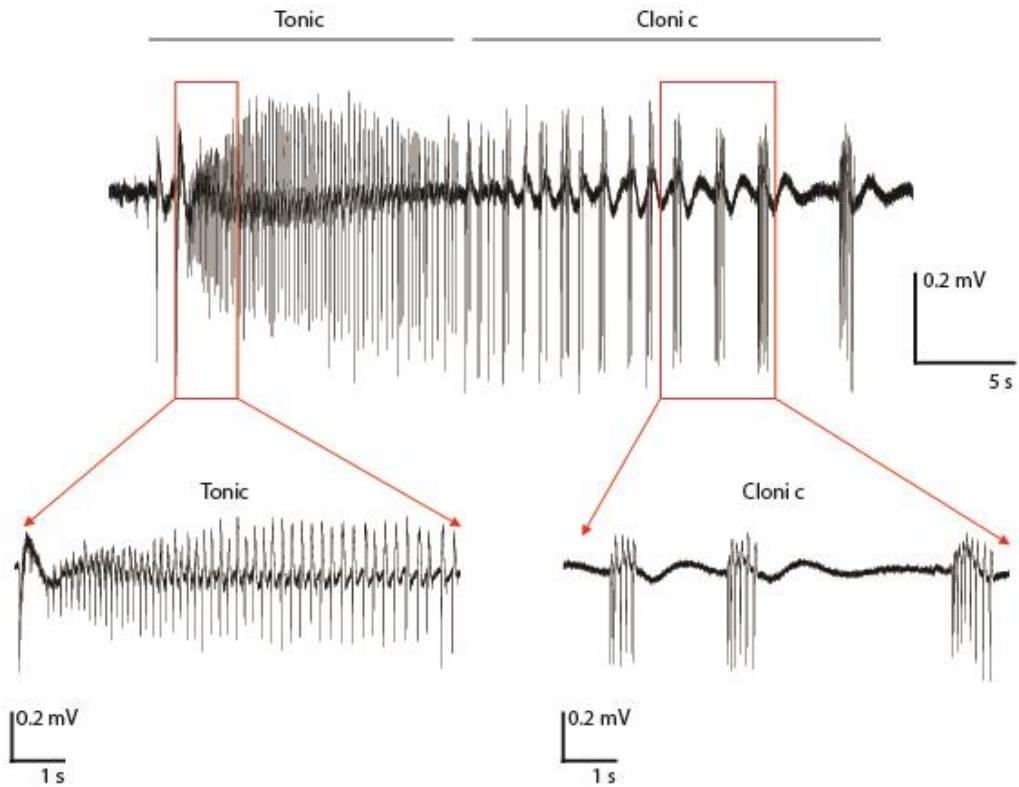
Despite these clear reductions in KCC2 expression and the accompanying depolarizing GABA responses in these TBI models, we can only speculate about the importance of this process for the development of TLE in humans. As it is impossible to resect tissue from patients during the latent period, a pathological role for KCC2 downregulation in the process of epileptogenesis in humans cannot yet be confirmed.

KCC2 dysfunction increases Cl^- loading and seizure severity

Despite current experimental limitations in understanding the role of KCC2 dysfunction in seizure induction, many studies have demonstrated a clear increase in intracellular Cl^- levels and an erosion of synaptic inhibition during seizures, further supporting a role for dysregulation of Cl^- homeostasis to potentiate seizure activity. GABAergic signaling becomes depolarizing and even excitatory onto hippocampal principle cells during the clonic-like after discharge phase of a seizure (**see Fig. 1.5**) due to a collapse in the Cl^- gradient (Fujiwara-Tsukamoto et al 2010, Fujiwara-Tsukamoto et al 2003, Ilie et al 2012, Lillis et al 2012). Shifts in $[\text{Cl}^-]_i$ during seizures have also been detected *in vivo* (Timofeev et al 2002). This rise in $[\text{Cl}^-]_i$ likely results from concurrent inhibitory and excitatory signaling (i.e. prolonged postsynaptic membrane depolarization coinciding with excessive GABA release from hyperactive interneurons, which enhances the driving force for Cl^-) (Deeb et al 2013, Thompson & Gahwiler 1989). Perforated patch clamp studies in which glutamate exposure leads to membrane depolarization and enhanced concurrent IPSPs, causing rapid Cl^- loading and E_{GABA} depolarization, nicely demonstrates the speed at which E_{GABA} can depolarize under hyperexcitable challenges (Deeb et al 2013).

While fluctuations in Cl^- occur in healthy brains, this rise in $[\text{Cl}^-]_i$ is typically short lasting due to rapid Cl^- extrusion by KCC2. Indeed, even in the case of seizure-induced Cl^- loads, KCC2 can extrude this excess Cl^- which corresponds the timing of seizure termination (Lillis et al 2012). We can anticipate, however, that insufficient KCC2 function in epileptic patients would delay such Cl^- extrusion,

Figure 1:7: Tonic versus clonic seizure activity



Trace of a seizure-like event from a brain slice exposed to 0-Mg^{2+} . These events are composed of a high frequency tonic component, followed by low frequency high amplitude after discharges termed the clonic phase of the seizure-like event.

potentially exacerbating seizure activity. Indeed, this idea is supported by several studies; inhibition of KCC2 function using a KCC2-specific pharmacological compound, VU0463271, prevents seizure termination *in vitro* seizure models resulting in activity reminiscent of SE (Kelley et al 2016, Sivakumaran et al 2015). Brain slices from mice with reductions in KCC2 function by phosphomodulation of KCC2-S940 (KCC2-S940A) results in a similar failure of seizure termination in *in vitro* and *in vivo* seizure models (Silayeva et al 2015). Given the relatively mild KCC2 hypofunction in these KCC2-S940A mice, it appears that even small changes in the ability of neurons to extrude Cl^- can have dramatic pathological consequences.

In extreme contrast to all the data discussed so far, several studies suggest KCC2 is pro-convulsant, by facilitating Cl^- loading during seizures (DeFazio et al 2000, Gonzalez et al 2018, Hamidi & Avoli 2015, Jarolimek et al 1999, Payne 1997, Staley & Proctor 1999, Viitanen et al 2010). This hypothesis arose from the thermodynamic equation that governs K-Cl flux across the membrane: $[\text{K}^+]_o \times [\text{Cl}^-]_o = [\text{K}^+]_i \times [\text{Cl}^-]_i$, which dictates that increases in $[\text{K}^+]_o$ cause a reflexive increase in $[\text{Cl}^-]_i$ that is mediated by KCC2. $[\text{K}^+]_o$ rises during seizures, and it is argued that this would drive Cl^- into the cell through a reversal in the driving force for K^+ and subsequently in the direction of K-Cl transport by KCC2. This would raise intracellular Cl^- levels, collapse the Cl^- gradient and abolish fast synaptic inhibition (Kaila et al 2014). It is argued that preventing KCC2 activity could mitigate these Cl^- loads, subsequently maintaining effective fast synaptic inhibition (Kaila et al 2014). However, if seizure induced hyper-activation of GABA_A receptors occurs

prior to elevations in extracellular K^+ , which indeed there is evidence to support (Lillis et al 2012), then KCC2 would not reverse due to the fact that $[Cl^-]_i$ will have already risen. Indeed, it should be noted that even if a reversal of K-Cl transport does occur which aids in the buffering of $[K^+]_o$, then deficits in KCC2 function would likely still be detrimental. A role for KCC2 as either pro-convulsant or anti-convulsant therefore remains controversial.

Restoring Cl^- homeostasis as a treatment for seizures

As I have described, there is now an abundance of evidence linking KCC2 dysfunction to seizures. However, this evidence alone does not necessarily imply that enhancing Cl^- extrusion would have any therapeutic benefit for seizures. Fortunately, many studies have addressed this very question, providing evidence that removal of excess intraneuronal Cl^- reduces seizure activity and promotes seizure termination.

Optogenetic silencing of PV^+ interneurons during *in vitro* seizure activity facilitates seizure termination, highlighting a paradoxical role for excessive interneuron activity during seizures (Ellender et al 2014). This is due to the impact of excessive $GABA_A$ receptor activity, concurrent with membrane depolarization, on the driving force for Cl^- . Under these conditions, Cl^- is driven into the cell which degrades fast synaptic inhibition. Furthermore, a direct role for high $[Cl^-]_i$ in promoting seizure activity was demonstrated *in vitro* by optogenetically removing Cl^- from neurons during seizure-like activity; this reduced the severity of

epileptiform activity (Alfonsa et al 2016). As neither of these strategies can be used in patients, targeting physiological mechanisms that act to reduce $[Cl^-]_i$ would be necessary to confirm the role of elevated $[Cl^-]_i$ in potentiating seizure activity. An obvious potential target is therefore KCC2. Unfortunately, this hypothesis has not yet been addressed as no pharmacological activators of KCC2 currently exist. However, studies using the NKCC1 inhibitor bumetanide have provided support that targeting Cl^- transport could have therapeutic benefits against seizures.

Bumetanide is an FDA-approved drug used in the treatment of edema and high blood pressure. Bumetanide depresses seizure activity *in vitro* (Dzhala et al 2008) and has anticonvulsant effects in rodent models of neonatal seizures (Mazarati et al 2009). Moreover, bumetanide in combination with diazepam is more effective than either drug alone in treating SE in mice (Sivakumaran & Maguire 2016). Excitingly, clinical trials are underway for the use of bumetanide to treat seizures in human neonates. While a reduction in seizure frequency and duration has occurred in one neonate patient after bumetanide administration, this patient had intractable multifocal seizures and died during the procedure (Kahle et al 2009), making conclusions on the effectiveness of bumetanide difficult.

Bumetanide also has unfavorable pharmacological properties including poor brain penetrance (Romermann et al 2017). Moreover, unlike KCC2, NKCC1 is also present in all non-neuronal cells, resulting in numerous side-effects including alkalosis, hypokalemia and diuresis when NKCC1 is inhibited (Puskarjov et al 2014a). Bumetanide has also been shown to cause deafness in 27% of infants that

were administered the drug (Pressler et al 2015). However, the development of pro-drugs with improved brain penetrance and reduced peripheral side effects retains the potential of targeting NKCC1 as a viable therapeutic strategy (Tollner et al 2014).

Despite this potential, a lack of KCC2 redundancy would prevent NKCC1 inhibition from reestablishing hyperpolarizing GABA_A currents if KCC2 function is impaired. At most, NKCC1 inhibition could restore E_{GABA} to levels equal to that of the resting membrane potential, but Cl⁻ must be extruded in order for an inwardly directed Cl⁻ flux to occur upon GABA_A receptor activation. This Cl⁻ extrusion can only be performed by KCC2. Therefore, it is likely that potentiating KCC2 function would not only be a more specific method of reducing neuronal [Cl⁻]_i leading to fewer side-effects, but would also be more efficacious in restoring synaptic inhibition.

Thesis Aims

Hypothesis

The function of KCC2 in vivo is tightly regulated by the phosphorylation state of threonine residues 906 and 1007 on KCC2 and preventing their phosphorylation will increase KCC2 function in the brain. Increasing KCC2 activity in vivo will be seizure-protective.

To test this hypothesis Prof. Stephen Moss generated a KCC2-T906A/T1007A knock-in mouse model which I have used as tool to investigate the impact of T906/T1007 phosphorylation on KCC2 function. In this thesis I present data that demonstrates KCC2 function is increased by these KCC2-T906A/T1007A mutations. I have subsequently investigated the impact of the KCC2-T906A/T1007A mutations on chemoconvulsant-induced seizure activity.

The aims of this thesis are as follows:

1. Characterize the impact of KCC2-T906A/T1007A mutations on KCC2 function
2. Determine the impact of KCC2-T906A/T1007A mutations on the severity of chemoconvulsant-induced seizures
3. Investigate the mechanisms through which KCC2-T906A/T1007A mutations increase KCC2 function and reduce seizure activity

Chapter 2 : Materials and Methods

Knock-in mouse Generation and Colony Maintenance

Generation of KCC2-T906A/T1007A knock-in mice

The KCC2-T906A/T1007A knock-in mouse line was generated by Genoway, a company that specializes in the generation of transgenic mice. The KCC2 gene was disrupted by knock-in insertion of T906A and T1007A mutations in exons 22 and 24. A targeting vector containing a region homologous to the genomic KCC2 sequence was constructed, and was used for ES cell electroporation to integrate T906A and T1007A point mutations into the gene. These ES cells were then injected into C57BL/6 blastocysts, reimplanted into OF1 pseudo-pregnant mice and allowed to develop to term. These chimeras were then bred with mice constitutively expressing Cre recombinase to remove the neomycin selection cassette (Neo) and thus create the Neo-excised point mutant knock-in line which

are heterozygous for the T906A and T1007A mutations and were subsequently the F1 generation of the mouse line. Mice were then backcrossed on the C57Bl/6 background, and bred to produce the homozygous and WT mice used for experimentation (**Fig. 2.1**). Male 5-7 week old mice were used for all experiments.

To confirm that the T906A/T1007A mutations were introduced into the KCC2 gene in the knock-in mice, Genoway sequenced the KCC2 gene from the heterozygous mice. The T906A and T1007A mutations were confirmed through the detection of a GCC codon which codes for alanine, in replacement of ACA and ACC for T906 and T1007 respectively (**Fig. 2.1**).

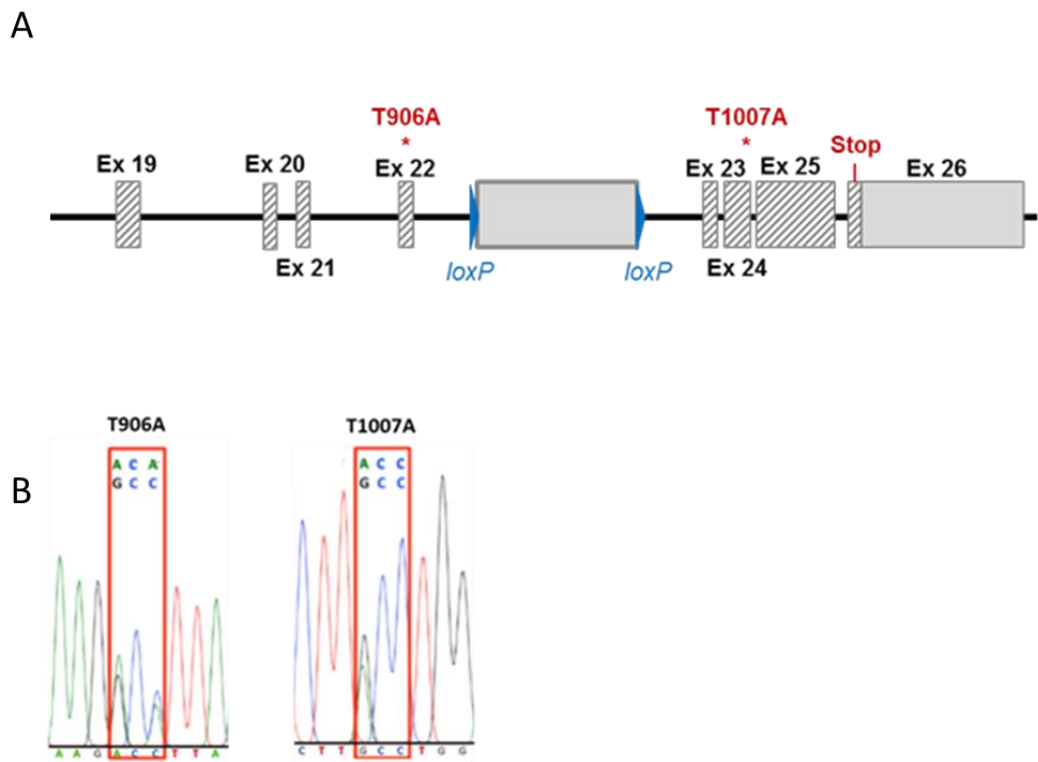
Animal care

All animal studies were performed with protocols approved by the Institutional Animal Care and Use committee of Tufts New England Medical Center. Animals are housed in Tufts University's AAALAC-approved facility adjacent to the laboratory. Animals live in temperature-controlled rooms on a 12 hour day/light cycle, fed ad libitum, and cages changed twice weekly.

Genotyping

Mice were genotyped by polymerase chain reaction (PCR) to determine if they were WT, heterozygous or homozygous for the KCC2-T906A/T1007A mutations.

Figure 2:1: Creation and sequencing of KCC2-T906A/T1007A knock-in mice.



A. Diagram of the KCC2-T906A/T1007A targeting construct indicating the location of the T906A and T1007A allele of KCC2. **B.** The chromatogram indicates the presence of the T906A and T1007A KCC2 mutations in heterozygous KCC2-T906A/T1007A mice.

Small tail clipping were taken from the mice while they were under isoflurane anesthesia. DNA was extracted from the tails using 200 µl of DirectPCR lysis reagent (Viagen, cat# 102-T) and 5 µl of Proteinase K solution (Viagen, 501-PK). Tails, fully submerged in the lysis solution, were put in a heat block for 16 hours at 55°C. The samples were then heated for 1 hour at 80°C, followed by centrifugation at 16,000 rcf for 10 min to pellet the insoluble material.

For detected of the Cre-excised point mutant knock-in allele, the primer set was designed flanking the remaining loxP site. The WT mice yielded a product of 298bp, whereas the homozygous mice yielded a product of 387bp.

The primers used for genotyping were as follows:

The forward primer sequence used was: AGACAAGGGTTCATGTAACAGACTCGCC

The reverse primer sequence used was: GTGGTTCGCCTATGGGATCTGCTACTC

Both primers were made up to 10 mM. The recipe used for the PCR reaction was: 5.35 µL dH₂O, 0.2 µL forward primer, 0.2 µL reverse primer, 6.25 µL HiFi HotStart Ready Mix PCR Kit (KAPA BioSystems) and 0.5 µL DNA. The following PCR protocol was then used to amplify the DNA (PCR lid temp: 105°C):

1. 95°C for 3 min
2. 95°C for 15 sec
3. 60°C for 15 sec
4. 72°C for 1 min
5. Repeat steps 2-4 35 times
6. 72°C for 5 min
7. Cool to 12°C

Tissue Preparation

P1 mouse pup dissection and culturing

P1 mouse pups were cooled on ice before decapitation and brain removal. Brains were submerged in ice-cold HEPES-buffered saline solution (HBSS), meninges removed from the brain surface, and hippocampi dissected out. Hippocampi were transferred to 10 mL of 0.25% trypsin in HBSS at 37°C for 9 min to dissociate the tissue. Trypsin was then removed from the hippocampi by washing the tissue three times in culture media (Neurobasal A media containing B27 (2%), glucose (0.6%), Glutamax (1%), and penicillin/streptomycin (1%)). 10 mL of fresh media was then added to the cells, and the cells were triturated with a 10 mL pipette, by gently pipetting up and down 15 times. Cells were then strained using sterile 40 µM nylon mesh to remove non-dissociated tissue. 400,000 cells were plated onto pre-prepared poly-L-lysine (PLL) coated glass coverslips in 30 mm dishes each containing 3 mL culture media (warmed to 37°C). Cells were maintained at 37°C in a humidified 5 % CO₂ incubator.

Hippocampal dissection from adult mice

Mice were deeply anesthetized with isofluorane before decapitation at the second cervical vertebrae. Brains were carefully removed from the skull and rinsed in ice-cold phosphate buffered saline (PBS). The hippocampus was then dissected with fine forceps, and immediately put into ice-cold RIPA lysis buffer (2% Triton-X-100, 0.5% deoxycholic acid, 5mM EDTA, 5mM EGTA, 1mM sodium

orthovanadate, 25mM sodium fluoride, 10mM sodium pyrophosphate, 100mM NaCl, 10mM sodium phosphate monobasic, pH 7.4) containing protease inhibitors (1 µg/mL aprotinin, 10 µg/mL leupeptin, 1 µg/mL pepstatin, 10 µg/mL antipain and 250 µg/mL AEBSF). Here, the tissue was dissociated with a 26G needle and rotated a 4°C for 30 min to lyse the tissue. The samples were then centrifuged at 16,000 rcf for 15 min at 4°C to pellet all insoluble material. The supernatant was used for western blotting.

Brain slicing for electrophysiology and biochemistry experiments

Acute horizontal or coronal slices (400 µM) were used for electrophysiology and biochemistry experiments. Mice were anesthetized with isoflurane and brains were removed and cut in ice-cold cutting solution on a Leica VT1000s vibratome. The cutting solution contained (in mM): NaCl 87, NaHCO₃ 25, NaH₂PO₄ 1.67, KCl 3, MgCl₂ 7, CaCl₂ 2.5, sucrose 50 and glucose 25. Slices were placed in a submerged chamber for a 60 min recovery period at 32°C in artificial cerebrospinal fluid (ACSF) containing, in mM: NaCl 126, NaHCO₃ 26, KCl 2.5, MgCl₂ 2, CaCl₂ 2, glutamine 1, NaH₂PO₄ 1.25, Na-pyruvate 1.5, and glucose 10, bubbled with 95% O₂/5% CO₂ gas mixture.

Cardiac Perfusion

Mice were deeply anesthetized with isofluorane, and pinned to a Styrofoam board. Quickly, a horizontal incision was made below the sternum, and then the diaphragm cut. The sides of the chest were cut to expose the heart. While the heart was still beating, a perfusion needle attached to a pump was inserted into the left ventricle and 30 mL ice-cold PBS was pumped through the body. This cleared the brain of blood before fixation. 30 mL of ice-cold 4% paraformaldehyde (PFA) in PBS was then pumped through the body to fix the brain. Mice were then decapitated and the brain was carefully removed from the skull and post-fixed in 4% PFA for 3 hours. The brains were then transferred to 30% sucrose in PBS for at least 16 hours before slicing.

Brain slicing for Nissl Staining

A microtome (Leica SM 2000R) was used to slice 40 μ M coronal sections from brains fixed with PFA (see above). A small amount OCT compound was placed onto the slicing platform, and the brain placed in the OCT. Dry ice was used to freeze the OCT and the brain, securing the brain to the platform, and thus stabilizing the brain for slicing. 40 μ m slices were cut and then submerged in PBS. Slices were washed three times in PBS, mounted onto gelatin coated slides, and then allowed to dry for at least 24 hours.

Biochemistry

Antibodies

All antibodies used are listed below:

Anti-Vesicular GABA Transporter (Millipore, rabbit polyclonal, cat# ab2257)

Anti-Postsynaptic density protein 95 (NeuroMab, mouse monoclonal, cat# 75-028)

Anti-GABA_A receptor subunit alpha-2 (Phosphosolutions, rabbit polyclonal, cat# 822GA2C)

Anti-GABA_A receptor subunit beta-3 (NeuroMab, mouse monoclonal, cat # 75-149)

Anti-KCC2 (Millipore, rabbit polyclonal, cat # 07-432)

Anti-KCC2 (NeuroMab, mouse monoclonal, cat# 75-013)

Anti-beta-actin (Sigma, mouse monoclonal, cat# A1978)

Anti-GAPDH (Santa Cruz, mouse monoclonal, cat# SC32233)

Anti-Gephyrin (Synaptic systems, rabbit polyclonal, A2220)

Anti-AMPA receptor subunit GluA1 (NeuroMab, mouse monoclonal, cat# 73-327)

Anti-KCC2-pT1007 (Phosphosolutions, rabbit polyclonal, made specifically for Prof. Stephen Moss)

Anti-Transferrin receptor (ThermoFisher, mouse monoclonal, cat# 13-6800)

Donkey anti-mouse IgG, HRP (Jackson ImmunoResearch, donkey polyclonal, cat#715-035-150)

Donkey anti-rabbit IgG, HRP (Jackson ImmunoResearch, donkey polyclonal, cat#711-035-152)

Protein assay

Protein concentrations were calculated using a colorimetric Bicinchonic Acid (BCA) assay. 1 μ l of each protein sample was added to individual wells in a 96 well plate, along with additional wells containing bovine serum albumin standards of known concentrations. 100 μ L of BCA working reagent (Pierce BCA protein assay kit, ThermoFisher) was added to each well and incubated at 37°C for 30 min and then cooled to room temperature. This induces a color change from green to purple proportional to protein levels, the concentration of which was then measured by passing 562nm wavelength light through the solution using a BioRad xMark Microplate Spectrophotometer. The absorbance at this wavelength is nearly linear with increasing protein concentration, thus protein concentration in each sample was calculated by comparing the absorption of each sample to the absorption of the protein standards used.

Immunoprecipitation

Total KCC2 was immunoprecipitated from hippocampal lysate prior to detection of KCC2-T1007 phosphorylation. The specificity of this antibody for phosphorylated KCC2-T1007 was previously characterized by (Conway et al 2017). A total of 20 μ L of protein A/G plus agarose (santa Cruz Biotechnology) was washed in IP Buffer (10 mM Tris-HCl, pH 8.0, 7.5 mM NaCl, 0.5% Triton X-100). and then mixed with 350 μ g of protein lysate and 1 μ g/mL of either anti-KCC2 antibody (mouse) or ChromPure mouse IgG (Jackson ImmunoResearch) in RIPA lysis buffer (2% Triton-X-100, 0.5% deoxycholic acid, 5mM EDTA, 5mM EGTA, 1mM sodium orthovanadate, 25mM sodium fluoride, 10mM sodium pyrophosphate, 100mM NaCl, 10mM sodium phosphate monobasic, pH7.4) containing protease inhibitors (1 μ g/mL aprotinin, 10 μ g/mL leupeptin, 1 μ g/mL pepstatin, 10 μ g/mL antipain and 250 μ g/mL AEBSF) for 16 hours at 4°C with rotation. Beads were then washed 3 times in IP Buffer. After the final wash, beads were mixed with 2X NuPAGE LDS Sample Buffer diluted from 4X in dH₂O (4X from Invitrogen) with 0.7% β -mercaptoethanol and incubated for 1 minute at 95 °C. Beads were then centrifuged for 2 min at 455 rcf, and the supernatant was processed by SDS-PAGE and western blotting.

Slice Biotinylation

Horizontal slices (400 μ M) were incubated with biotin solution (1 mg/mL EZLink Sulfo-NHS-LC-Biotin in ACSF containing, in millimoles: NaCl 126, NaHCO₃ 26, KCl

2.5, MgCl₂ 2, CaCl₂ 2, glutamine 1, NaH₂PO₄ 1.25, Na-pyruvate 1.5, and glucose 10, bubbled with 95% (vol/vol) O₂/5% (vol/vol) CO₂ gas mixture) for 45 minutes at 4°C with gentle shaking. Following biotin incubation, slices were washed 3 times with ice-cold glycine (100 mM glycine in ACSF), with the final wash carried out for 15 minutes at 4°C with gentle shaking. Slices were then washed twice with ice-cold ACSF and subsequently lysed in RIPA Buffer (2% Triton-X-100, 0.5% deoxycholic acid, 5mM EDTA, 5mM EGTA, 1mM sodium orthovanadate, 25mM sodium flouride, 10mM sodium pyrophosphate, 100mM NaCl, 10mM sodium phosphate monobasic, pH7.4) containing protease inhibitors (1µg/mL aprotinin, 10µg/mL leupeptin, 1µg/mL pepstatin, 10µg/mL antipain and 250µg/mL AEBSF) by rotating samples for 30 min at 4°C. Insoluble material was removed by centrifugation for 15 min at 16,000 rcf. 350 µg of the supernatant was added to 50 µL of streptavidin agarose resin (Thermoscientific) in RIPA buffer containing protease inhibitors and incubated for 16 hours at 4°C with rotation. Beads were then washed (10 mM Tris-HCl, pH 8.0, 7.5 mM NaCl, 0.5% Triton X-100) 3 times. Beads were then mixed with 2X NuPAGE LDS Sample Buffer diluted from 4X in dH₂O (4X from Invitrogen) with 0.7% β-mercaptoethanol and incubated for 1 minute at 95°C, and subsequently loaded onto acrylamide gels and processed by Sodium dodecyl sulphate polyacrylamide gel electrophoresis (SDS-PAGE). KCC2 levels were then measured by western blotting.

Sodium dodecyl sulphate polyacrylamide gel electrophoresis (SDS-PAGE)

2X NuPAGE LDS Sample Buffer (4X from Invitrogen) with 0.7% β -mercaptoethanol was added to samples as described above. Samples were then vortexed and heated at 95°C for 1 min before being loaded onto polyacrylamide gels for electrophoresis.

The composition of the polyacrylamide gels used for separation of proteins is listed below:

- 8% (v/v) acrylamide:bis solution 29:1
- 0.38M Tris (pH8.8)
- 0.1% (w/v) Sodium dodecyl sulfate (SDS)
- 0.1% (w/v) ammonium persulphate (APS)
- 0.06% (v/v) tetramethylethylenediamine (TEMED)
- In dH₂O

After mixing of the solution, it was poured into mini PROTEAN 3 system gel casting stand (Bio-Rad) for setting. 70% ethanol was added to the top of the solution to ensure the top of the gel set in a straight horizontal line. This was left for 30 min at room temperature to set. After 30 min the ethanol was washed from the top of the gel using dH₂O. An additional acrylamide solution, the stacking gel, was then added to the top of the gel, along with a comb to create wells in which the protein samples can be added. The composition of the stacking gel is listed below:

- 5% (v/v) acrylamide/bis solution 29:1

- 0.13M Tris (pH 6.8)
- 0.11% (w/v) SDS
- 0.1% (w/v) ammonium persulphate (APS)
- 0.1% (v/v) Tetramethylethylenediamine TEMED
- In dH₂O

After 30 min, in which time the stacking gel sets, the gels were assembled into a mini PROTEAN 3 system gel running tank (Bio-Rad). Running buffer was then added to the setup, the composition of which is listed below:

- 25mM Tris
- 190mM Glycine
- 3.5mM SDS
- In dH₂O

Samples were loaded into the wells, along with a molecular weight marker (ThermoScientific, cat #26634) to enable the molecular weight of the protein of interest to be determined. Proteins were then separated on the gels by electrophoresis, which was carried out at 100mV for approximately 2 hours.

Western blotting

After electrophoresis, gels were electrotransferred onto nitrocellulose membranes, which have a high protein-binding affinity and immobilize proteins. The membrane was placed on top of the gel, with a piece of filter paper and

sponges either side. This was assembled into a Mini Transblot cell unit (Bio-Rad), submerged in transfer buffer, the components of which are listed below:

- 48mM Tris
- 39mM Glycine
- 1.3mM SDS
- 20% Methanol
- In dH₂O

Gels were subjected to a current of 50 mA for 16 hours at 4°C to transfer the proteins from the gel to the membrane. Following electroblotting, the nitrocellular membrane was removed from the cassette and ponceau stained (0.1% w/v ponceau, 5% acetic acid in dH₂O) to check for successful protein transfer. Membranes were then washed briefly in PBS with 0.1% Tween (PBS-T). Blocking solution (5% milk, 1% BSA in PBS-T) was then applied to the membrane for 1 hour. Membranes were then incubated with primary antibody diluted in blocking solution overnight at 4°C. Membranes were then washed 3 times in PBS-Tween and incubated with the respective HRP-conjugated secondary antibody. Secondary antibody incubations were carried out in blocking solution for 1 hour at room temperature. Membranes were then washed 3 times in PBS-Tween, followed by 1 wash in PBS. Chemiluminescence signal was detected using SuperSignal West Dura Extended Duration Substrate (Thermo Scientific). Quantification of chemiluminescence signal was carried out using Image Lab 5.0 (BioRad).

Histology

Nissl Staining

Cresyl Violet Acetate solution was used to stain Nissl substance in the cytoplasm of neurons in slices fixed with PFA, which stains the neuropil a granular purple/blue. This allows gross brain structure to be visualized. Slice mounted onto gelatin-coated slides were sequentially exposed to the following solutions:

1. 70% Ethanol (1min)
2. 95% Ethanol (1 min)
3. 100% Ethanol (1 min)
4. dH₂O (1 min)
5. 0.1% Cresyl violet stain 5 min
6. dH₂O (~30 sec)
7. 70% Ethanol (2 min)
8. 95% Ethanol (2 min)
9. 95% Ethanol/0.5% Acetic Acid (1min)
10. 100% Ethanol (1 min)
11. Xylene (2 min)

Glass slips were then used to cover the slices. Slices were then visualized with a brightfield microscope and images taken using Nikon instruments software-elements (NIS-elements).

Patch clamp electrophysiology

Solutions

Bath saline (in mM): NaCl 140, KCl 2.5, CaCl₂ 2, MgCl₂ 1.5, Hepes 10, glucose 11, pH 7.4 NaOH. Saline was made fresh every day from a 5X stock.

TTX was used at a final concentration of 500 nM, diluted in bath saline from 1mM stock aliquots (made up in dH₂O and stored at -20°C).

Muscimol was used at a final concentration of 1μM, diluted in bath saline from 1mM stock aliquots (made in dH₂O and stored at -20°C).

Glutamate was used at a final concentration of 20 μM, diluted in bath saline from 20mM stock aliquots (made in NaOH 0.1N and stored at -20°C).

The selective KCC2 inhibitor VU0463271 was dissolved in DMSO to make 20 mM stock solutions, aliquots of which were stored at -20°C. VU0463271 stocks were diluted in bath saline to a final concentration of 1 μM (final DMSO concentration of 0.001%) for experiments.

Gramicidin stock solutions were prepared at 10mg/mL in DMSO and stored at -20°C. For experiments, stock solutions were diluted to a final concentration of 50μg/mL in (in mM): KCl 140, HEPES 10, pH 7.4 KOH. This was used as the internal patch pipette solution for gramicidin perforated patch clamp experiments.

Whole cell patch clamp pipette solution contained (in mM): KMeSO₄ 115, KCl 30, MgCl₂ 2, HEPES 10, Na-ATP 4, Na-GTP 0.4, pH 7.2, aliquots of which were stored at -20°C. Solution was kept at 4°C throughout experiment.

Set up

Recordings were conducted at 32°C (maintained using a Warner Instrument temperature controller TCB443). Cells on coverslips were submerged in bath saline in a Warner Instrument RC-26 recording chamber. All solutions (except the bath saline entering from a bath inlet pipe) were applied through a three-barrel microperfusion system (700 μm , Warner Instruments, Hamden, CT) closely positioned above the cell. These solutions were applied through the perfusion pipette at a rate of 0.5 mL/min and I used a computer-controlled perfusion fast-step device (Warner Instruments) to ensure fast and complete exchange of solutions.

Patch pipettes (3-6 M Ω) were made using a P-1000 micropipette puller from Sutter Instrument, and were used for both gramicidin perforated patch clamp experiments and whole cell patch clamp experiments.

E_{GABA} Measurements

Gramicidin perforated patch clamp experiments began once adequate perforation had been achieved, classed here as a series resistance <50 M Ω . Whole cell experiments began once seals of >1G Ω were formed in the cell-attached configuration, and negative pressure was applied to break into the cell and achieve the whole cell configuration.

E_{GABA} was measured by application of muscimol (1 μ M) during positive going voltage ramps (10 mV or 20 mV, 1 s duration). The same voltage ramp was performed in the absence of muscimol to acquire the leak currents. Only cells with stable membrane potentials less than -50 mV were accepted for analysis to ensure only healthy cells were used for experiments. Data were acquired at 10 kHz and low pass Bessel filtered at 2kHz with an Axopatch 200B amplifier. Subsequent calculation of the reversal potential of the leak-subtracted muscimol currents was obtained using linear regression fit analysis in Clampex 10 software (Molecular Devices, Sunnyvale, CA). E_{GABA} values were then corrected to account for liquid junction potentials of 4.9mV for perforated patch clamp experiments and 13.9 mV for whole cell patch clamp experiments. Once E_{GABA} values were obtained, these were used to determine the intracellular Cl^- concentration of the cells. E_{GABA} values are considered equal to E_{Cl^-} values as Cl^- is the major permeant anion of $GABA_A$ receptors. E_{Cl^-} values were calculated using the Nernst equation:

$E_{Cl^-} = RT/zF \times \ln[Cl^-]_o/[Cl^-]_i$, detailed below:

E_{Cl^-} (Cl^- reversal potential)

R (universal gas constant) = 8.324 J K⁻¹ mol⁻¹

T (temperature in kelvin) = 305

Z (charge of the ion) = -1 in the case of Cl^-

F (faraday constant) = 9.6485 x10⁴Cmol⁻¹

$[Cl^-]_o$ = bath Cl^- concentration

$[Cl^-]_i$ = intracellular Cl^- concentration

Resting Membrane Potential (RMP) Measurements

RMP was estimated in current clamp ($I=0$) and then measured in voltage clamp by performing a 10 mV voltage ramp covering the estimated RMP value. Linear regression fit analysis was then used to determine the RMP.

Input Resistance Measurements

The input resistance of each cell was determined using a current injection protocol, using a series of hyperpolarizing current steps (-50 pA - 0 pA in 10 pA increments, with a duration of 1 s). Input resistance was calculated as the change in membrane potential in response to a negative current injection divided by the magnitude of that current. The input resistance was then determined by the slope of a linear regression line fitted to the linear portion of the I-V plot.

Glutamate Challenge Assay

This assay was performed using the gramicidin perforated patch clamp technique. Baseline E_{GABA} measurements were taken in the presence of 500 nM TTX. After 3 min, TTX was removed from the bath by applying bath saline through the inlet pipe. 20 μ M glutamate was then applied to the cell for 3 x 10 s, each exposure spaced 30 s apart. E_{GABA} was then measured after 3 min exposure to TTX (the

“recovery” E_{GABA} value). The glutamate exposure was then repeated, but E_{GABA} was measured immediately after the 3 glutamate pulses, with no recovery period (the “challenge” E_{GABA} value).

Cl⁻ loading Assay

This assay was performed using whole cell patch clamp. 500 nM TTX was applied throughout. Baseline E_{GABA} values were taken 4 min after achieving whole cell, followed by a 3 min exposure to the specific KCC2 inhibitor VU0463271, after which a further E_{GABA} measurement was taken.

Extracellular Field Recordings

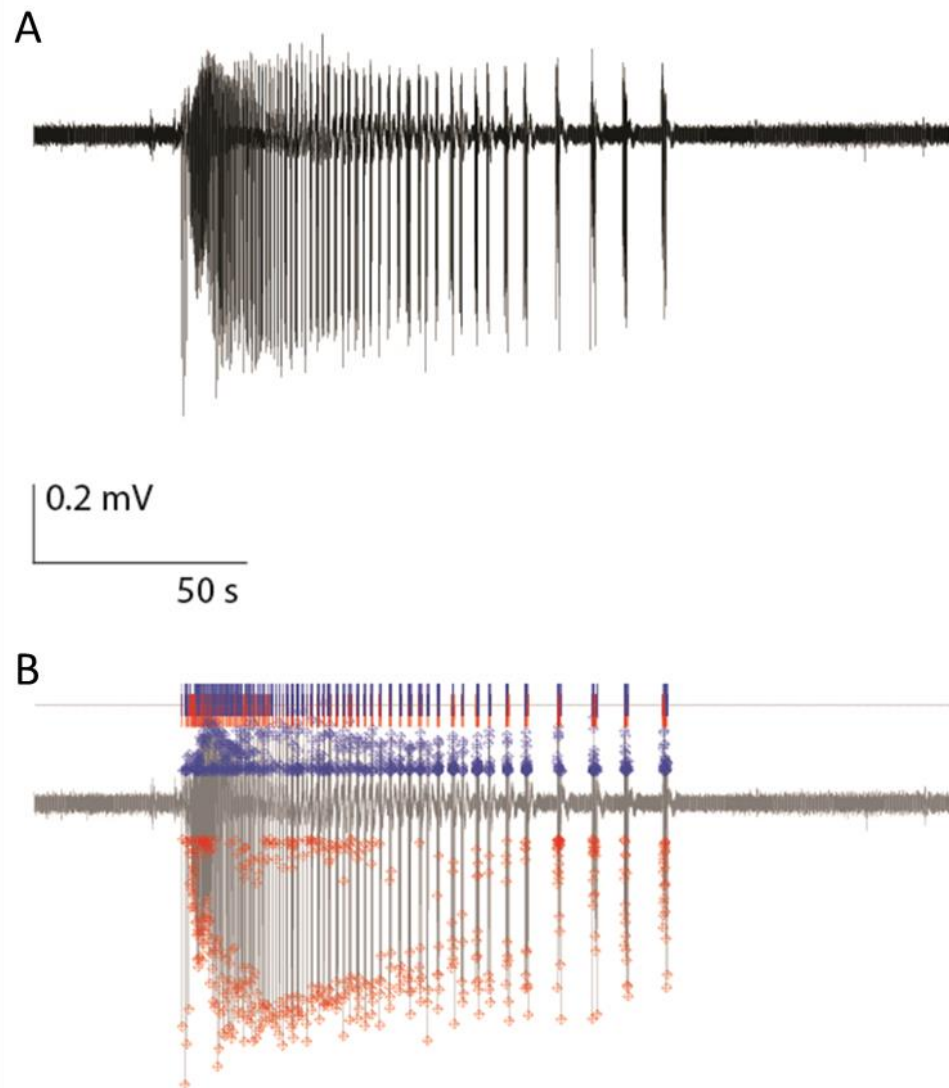
In vitro seizure assays

1 hour post slicing, slices were transferred to a Warner Instruments recording chamber (RC-27L). Electrodes of 0.5-1M Ω were inserted into layer III/IV of the medial entorhinal cortex, several cell layers deep. Slices were perfused for 10 min with ACSF containing, in mM: NaCl 126, NaHCO₃ 26, KCl 2.5, MgCl₂ 2, CaCl₂ 2, glutamine 1, NaH₂PO₄ 1.25, Na-pyruvate 1.5, and glucose 10) (4 mL/min, 32 °C) before changing to either 0-Mg²⁺ ACSF (containing in mM: NaCl 126, NaHCO₃ 26, 5KCl, 2 Ca²⁺, glutamine 1, NaH₂PO₄ 1.25, Na-pyruvate 1.5, and glucose 10) or 4-aminopyridine (4-AP) ACSF, containing in mM: 100uM 4-AP in NaCl 126, NaHCO₃ 26, KCl 5, MgCl₂ 0.6, CaCl₂ 1.2, glutamine 1, NaH₂PO₄ 1.25, Na-pyruvate 1.5, and

glucose 10. All solutions were bubbled with 95% (vol/vol) O₂/5% (vol/vol) CO₂ gas mixture. The selective KCC2 inhibitor VU0463271 was dissolved in DMSO to make stock solutions (final DMSO concentration of 0.001%), and subsequently solubilized in ACSF. Recordings were performed with a Multiclamp 700B amplifier (Molecular Devices) with Clampex 10 acquisition software (Molecular Devices). Data were filtered at 10 kHz and analyzed offline with Clampfit (Molecular Devices). Recordings were highpass filtered above 1Hz to remove baseline wobble. Time spent in seizure-like activity was measured using threshold detection software in Clampfit. 3 x the standard deviation of a 1 min period of the baseline immediately prior to 0-Mg²⁺/4-AP onset was used as the lower cut off for event detection. The duration between each above-threshold event was calculated, and inter-event durations of <20s were considered as a continuation of the same seizure-like event. Inter-event durations of >20s were considered silent (non-seizing) periods (**Fig. 2.2**). Total time in seizure activity was added and expressed as a percentage of total time.

Power analysis was performed using Labchart software. Fast-fourier transform (FFT) was used to transform the local field potential signals from the time domain into the frequency domain to form a power spectral density plot (FFT size 16K, 93.7% overlap). The power of each frequency was binned into different frequency bands, the consensus of which are delta (1-4 Hz), theta (4-8 Hz), alpha (8-13 Hz), beta (13-30 Hz), and low gamma (30-50 Hz).

Figure 2:2: Threshold analysis for quantifying seizure-like activity in *in vitro* seizure models



A. Local field potential recording of an individual seizure-like event induced by 0-Mg²⁺. **B.** Time spent in seizure-like activity was measured using threshold detection software in Clampfit. All events above threshold are detected, indicated here by the blue and red markers. The duration between each event was calculated and inter-event durations of <20s were considered as a continuation of the same seizure-like event.

Field EPSPs

Coronal slices (400 μm) were transferred to a Warner Instruments recording chamber (RC-27L) after 1 hour of recovery in ACSF. A stimulating electrode (FHC, model CBARC75) was positioned to stimulate Schaffer collaterals and commanded by a Stimulus Isolator (World Precision Instruments), and responses were recorded in the stratum radiatum using 0.5-1M Ω electrodes inserted several cell layers deep. The stimulus intensity was determined by a threshold response at stimulus duration (width) of 120 μs , with no response at 80 μs . The width of the stimulus was increased stepwise by 40 μs to create input-output curves from 120 μs -1000 μs . The maximum slope of the response (volts per second) was measured within the linear phase of the fEPSP initial slope (approximately 0.5-1ms window).

Behavior

For all behavioral experiments, mice were habituated in the testing rooms for 1 hour prior to testing. Testing was performed at similar times of the day (between 1 and 3pm), in temperature controlled rooms (70-74 F). Littermates were always tested at the same time. Following completion of each experiment, mice were returned to their home cage. Equipment was cleaned between each mouse using 70% ethanol, followed by Clidox (chlorine dioxide based sterilant).

Open Field

Mice were placed into the center of a 60 cm x 60 cm arena and allowed to explore for 10 min. Photobeam break technology and MotorMonitor software was used to track the distance travelled by the mice, as well as time spent in the center of the arena versus the periphery.

Rotarod

Mice were placed onto a rotating cylinder, 4 cm in diameter, fixed 20 cm above the ground, gradually accelerating from 0-40 rotations per minute over 5 minutes. The cylinder was coated in rubber coating to facilitate traction. The time for the mice to fall off the cylinder or to lose control (defined as three rotations around the cylinder) was measured using beam break technology. Mice were tested 4 times, spaced 15 minutes apart, and the average of the final 3 trials was taken.

Elevated Plus

Mice were placed into the center of an elevated plus-shaped apparatus, with two open and two enclosed arms, and were given 10 min to explore. The time the mice spent in the open and closed arms, and the number of entries into the open arms was tracked using beam break technology and MotorMonitor software.

EEGs

Surgery

WT and KCC2-T906/T1007A littermates were used for EEG studies. Mice were anesthetized with 100 mg/kg ketamine and 10 mg/kg xylazine according to a protocol approved by IACUC. Mice were then given 0.1 mg/kg intraperitoneal injection of buprenorphine as an analgesic. All instruments were sterilized with a heated beads sterilizer. The fur covering the scalp was shaved off then the mouse was placed into a stereotax and head secured in position. The scalp was sterilized by 3 x application of β -iodine, and washed with 70% ethanol between each application. Scissors were then used to make an incision down the length of the scalp to expose the skull. The skull was washed with β -iodine and 70% ethanol in the same way as the scalp. Superglue was used to secure an EEG/EMG implant to the skull, just in front of lambda. Holes were then drilled through the skull in each corner of the EEG implant and screws placed in each hole. Silver epoxy was placed under each screw head to provide electrical connectivity between the electrodes and the headmount. Dental cement was then used to close the scalp and further secure the headmount to the skull. Mice were then allowed to recover for 5 days before EEG recordings were obtained.

Recordings

Mice were acclimated to the EEG room 1 hour prior to experiments. Sirenia Acquisition software was used to obtain EEG recordings. After baseline recordings

were obtained, mice were intraperitoneally injected with 20 mg/kg kainate to induce seizures. Onset to first tonic seizure was calculated by visual inspection of the EEG trace using Labchart software and the data was expressed as the onset time relative to its WT littermate control. Power analysis was performed using Labchart software. Fast-fourier transform (FFT) was used to transform the EEG signals from the time domain into the frequency domain to form a power spectral density plot (FFT size 16K, 93.7% overlap). The power of each frequency was expressed as a percentage of the total power of the signal, and then binned into different frequency bands, the consensus of which are delta (1-4 Hz), theta (4-8 Hz), alpha (8-13 Hz), beta (13-30 Hz), low gamma (30-50 Hz) and high gamma (50-100 Hz).

Statistical Analysis

All data are presented as the mean \pm SEM and were analyzed with the unpaired t-test except for E_{GABA} shifts detected on the same cells, where paired T-tests were used (paired T-tests are indicated in the results sections where appropriate). P values < 0.05 are considered statistically significant.

Chapter 3 : KCC2-T906A/T1007A mutations increase KCC2 function

Summary

Phosphorylation of KCC2 at sites T906 and T1007 are thought to inhibit KCC2 function. Using a KCC2-T906A/T1007A knock-in mouse, I explored the importance of these phosphorylation sites for KCC2 regulation. These mutations increased KCC2-mediated Cl^- extrusion in mature neurons, as well as during postnatal neuronal development resulting in an accelerated developmental excitatory-to-inhibitory E_{GABA} shift. This potentiation of KCC2 function does not stem from an increase in KCC2 surface expression and is therefore likely altering the kinetic properties of the transporter. Synaptic function and network activity are unaffected by these KCC2-T906A/T1007A mutations. Moreover, these KCC2-T906A/T1007A mutations did not impact gross brain morphology, or baseline motor and anxiety behaviors. In summary, this chapter identifies the T906 and

T1007 phosphorylation state of KCC2 as a powerful regulator of neuronal Cl⁻ extrusion, both during development and in mature neurons, which results in no overt phenotype in mice.

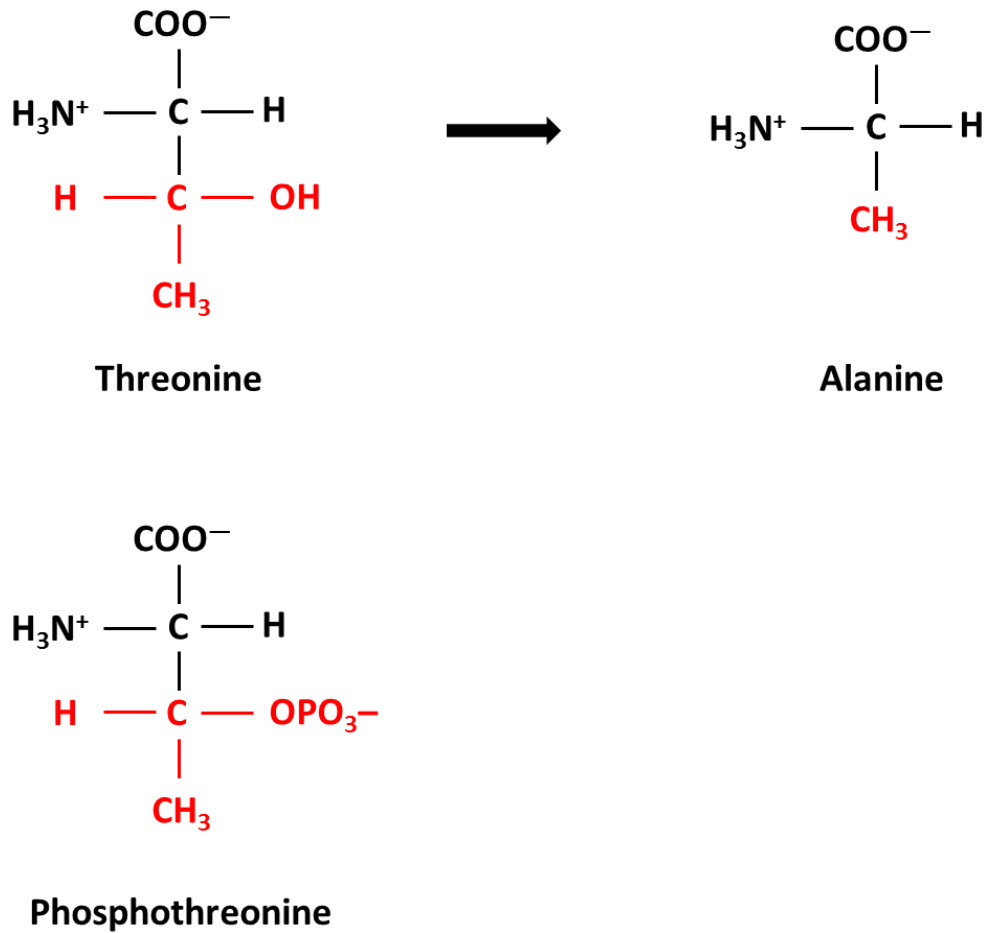
Introduction

Identification of phosphorylation as a critical regulator of KCC2 function

Initial evidence to suggest that KCCs are regulated by phosphorylation came from the observation that KCC activity is increased when ATP and Mg^{2+} are depleted (Delpire & Lauf 1991, Lauf 1985). Furthermore, both cell swelling and N-ethylmaleimide (NEM) lead to activation of KCCs, but a delay to full KCC activation suggested that inhibition of specific kinases may underlie this activation (Jennings & Alrohil 1990). Strong evidence for this arose from the observation that KCCs fail to be activated by swelling or NEM in the presence of specific phosphatase inhibitors (calyculin A and okadaic acid) (Jennings & Alrohil 1990, Jennings & Schulz 1991).

The identification of several phosphorylation sites on KCC2 has aided in our understanding of this process. In fact, recently it was confirmed that a phosphorylation site on KCC2, threonine T1007 (T1007), is responsible for mediating the NEM-dependent increase in KCC2 function. NEM dephosphorylates KCC2-T1007 which results in an increase in KCC2 function (Conway et al 2017). Mutation of T1007 to a glutamate residue (T1007E), the negative charge of which mimics phosphorylation, abolishes sensitivity to NEM, demonstrating NEM's actions work exclusively through phosphomodulation of this site.

Figure 3:1: Structure of threonine, phosphothreonine and alanine



A hydroxyl group is present in the side chain of threonine amino acids. Phosphorylation involves the transfer of a phosphate group from ATP to the hydroxyl group on the amino acid side chain. By mutating threonine sites to alanine, this hydroxyl group is removed, eliminating the site as a substrate for phosphorylation.

A role for KCC2-T906/T1007 phosphorylation in the modulation of KCC2 function

Phosphoregulation of KCC2-T1007 in addition to a further threonine residue on KCC2 (T906), are thought to play a central role in the physiological regulation of KCC2 function. High levels of KCC2-T906/T1007 phosphorylation are present in the immature nervous system, but phosphorylation of these sites decreases as neurons mature (Friedel et al 2015, Rinehart et al 2009), correlating with the developmental increase in KCC2 activity. It was speculated that KCC2-T906/T1007 phosphorylation may maintain KCC2 in an inhibited state. Support for this has come from many studies assessing the impact that preventing phosphorylation of these sites has on KCC2 function, which was achieved by mutating these T906/T1007 to alanine residues (KCC2-T906A/T1007A), which removes the hydroxyl group needed for phosphorylation to occur (**Fig. 3.1**). By transfecting KCC2-T906A/T1007A constructs into HEK-293 cells and assessing KCC2 transport function through the use of a chloride transport dependent $^{86}\text{Rb}^+$ flux assay, it was discovered that KCC2-T906A/T1007A transport function is 4-fold higher than that of WT KCC2 (Rinehart et al 2009). *In utero* electroporation of KCC2-T906A/T1007A in the cortex similarly enhances KCC2 function and prematurely hyperpolarizes E_{GABA} during development (Inoue et al 2012), demonstrated by obtaining E_{GABA} values using gramicidin perforated patch clamp. This increase in KCC2 function when KCC2-T906/T1007 sites are replaced with alanine residues has been corroborated by others (Friedel et al 2015, Titz et al 2015, Weber et al 2014).

Several studies involving pharmacological reduction of KCC2-T906/T1007 phosphorylation have provided further support that dephosphorylation of these residues increases KCC2 function. This was achieved through inhibition of known regulatory kinases which subsequently reduces KCC2-T906/T1007 phosphorylation. STE20/SPS1-related proline-alanine-rich protein kinase (SPAK) and the related kinase, oxidative stress–responsive 1 protein (OSR1), are thought to phosphorylate T906/T1007 on KCC2, and the equivalent sites on KCC 1, 3 and 4. A role for SPAK/OSR1 in regulating KCCs was discovered when these two kinases were found to physically bind to the N-terminus of KCC3 in a yeast two-hybrid screen (Piechotta et al 2002). With-no-lysine kinase 1 (WNK1)-mediated phosphorylation of SPAK at S373, and S325 on OSR1, correlates with the activation of these kinases (Friedel et al 2015), and the phosphorylation of KCC2-T906/T1007. Small interfering (si)-RNA-mediated knockdown of WNK1 in model cell systems partially suppresses KCC2-T906/T1007 phosphorylation *in vitro* (Rinehart et al 2009). Similarly shRNA knock-down of WNK1, as well as pharmacological inhibition of WNK1, decrease KCC2-T906/T1007 phosphorylation and enhances KCC2 function in neurons. These findings support KCC2-T906/T1007 (de)phosphorylation as a key mechanism through which KCC2 function is regulated.

A role for KCC2-T906/T1007 dephosphorylation in the developmental upregulation of KCC2 function has been proposed. The phosphorylation and function of SPAK/OSR1 decreases over development due to a reduction in WNK1 activity as neurons mature. This correlates with a decrease in KCC2-T906/T1007

phosphorylation, increased KCC2 function, and subsequent hyperpolarization of E_{GABA} over development (Friedel et al 2015). Moreover, *in utero* electroporation of KCC2-T906A/T1007A in the cortex prematurely enhances KCC2 function in immature neurons (Inoue et al 2012). This highlights a potential role for KCC2-T906/T1007 phosphoregulation in controlling this developmental excitatory-to-inhibitory GABAergic shift.

As these previous studies on KCC2-T906A/T1007A involve *in vitro* systems, ectopic overexpression of KCC2 *in vivo*, or non-specific pharmacological kinase inhibitors, it remains unclear whether the phosphorylation state of KCC2-T906/T1007 is responsible for modulation of KCC2 function *in vivo*. Similarly, whether KCC2-T906/T1007 (de)phosphorylation is responsible for the depolarizing to hyperpolarizing E_{GABA} shift is still unconfirmed. Increasing KCC2 function *in vivo* would enable the first investigations into the impact of increased KCC2 activity on brain function. Importantly, a potential benefit of increasing KCC2 function as a therapeutic strategy for seizure-associated disorders could be investigated. With this motivation, Prof. Stephen Moss created a KCC2-T906A/T1007A knock-in mouse (through Genoway), and my first aim is centered on characterizing the impact of these mutations on KCC2 function both during development and in the adult brain, as well as their impact on brain function.

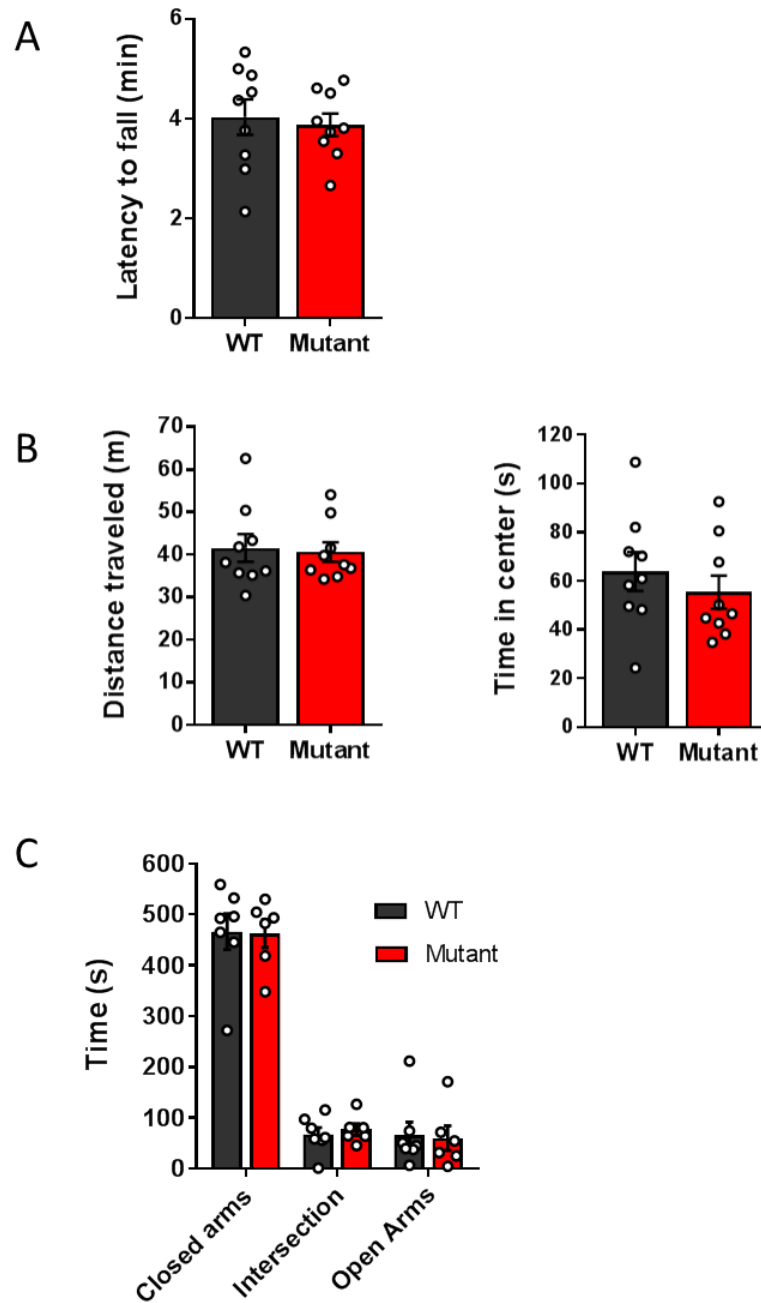
Results

Generation and behavioral characterization of KCC2-T906A/T1007A knock-in mice

To determine if phosphorylation of KCC2-T906/T1007 regulates KCC2 function *in vivo*, Prof. Stephen Moss generated mice in which KCC2-T906/T1007 are mutated to alanine residues (KCC2-T906A/T1007A). Homozygous KCC2-T906A/T1007A mice were viable, survived through adulthood, and exhibited no overt phenotype. These mice had normal motor coordination, assessed as latency to fall off an accelerating rotarod (WT: 4.03 ± 0.35 min, $n = 9$; T906A/T1007A: 3.88 ± 0.23 min, $n = 9$; $p = 0.7206$) (**Fig. 3.2A**), and normal locomotor activity, assessed as distance travelled in an open field arena (WT: 41.6 ± 3.3 m, $n = 9$; T906A/T1007A: 40.6 ± 2.3 m, $n = 9$; $p = 0.8145$) (**Fig. 3.2B**).

To assess anxiety-like behavior in the KCC2-T906A/T1007A mice, I measured the time the mice spent in the center of the open field area and detected no difference between the WT and KCC2-T906A/T1007A mice (WT: 63.82 ± 7.908 , $n=9$; T906A/T1007A: 55.4 ± 6.729 , $n=9$; $p = 0.4292$) (**Fig. 3.2B**). Furthermore, in an elevated plus maze, there was no difference in time spent in the open arms of the maze between WT and KCC2-T906A/T1007A mice (WT: 66.49 ± 25.38 s, $n=7$; T906A/T1007A: 59.87 ± 24.22 s, $n=6$; $p = 0.8553$) (**Fig. 3.2C**), suggesting comparable levels of anxiety is present in the WT and KCC2-T906A/T1007A mice.

Figure 3:2: Motor and anxiety-like behaviors are normal in KCC2-T906A/T1006A mice



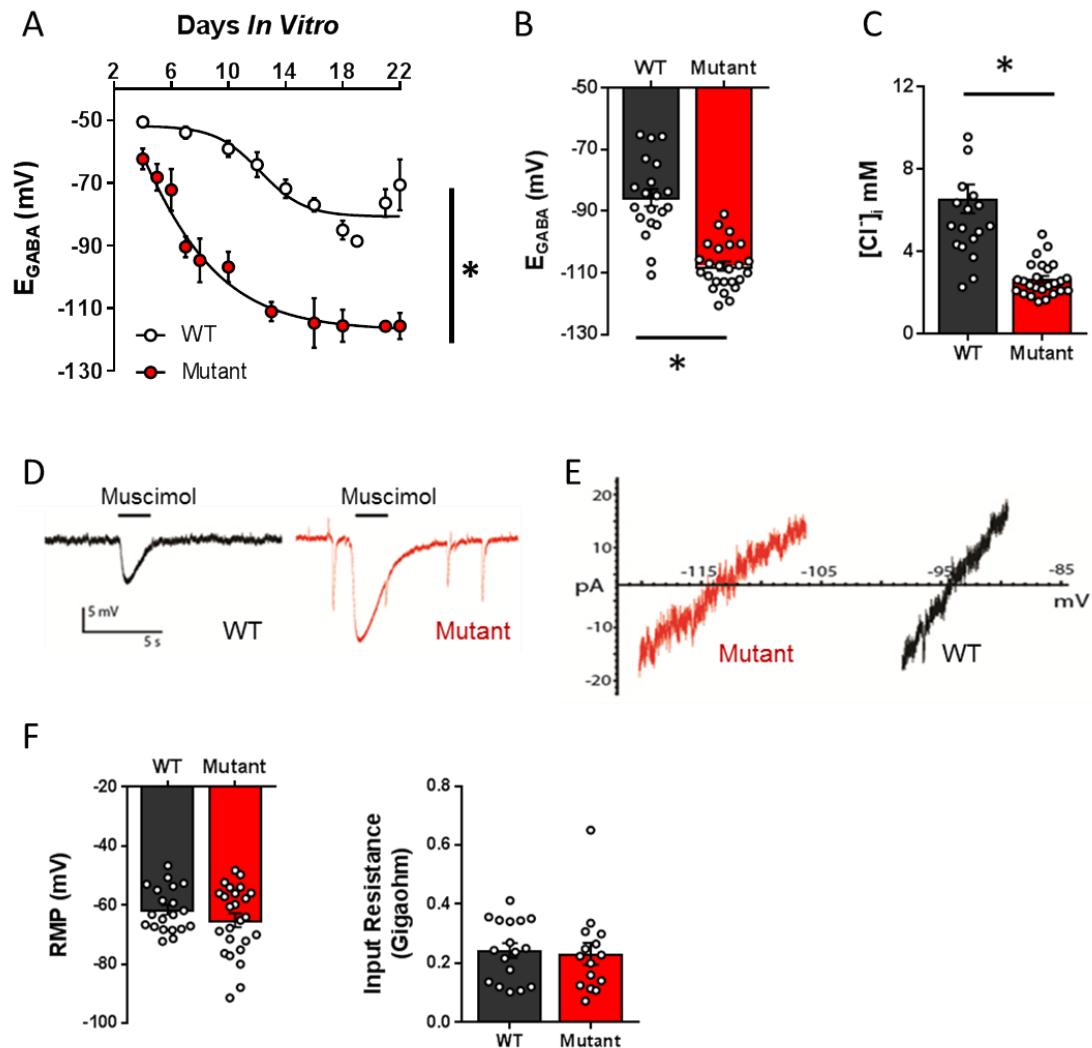
A. Latency to fall off an accelerating rotarod was comparable between WT and KCC2-T906A/T1007A mice. **B.** No differences in distance travelled in an open field, as well as time spent in the center of the arena, were detected between WT and KCC2-T906A/T1007A mice. **C.** Time spent in the closed arms, intersection and open arms of an elevated plus maze was comparable between WT and KCC2-T906A/T1007A mice.

KCC2-T906A/T1007A mutations increase KCC2 function at all stages of neuronal development

To determine if the KCC2-T906A/T1007A mutations impact KCC2 function, I performed gramicidin perforated patch-clamp experiments on hippocampal neurons cultured from WT and KCC2-T906A/T1007A P1 mice and recorded E_{GABA} at 4-21 DIV. E_{GABA} was strongly hyperpolarized in KCC2-T906A/T1007A neurons at all stages of neuronal development (**Fig. 3.3A**), and in mature neurons (18-21DIV) (WT: -86 ± 3 mV, $n = 20$ neurons; T906A/T1007A: -108 ± 3 mV, $n = 25$ neurons; $p < 0.0001$) (**Fig. 3.3 B,D,E**), indicating increased KCC2 function in the KCC2-T906A/T1007A neurons. I calculated the $[\text{Cl}^-]_i$ values from the E_{GABA} values using the Nernst equation, which revealed significantly lower $[\text{Cl}^-]_i$ in the 18-21 DIV KCC2-T906A/T1007A neurons compared to the age-matched WT neurons (WT: 6.6 ± 0.7 mM, $n = 20$; T906A/T1007A: 2.7 ± 0.2 mM, $n = 25$; $p < 0.0001$) (**Fig. 3.3C**). In contrast, both the resting membrane potential (RMP) (WT: -62 ± 2 mV, $n = 20$; T906A/T1007A: -65 ± 2 mV, $n = 25$; $p = 0.2445$) and input resistance (R_i) (WT: 243 ± 25 M Ω , $n = 17$; T906A/T1007A: 232 ± 36 M Ω , $n = 15$; $p = 0.7946$) did not significantly differ between WT and KCC2-T906A/T1007A neurons (**Fig. 3.3F**), demonstrating that increased KCC2 function does not impact these parameters.

To determine the mechanism responsible for increased Cl^- extrusion in KCC2-T906A/T1007A neurons, I assessed whether the mutations influenced the total and/or surface expression of KCC2. I first characterized the best conditions for assessing total and surface expression of KCC2 by western blotting. To determine what protein concentration would allow me to visualize a sufficient level of KCC2

Figure 3:3: KCC2 function is increased in KCC2-T906A/T1007A hippocampal neurons

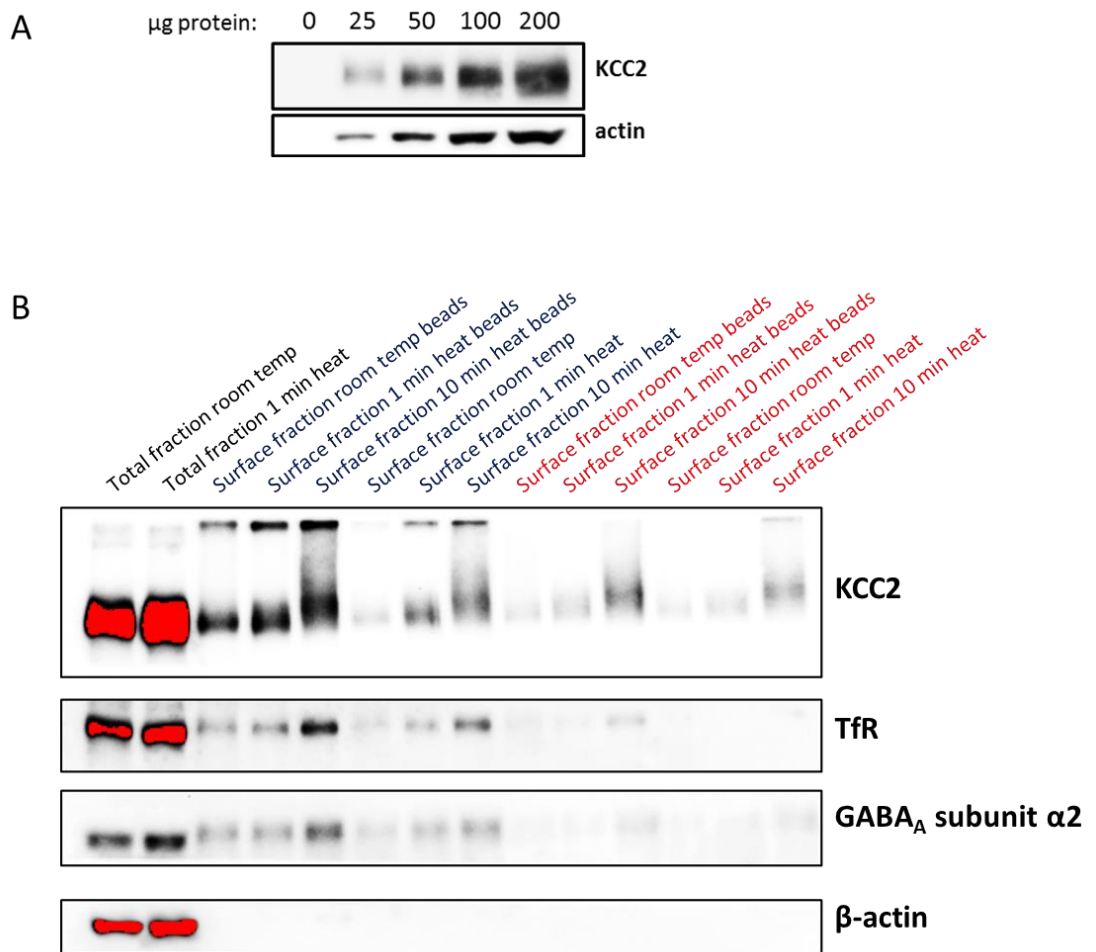


A. Graph depicting E_{GABA} values in WT and KCC2-T906A/T1007A hippocampal neurons between 4 and 21 DIV. KCC2-T906A/T1007A E_{GABA} values were significantly more negative at all stages of development. **B.** Summary of all E_{GABA} values in mature (18-21 DIV) hippocampal neurons in WT and KCC2-T906A/T1007A neurons. **C.** The $[Cl^-]_i$ values corresponding to the measure E_{GABA} values from the mature WT and KCC2-T906A/T1007A neurons are shown, demonstrating reduced $[Cl^-]_i$ in KCC2-T906A/T1007A neurons compared to WT. **D.** Traces depict hyperpolarizing GABA_A responses to muscimol application, with increased amplitude response in the KCC2-T906A/T1007A neurons. **E.** Example I-V plots depicting the reversal potentials of muscimol activated currents of an individual WT and KCC2-T906A/T1007A hippocampal neuron. **F.** Input resistance and RMP were unaffected by the KCC2-T906A/T1007A mutations

expression, while still enabling me to visualize both increases and decreases in KCC2 protein expression, I performed SDS-PAGE and western blotting of several different protein concentrations (0-200 μg) from protein lysates of brain slices. 50 μg enabled clear visualization of reductions and increases in KCC2 expression, thus I used this concentration for assessing total KCC2 expression (**Fig. 3.4A**).

To determine the best conditions for adequate signal levels of surface proteins on western blotting, I tried several different conditions. I used WT slices that were exposed to biotin for 45 min, and I varied the time in which the surface proteins were isolated with streptavidin beads, trying both 16 hour incubations, as well as a shorter time period of 2 hours. I also tried different elution methods, specifically a 20 min room temperature elution, a 1 min at 95°C elution, and a 10 min 95°C elution. Furthermore, I tested whether loading the streptavidin beads into the wells, versus loading the supernatant, was more effective to detect KCC2 by western blotting. This revealed that the best condition for visualizing surface KCC2 was incubation of the sample with the streptavidin beads for 16 hours followed by elution at 95°C for 1 min and then loading the streptavidin beads onto the polyacrylamide gel (as opposed to just the supernatant). While the 10 min boil produced more protein, it resulted in smearing of the KCC2 signal, thus I chose to use the 1 min boil condition. I also probed for GABA_A receptor subunit $\alpha 2$ as a control due to its abundance at the plasma membrane, and transferrin receptor (TfR) as this will be used as a loading control for the biotinylation experiments. A lack of β -actin in the surface lanes revealed there was very little

Figure 3:4: Assessing the ideal conditions required to visualize total and surface expression of KCC2 from brain slices by western blot



A. Protein concentrations ranging between 0-200µg were visualized by western blot. 50µg of protein provided adequate signal for visualization of total KCC2, while enabling the detection of increases and decreases in expression and was thus the selected protein concentration for assessing total KCC2 expression. **B.** Surface KCC2 expression was best visualized by incubating protein lysate with streptavidin beads for 16 hours followed by heating of the sample for 1 min at 95°C, followed by loading the beads onto the gel. Total lysate samples are overexposed (red bands) in order to visualize the surface fraction. Blue text indicates samples incubated with streptavidin beads for 16 hours and red text indicates sampled incubated with streptavidin beads for 2 hours.

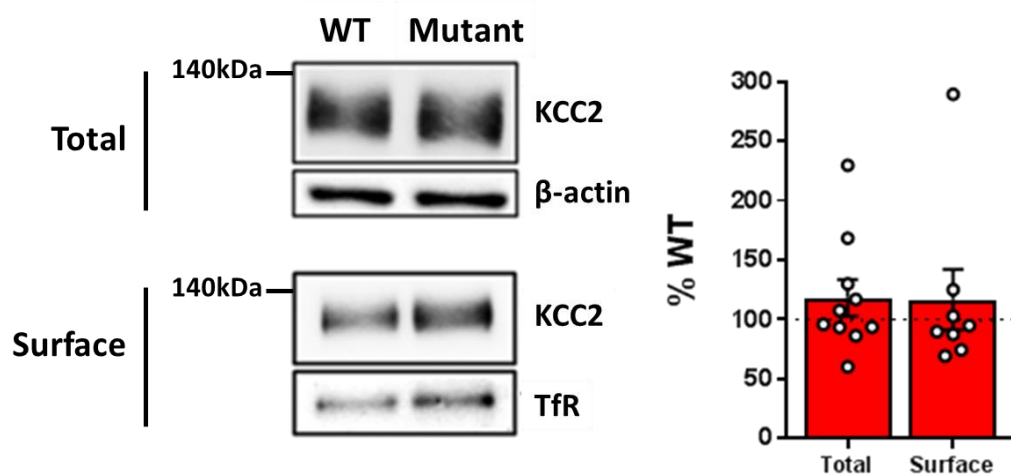
slice damage during my slicing and biotinylation, confirming the slices were healthy (**Fig. 3.4B**).

After establishing the ideal experimental conditions, I compared KCC2 total and surface expression between WT and KCC2-T906A/T1007A brain slices. I detected no difference in either total (118 ± 15 % WT, $n = 10$; $p = 0.2523$) or surface (117 ± 25 % WT, $n = 8$; $p = 0.5236$) KCC2 protein levels between WT and KCC2-T906A/T1007A mice (**Fig. 3.5**), indicating the mutations do not increase Cl^- extrusion through enhanced surface levels but are likely exerting their effects by modulating an intrinsic property of the transporter (**explored in aim 3**).

Gross brain morphology and neuronal network excitability is normal in KCC2-T906A/T1007A mice

The KCC2-T906A/T1007A mouse line is the first mouse model with increased KCC2 function, so it was important to characterize effects of the mutations on gross morphology and brain function. To visualize gross brain morphology, I performed Nissl staining on coronal slices from PFA perfused brains, and no abnormalities were detected in the KCC2-T906A/T1007A mice. Hippocampal images are shown in (**Fig. 3.6**). To assess for changes in inhibitory and excitatory synapses in KCC2-T906A/T1007A mice, I performed immunoblotting on total protein lysates from brain slices for markers of excitatory (PSD-95 and GluA1) and inhibitory (gephyrin, VGAT and GABA_A receptor subunits $\alpha 2$ and $\beta 3$) synapses. The total expression of PSD-95 (103 ± 9 % WT, $n = 5$; $p = 0.7739$), Gephyrin (85 ± 7 % WT, $n = 5$; $p =$

Figure 3:5: KCC2 total and surface expression is unaffected by KCC2-T906A/T1007A mutations



Biotinylation was performed on WT and KCC2-T906A/T1007A brain slices. Western blot revealed total and surface expression of KCC2 is unchanged in KCC2-T906A/T1007A mice compared to WT. Total KCC2 was normalized to beta-actin expression. Surface KCC2 was normalized in TfR surface expression. Data are expressed as the percentage of WT expression.

0.0717), GABA_A receptor subunit β 3 (89 ± 5 % WT, $n = 5$; $p = 0.0795$), and GABA_A receptor subunit α 2 (109 ± 9 % WT, $n = 5$; $p = 0.3592$) are comparable between WT and KCC2-T906A/T1007A mice, while small reductions in GluA1 (85 ± 6 % WT, $n = 5$; $p = 0.0380$) and VGAT (83 ± 4 % WT, $n = 5$; $p = 0.0029$) were detected (**Fig. 3.7**).

To determine if these reductions alter the efficacy of excitatory transmission, I analyzed the input/output (I/O) relationship in the hippocampus. Field EPSPs were measured in the stratum radiatum in response to Schaffer collateral stimulation of varying stimulus widths. I/O curves from WT and KCC2-T906A/T1007A slices were comparable, indicating that the KCC2-T906A/T1007A mutations do not impact the efficacy of excitatory transmission, at least in the hippocampus (**Fig. 3.8**).

I then assessed global network activity by obtaining *in vivo* cortical EEG recordings from awake mice. Spectral analysis did not reveal significant differences across a range of frequency bands between WT and KCC2-T906A/T1007A mice, indicating normal neuronal network excitability in the cortex of these mice (**Fig. 3.9**). Details of the measured values are below:

Delta (1-4Hz): WT: 18.81 ± 3.96 %, $n = 9$; T906A/T1007A: 19.36 ± 3.163 %, $n = 8$; $p = 0.9164$

Theta (4-9Hz): WT: 21.15 ± 2.7 %, $n = 9$; T906A/T1007A: 22.5 ± 2.123 %, $n = 8$; $p = 0.7043$

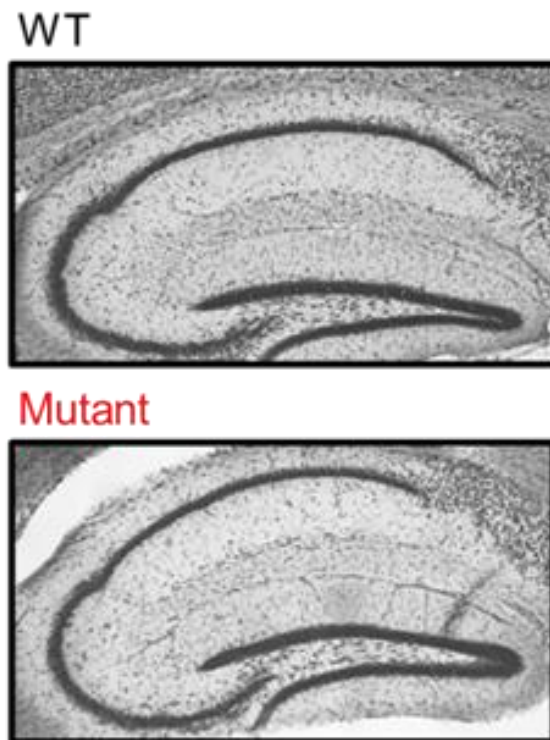
Alpha (9-13Hz): WT: 8.228 ± 0.7357 %, n = 9; T906A/T1007A: 9.072 ± 0.7954 %, n = 8; p = 0.4479

Beta (13-30Hz): WT: 16.49 ± 1.631 %, n = 9; T906A/T1007A: 17.87 ± 1.873 %, n = 8; p = 0.5825

Low gamma (30-50Hz): WT: 14.5 ± 1.824 %, n = 9; T906A/T1007A: 12.76 ± 1.858 %, n = 8; p = 0.5144

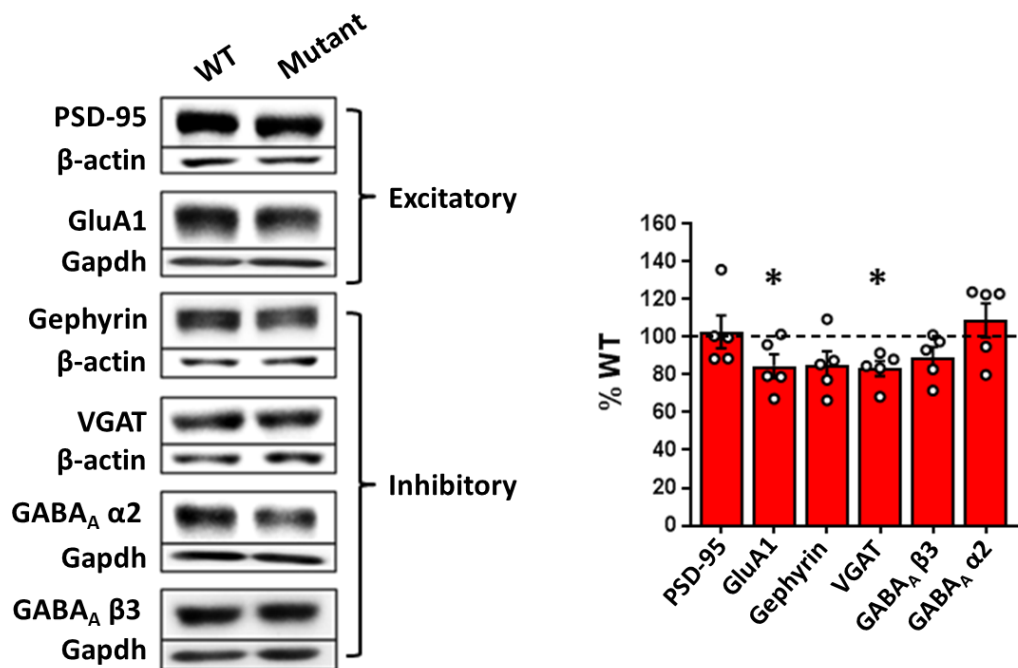
High gamma (50-100Hz): WT: 20.83 ± 2.643 %, n = 9; T906A/T1007A: 18.43 ± 2.625 %, n = 8; p = 0.5321

Figure 3:6: Assessing gross brain structure in WT and KCC2-T906A/T1007A mice



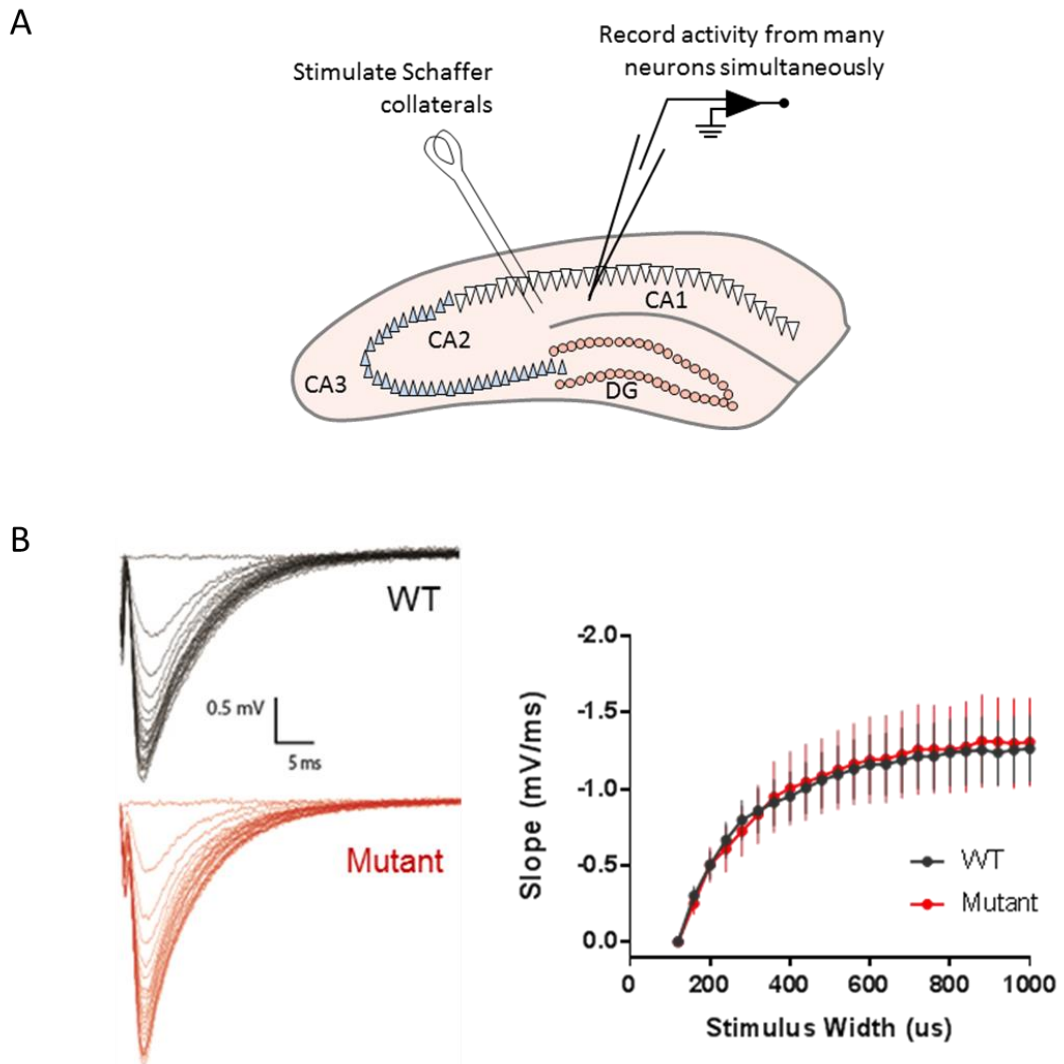
Nissl staining of coronal slices from PFA perfused brains revealed no gross differences in hippocampal structure between WT and KCC2-T906A/T1007A mice.

Figure 3:7: Assessing synaptic protein expression in WT and KCC2-T906A/T1007A mice



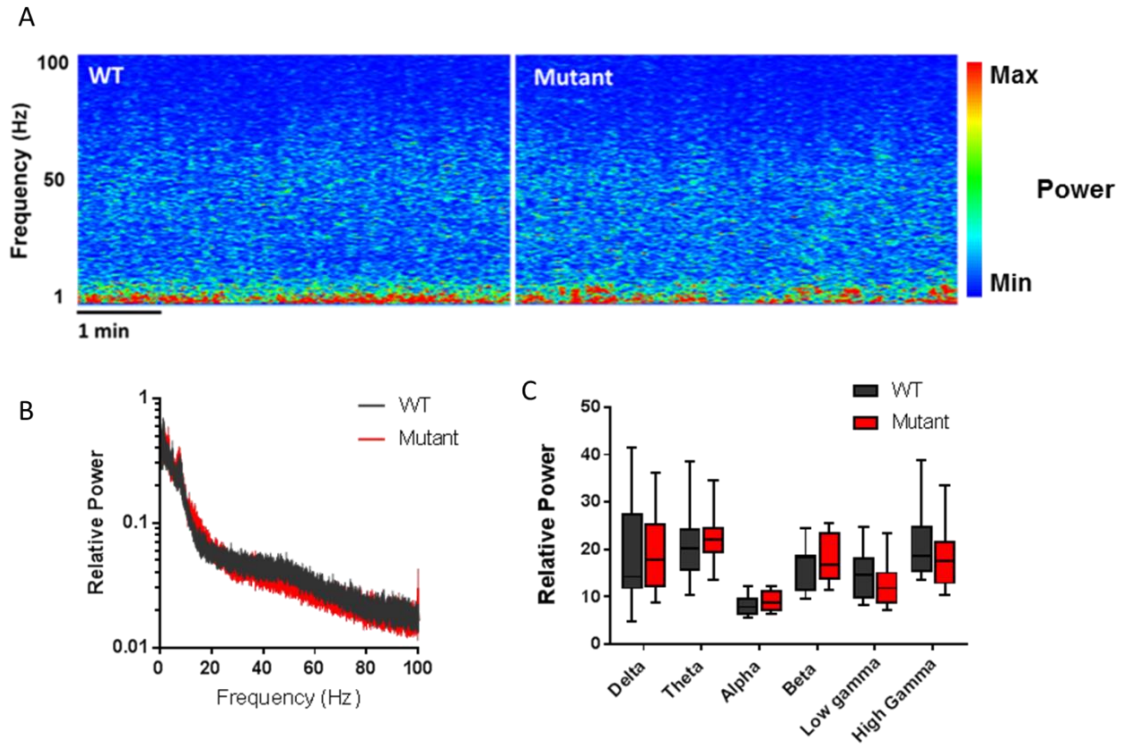
Western blots of several markers of excitatory (PSD-95; GluA1) and inhibitory (Gephyrin; VGAT; GABA_A receptor subunit β3; GABA_A receptor subunit α2) synapses indicating the total expression of PSD-95, Gephyrin, GABA_A receptor subunit β3, and GABA_A receptor subunit α2 were comparable between WT and T906A/T1007A mice, while small reductions in GluA1 and VGAT were detected. Values are expressed as the percentage of WT expression.

Figure 3:8: Excitatory synaptic function is normal in the hippocampus of KCC2-T906A/T1007A mice



A. Cartoon depicting experimental procedure. Field EPSPs were elicited in the stratum radiatum of acute coronal brain slices through stimulation of the Schaffer collaterals. **B.** Schaffer collaterals were stimulated at sequentially increasing durations (widths) from 120 ms to 1000 ms. An example field EPSP trace for WT and KCC2-T906A/T1007A slices is shown. An input/output curve of the field EPSP slope in response to stimulation revealed no differences between WT and KCC2-T906A/T1007A slices.

Figure 3:9: Resting state relative EEG power is comparable between WT and KCC2-T906A/T1007A mice



A. Spectrograms of resting state cortical EEG recordings (5 min) from WT and KCC2-T906A/T1007A awake mice. **B.** Power spectral density plot of the EEG data depicted in A. **C.** Power analysis binned into the delta (1-4Hz), theta (4-9Hz), alpha (9-13Hz), beta (13-30Hz), low gamma (30-50Hz) and high gamma (50-100Hz) frequency bands revealed no differences between WT and KCC2-T906A/T1007A mice. Power analysis is expressed as relative power (see **Methods**).

Discussion

The work presented in this chapter confirms previous *in vitro* studies demonstrating that (de)phosphorylation of KCC2 at sites T906 and T1007 is a powerful regulatory mechanism for modulating KCC2 function, hyperpolarizing E_{GABA} to values far more negative than those in WT neurons when phosphorylation of KCC2-T906/T1007 is prevented through mutation of these sites to alanine. Previous work on these sites employed cell lines transfected with KCC2-T906A/T1007A, as well as ectopic overexpression of KCC2-T906A/T1007A *in utero* (Inoue et al 2012, Rinehart et al 2009, Titz et al 2015, Weber et al 2014), thus the relevance of these phosphorylation sites to neuronal endogenous KCC2 remained undetermined. The work presented in this chapter furthers our understanding of the physiological role of phosphorylation in regulating KCC2 function. However, it is important to note that my findings characterize the impact of preventing phosphorylation of KCC2-T906/T1007 by mutating these sites to alanine, an artificial method of eliminating phosphorylation. Therefore, I cannot distinguish between the roles of phosphorylation in modulating KCC2 function versus the necessity of these threonine residues for interaction with regulatory proteins. However, as previous studies have demonstrated that developmental (Friedel et al 2015, Rinehart et al 2009) and pharmacological (Conway et al 2017, de Los Heros et al 2014, Friedel et al 2015) dephosphorylation of KCC2-T906/T1007 correlates with increased KCC2 activity, and alanine mutations at these sites similarly increase KCC2 function, it is likely that the major factor underlying the enhanced KCC2 function by the KCC2-

T906A/T1007A mutations is the prevention of phospho-inactivation rather than interrupting the binding sites for regulatory proteins.

Interestingly, surface expression of KCC2 was unaffected by the KCC2-T906A/T1007A mutations. This suggests that increased KCC2 function resulting from these mutations may be due to a modification of the kinetic properties of the transporter (**explored in aim 3**). This finding does contrast with a previous report that neurons transfected with KCC2-T906A/T1007A constructs have increased KCC2 surface expression compared to WT (Friedel et al 2015). It is unclear what may underlie this discrepancy with my own results, although the overexpression in their study versus the endogenous levels of protein in my own work may be responsible. This previous study specifically assessed changes in KCC2 surface expression in the soma of individual hippocampal pyramidal neurons using single cell fluorescence imaging. The lack of change in KCC2 surface expression that I detect in total brain slices may reflect a hippocampus specific increase in KCC2 surface expression that would be obscured when assessing protein from total brain slices. Moreover, the overwhelming majority of KCC2 is expressed in spines which would preclude specific changes in the cell soma being detected on western blot.

Not only did preventing KCC2-T906/T1007 phosphorylation increase KCC2 function in mature neurons, there was also a substantial increase in KCC2 function during development, resulting in a prominent acceleration in the developmental hyperpolarization of E_{GABA} , as measured between 4 and 21 days. This confirms previous suggestions that phosphorylation of these sites plays a role

in the maintenance of KCC2 inhibition in early stages of neuronal development (Friedel et al 2015, Rinehart et al 2009).

While an acceleration of the developmental depolarizing-to-hyperpolarizing GABAergic shift is informative about the role that KCC2-T906/T1007 phosphorylation plays in regulating KCC2 function during this time period, I also wanted to determine what impact a loss of depolarizing GABA during development has on brain function. This stemmed from several reports indicating that neuronal maturation and spine formation is abnormal when depolarizing GABA is prematurely abolished during development. Overexpression of KCC2 in rat ventricular progenitors and cortical neurons derived from these progenitors prematurely hyperpolarizes E_{GABA} , and impairs the morphological maturation of these neurons, reducing neuronal length and branch number (Cancedda et al 2007). Knock-down of NKCC1 in newborn neurons also leads to deficits in spine formation and dendritic development (Ge et al 2006). However, both of these studies involved changing the expression of KCC2/NKCC1 which prevents exclusion of these effects being mediated by non-transport function of these proteins rather than accelerated onset of hyperpolarizing GABAergic inhibition. Indeed, recent work indicates a 'moonlighting' transport-independent role for KCC2, with alterations in KCC2 protein expression able to modulate dendritic spine formation and the efficacy of excitatory transmission (Blaesse & Schmidt 2015). As the KCC2-T906A/T1007A mice exhibit normal expression levels of KCC2, these mice presented the opportunity for a more informative assessment of the impact of accelerated developmental E_{GABA} hyperpolarization.

Interestingly, no overt phenotype was detected in these mice, including no changes in brain structure or neuronal function, and no motor or anxiety behavioral abnormalities. The only clear changes I detected within the brain of KCC2-T906A/T1007A mice were small but significant reductions in GluA1 and VGAT expression, suggesting that both excitatory and inhibitory synapses are impacted by increased KCC2 function and/or the presence of the alanine mutations, possibly causing a reduction in synapse number. Examination of synaptic function by measuring the amplitude and frequency of inhibitory and excitatory post-synaptic potentials would provide information about the functional consequence of these changes in GluA1 and VGAT on synaptic activity. However, a lack of change in the ability of Schaffer collateral stimulation to elicit EPSPs in CA1 neurons of KCC2-T906A/T1007A slices does suggest that these small changes in synaptic protein expression may not have any impact on the efficacy of excitatory synaptic function.

Moreover, a lack of overt phenotype in the KCC2-T906A/T1007A mice suggests that depolarizing GABA_A currents present in the immature nervous system may not have as important a physiological role as has previously been proposed, although many more behavioral experiments exploring cognitive function of the KCC2-T906A/T1007A mice would be needed to confirm this.

Further to this, no detectable changes in the distribution of power across the delta, theta, alpha, beta or gamma frequency bands in resting state EEG recordings from KCC2-T906A/T1007A mice suggests that increased KCC2 function does not impact baseline neuronal network function or neuronal synchronization.

This lack of neurophysiological alterations in these mice explains the lack of motor deficits or changes in anxiety-like behavior in these mice, in contrast to other pharmacological agents that enhance GABAergic inhibition such as benzodiazepines (Perucca & Gilliam 2012). This is unsurprising given that increasing KCC2 function is mildly tuning the strength of synaptic inhibition, as opposed to benzodiazepines which cause a large increase in shunting inhibition due to increased GABA_A receptor activation and a resulting reduction in neuronal activity.

It would be revealing to examine anxiety-like behavior in the KCC2-T906A/T1007A mice after stress inducing conditions. Stress is known to decrease KCC2 function in the hypothalamic–pituitary–adrenal axis (HPA) promoting anxiety-like behavior (Hewitt et al 2009, Maguire & Salpekar 2013). KCC2 may remain active in the HPA of KCC2-T906A/T1007A mice under stress-inducing conditions potentially acting to reduce anxiety levels. While the open field test and the elevated plus maze are mildly anxiogenic, it may not be sufficiently anxiety provoking to downregulate KCC2 function, although this has not been examined. More severe stress-inducing paradigms would enable a potential anxiolytic action of enhanced KCC2 function to be addressed.

As discussed, phosphorylation of KCC2-T906/T1007 appears to exert powerful control over KCC2 function, and likely acts as a key physiological mechanism for modulating KCC2 activity. As phosphorylation changes likely occur more rapidly than changes in KCC2 protein expression and trafficking, (de)phosphorylation of these residues may enable rapid modification of the strength of fast synaptic

inhibition. Pharmacological prevention of KCC2-T906/T1007 phosphorylation would enable the time course of this KCC2 activation/inhibition to be assessed.

Chapter 4 : Increasing KCC2 function limits seizure onset and severity

Summary

In this chapter, I examine the impact of KCC2-T906A/T1007A mutations on the severity of chemoconvulsant-induced seizures. I have assessed seizure activity in two *in vitro* seizures models (4-aminopyridine; 0-Mg²⁺) through local field potential recordings in the entorhinal cortex; and in one *in vivo* model (kainate) through EEG recordings. Here, I present evidence that these KCC2-T906A/T1007A mice have a reduced seizure phenotype, detecting both a delay in seizure onset and a reduction in seizure activity.

I also examined the power spectral density of the seizure activity, providing a quantitative metric of the severity of the seizures. A common phenotype I observed across the different seizure models was a reduction in high frequency neuronal synchronization during seizure activity in KCC2-T906A/T1007A

brains/slices compared to WT mice. High frequency activity is associated with more severe seizures, proving further evidence that increased KCC2 function reduces seizure severity. Moreover, KCC2-T906A/T1007A mice exhibited a reduced kainate-induced lethality relative to WT mice. This work suggests that increasing KCC2 function may be a valid therapeutic target for the treatment of seizures in patients with epilepsy.

Introduction

KCC2 dysfunction in epilepsy

Epilepsy is a condition of imbalanced excitation and inhibition in the brain, ultimately leading to the excessive neuronal activation and synchronization that underlies seizures. For this reason, pharmacological agents acting to enhance the efficacy of GABAergic inhibition in the brain are commonly used as therapies to treat seizures; unfortunately, these fail to work for many patients and have too many side effects (Mayer et al 2002, Perucca & Gilliam 2012, Treiman et al 1998). Recent work highlights inadequately maintained neuronal chloride levels as a potential reason for this failure (Deeb et al 2013, Staley 1992). Neuronal Cl^- extrusion mediated by KCC2 is essential for maintaining appropriate levels of inhibition in the brain (Payne 1997, Rivera et al 1999). Without adequate control of $[\text{Cl}^-]_i$ homeostasis a reversal in the polarity of GABA_A currents occurs (E_{GABA} depolarization); in effect, fast synaptic inhibition can become fast synaptic depolarization/excitation (Sivakumaran et al 2015). Adequate levels of KCC2 function are therefore required to ensure appropriate levels of fast synaptic inhibition are maintained in the brain. This positions KCC2 as a critical determinant of the strength of neuronal inhibition, the loss of which has devastating consequences on brain function.

Indeed, the identification of several KCC2 loss-of-function mutations that cause severe infantile-onset epilepsy highlights the critical importance of adequate

KCC2 activity for maintaining normal brain function (Saitou et al 2016, Stodberg et al 2015). Importantly, KCC2 function is also downregulated in patients with idiopathic (Cohen et al 2002, Huberfeld et al 2007, Munoz et al 2007, Palma et al 2006) and acquired (Campbell et al 2015, Karlocai et al 2016) epilepsies, suggesting loss of this critical Cl⁻ extrusion mechanism may play a role in the development and severity of a broad spectrum of epilepsies.

Further support for KCC2 as an essential seizure-limiting protein has come from several animal studies. Deletion of the KCC2 gene (Slc12a5) in mice causes death immediately after birth (Hubner et al 2001), and disruption of only KCC2b, accounting for the majority of KCC2 in the mature brain, causes spontaneous seizure activity and complete mortality in the early postnatal period (Woo et al 2002), coinciding with the timing of the developmental upregulation of KCC2. Interestingly, mice with impaired KCC2 function through phosphomodulation of KCC2 have an enhanced seizure phenotype in the kainate-seizure model, and die shortly after seizure initiation (Silayeva et al 2015). Moreover, pharmacological inhibition of KCC2 enhances seizure severity *in vitro* and *in vivo* (Sivakumaran et al 2015). Collectively, this work suggests that loss of KCC2 may contribute to the enhanced excitability in the epileptic brain.

It has therefore been speculated that increasing KCC2 function could be therapeutically beneficial in the clinical management of seizure disorders. This hypothesis has not yet been addressed due to a lack of pharmacological activators

of KCC2. As I have demonstrated in aim 1, KCC2-T906A/T1007A mutations increase KCC2 function in the brain, thus the KCC2-T906A/T1007A knock-in mouse model has provided me with an opportunity to address this question.

Modelling seizures in mice

The electrographic criteria for valid seizure models are the detection of electrical activity that resembles the electrographic activity seen on the EEGs of patients during seizures. This includes a high frequency “tonic” component, followed by a “clonic” lower frequency high amplitude discharges (Anderson et al 1986) (**see Fig 1.5**). These components are observed in several *in vitro* and *in vivo* seizure models, making them ideal choices for studying seizure activity. Seizures or seizure-like events (SLEs) can be induced in mice or brain slices respectively through the use several chemoconvulsant pharmacological compounds/conditions. The use of 4-aminopyridine (4-AP), a voltage gated potassium channel blocker (Perreault & Avoli 1991), or removal of Mg^{2+} from the ACSF (0- Mg^{2+}) (Anderson et al 1986, Dreier & Heinemann 1991) are widely used *in vitro* models for investigating seizure activity. Both models induce a reproducible pattern of seizure-like activity, containing clear tonic and clonic components that resemble the human condition. These SLEs usually terminate within 1 min, although they can develop into “late recurrent discharges” or “status-like activity” which is continuous seizure-like activity that fails to terminate. I therefore chose to use these models in this study. An advantage of assessing seizure activity in *in vitro* preparations, specifically acute brain slices, is the ability to precisely control

the temperature and composition of extracellular solutions, as well as rapid drug application; this degree of control is not possible *in vivo*.

Despite the useful information that can be gained from *in vitro* seizure models, *in vivo* studies have many advantages. Assessing seizure activity *in vivo* enables the behavioral component of the seizures to be examined, which contains important information about the relevance of the electrographic activity for the actual induction of motor seizures. A combination of *in vitro* and *in vivo* seizure studies is therefore ideal.

As with *in vitro* studies, *in vivo* seizures can be induced with pharmacological chemoconvulsants; these include agents such as kainate (Lothman & Collins 1981) and pilocarpine (Turski et al 1983). I chose to use the kainate model, which induces severe tonic-clonic behavioral and electrographic seizures, and often leads to status epilepticus (SE), a period of prolonged seizure activity that fails to terminate. This period of SE is comparable electrographically to the 'status-like activity' often detected in *in vitro* seizure-models again highlighting the similarity between *in vitro* and *in vivo* seizure models. Kainate is one of the most severe seizure-inducing agents used to assess seizure activity *in vivo* and often results in death, providing a further metric in which to assess seizure severity in mice.

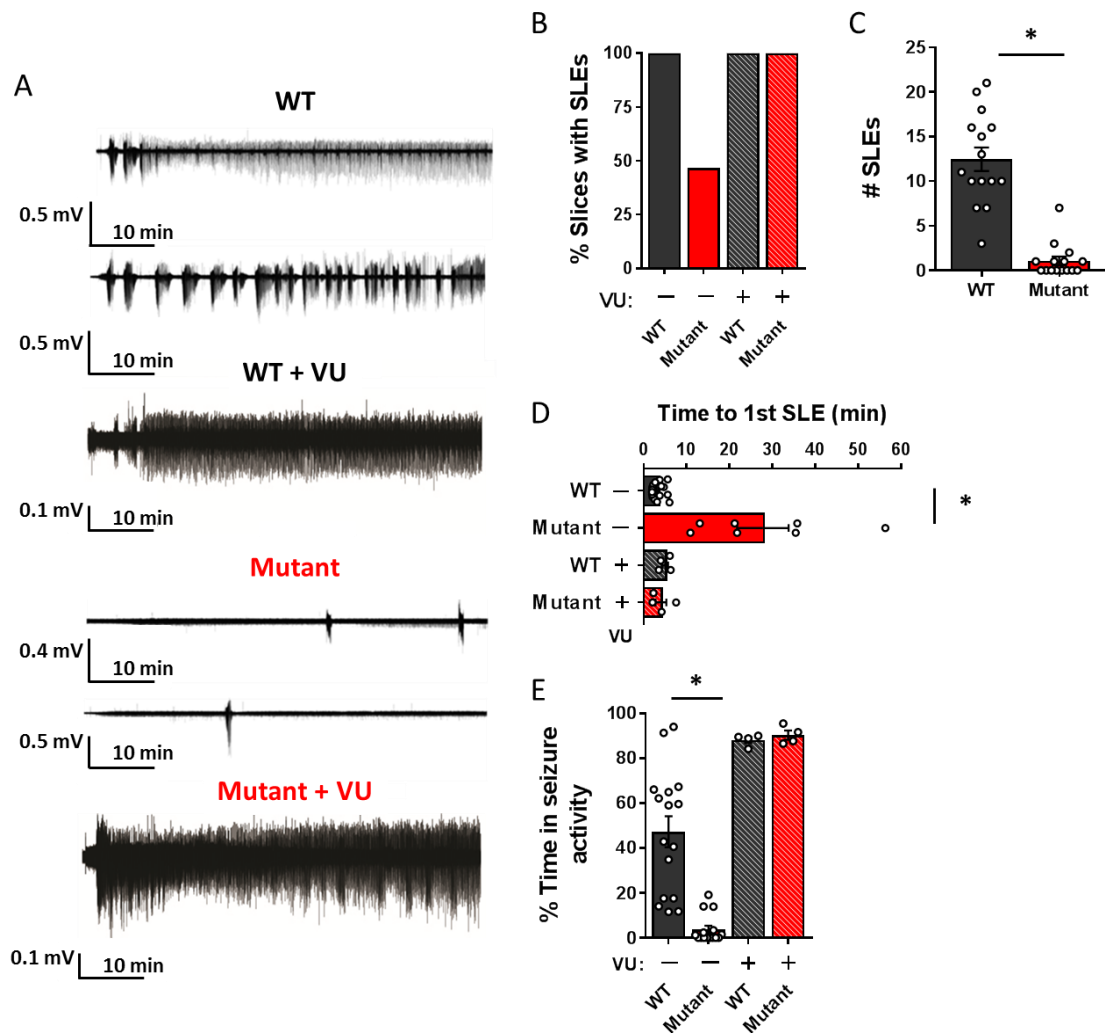
Results

KCC2-T906A/T1007A mice have reduced seizure-like activity *in vitro*

The voltage-gated K⁺ channel blocker 4-aminopyridine (4-AP) is commonly used to induce seizure-like activity in acutely prepared hippocampal slices (Kelley et al 2016). To enhance the severity of the 4-AP model I reduced the extracellular concentrations of Mg²⁺ and Ca²⁺, and increased the [K⁺]_o concentration as has been employed by others (Ziburkus et al 2006) (see Materials and Methods). Slices were exposed to ACSF for 10 min, followed by a 60 min exposure to 4-AP (**Fig. 4.1 A**). Under these conditions, all WT slices (16/16 slices) exhibited seizure-like events (SLEs) compared to only 46.7% (7/15 slices) of KCC2-T906A/T1007A slice (**Fig. 4.1 B**). Of the slices that did exhibit seizure-like activity, onset of the 1st SLE was delayed in the KCC2-T906A/T1007A slices (WT: 3.4 ± 0.4 min, n = 16; T906A/T1007A: 27.8 ± 6 min, n = 7; p < 0.0001) (**Fig. 4.1 D**). Furthermore, the percentage of time spent in epileptiform activity was reduced in KCC2-T906A/T1007A slices (WT: 47 ± 7 %, n = 16; T906A/T1007A: 3.7 ± 1.7 %, n = 15; p < 0.0001) (**Fig. 4.1 E**).

Importantly, as my Schaffer collateral stimulation experiments demonstrated (**see aim 1**), the high percentage of unresponsive KCC2-T906A/T1007A slices was not due to poor health of the tissue. Indeed, application of 4-AP plus the small molecule KCC2 inhibitor VU0463271 (1 μM) induced SLEs in all WT and KCC2-T906A/T1007A slices tested (n = 4 for both genotypes) (**Fig. 4.1 A,B**). VU0463271

Figure 4:1: KCC2-T906A/T1007A mutations were protective against 4-AP-induced epileptiform activity



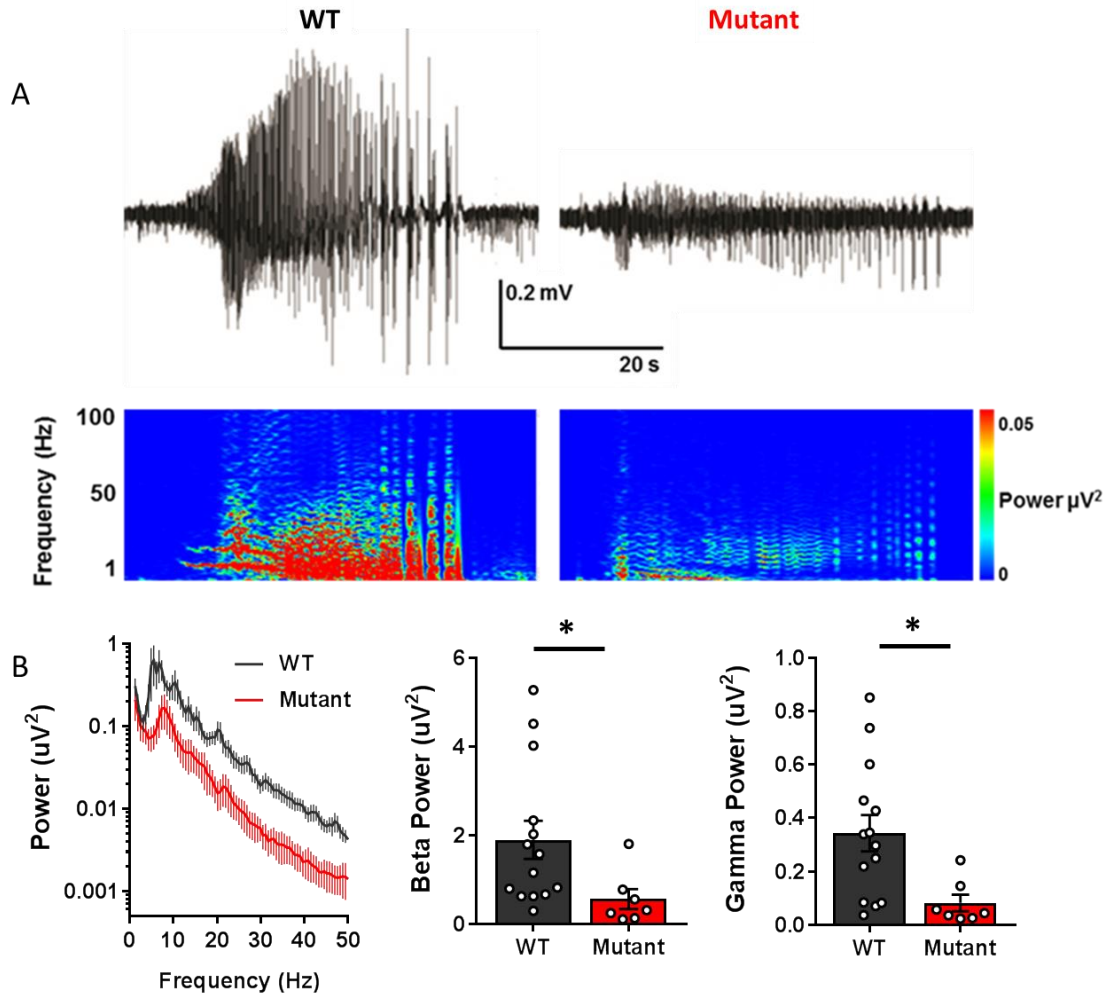
A. Example traces from local field potential recordings from layer III/IV of the entorhinal cortex in horizontal brain slices from WT and KCC2-T906A/T1007A slices exposed to 4-AP. Traces revealed a marked reduction in seizure-like events in recordings from KCC2-T906A/T1007A slices compared to WT slices. Exposure of slices to 4-AP plus the KCC2 inhibitor VU0463271 (VU) induced severe epileptiform activity in both WT and KCC2-T906A/T1007A slices. **B.** KCC2-T906A/T1007A slices showed a reduction in the percentage of slices exhibiting seizure-like events (SLEs). This effect was abolished with the application of VU. **C.** The number of individual SLEs was reduced in the KCC2-T906A/T1007A slices. **D.** The time to the first SLE was delayed in the KCC2-T906A/T1007A slices, but resembled WT onset times in the presence of VU. **E.** The % time spent in seizure activity was reduced in the KCC2-T906A/T1007A slices but was increased to WT time with the application of VU.

accelerated the onset times of SLEs in mutant slices to values statistically similar to WT onset times (WT: 4.0 ± 1.3 min, $n = 4$; T906A/T1007A: 5.0 ± 0.7 min, $n = 4$; $p = 0.5350$) (**Fig. 4.1D**). Similarly, the percentage of time spent in epileptiform activity in mutant slices was increased to WT levels when KCC2 was inhibited (WT: 88 ± 1 %, $n = 4$; T906A/T1007A: 90 ± 2 %, $n = 4$; $p = 0.3936$) (**Fig. 4.1E**).

To further assess seizure-like activity in the WT and KCC2-T906A/T1007A slices in the 4-AP *in vitro* model I wanted to analyze the individual SLEs more closely. I performed power spectral density analysis of the 1st SLE as increased power is a known correlate of enhanced network synchrony that underlies severe seizures (Zayachkivsky et al 2015). The power of 13-30 Hz beta frequency activity (WT: $1.90 \pm 0.43 \mu\text{V}^2$, $n = 14$; T906A/T1007A: $0.56 \pm 0.23 \mu\text{V}^2$, $n = 7$; $p = 0.0485$) and 30-50 Hz gamma frequency activity (WT: $0.34 \pm 0.07 \mu\text{V}^2$, $n = 14$; T906A/T1007A: $0.08 \pm 0.03 \mu\text{V}^2$, $n = 7$; $p = 0.0163$) was significantly lower during KCC2-T906A/T1007A SLEs compared to WT (**Fig. 4.2 A,B**).

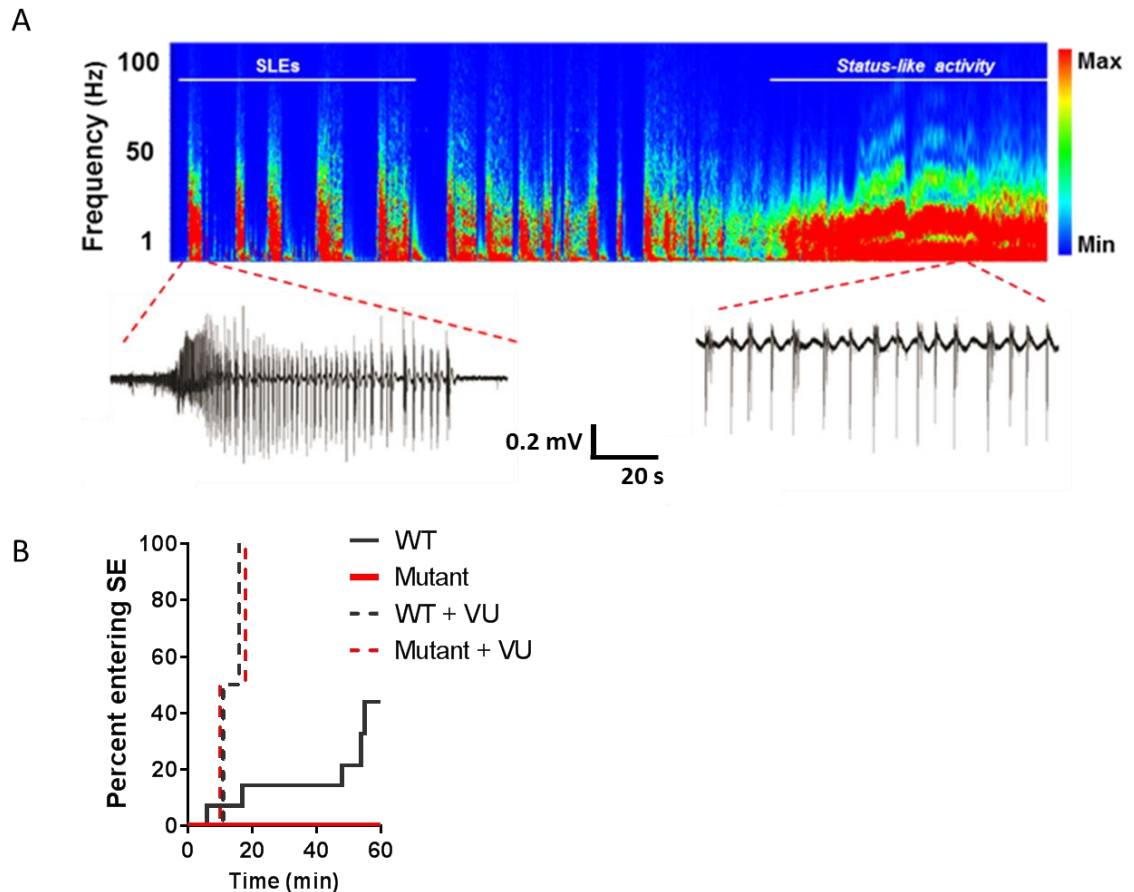
Moreover, no KCC2-T906A/T1007A slices (0/15 slices) degenerated into SE-like activity compared to 43.8% of WT (7/16 slices). 4-AP in the presence of the KCC2 inhibitor VU0463271 led to rapid SE entry in both WT and KCC2-T906A/T1007A slices (**Fig. 4.3**), demonstrating the resistance to SE entry in KCC2-T906A/T1007A slices is due to the enhanced KCC2 function. These data indicated that increasing KCC2 function by preventing phosphorylation of KCC2-T906/T1007 was highly anti-convulsant in this *in vitro* model.

Figure 4:2: KCC2-T906A/T1007A mutations reduced high frequency neuronal synchronization during 4-AP-induced SLEs



A. Local field potential recordings from layer III/IV of the entorhinal cortex of horizontal brain slices from WT and KCC2-T906A/T1007A mice. Traces depict individual SLEs induced by 4-AP exposure as well as the corresponding spectrograms visualizing the power distribution across the frequency range between 1 and 100Hz. The color represents the signal power, with warmer colors representing higher power and cooler colors representing lower power. **B.** Power spectral density plot of the 1st SLE from WT and KCC2-T906A/T1007A slices. The power of 13-30 Hz beta frequency activity and 30-50 Hz gamma frequency activity during the first SLE was lower in KCC2-T906A/T1007A slices compared to WT.

Figure 4:3: KCC2-T906A/T1007A mutations conferred resistance to 4-AP induced status-like activity.



A. Spectrogram of 4-AP-induced seizure-like activity in a WT slice, with traces depicting an individual SLE, and a period of continuous seizure activity considered as an *in vitro* form of status epilepticus (“status-like activity”). **B.** Quantification of the percentage of slices exhibiting status-like activity is displayed, as well as the time of SE onset. No KCC2-T906A/T1007A slices degenerated into SE-like activity, compared to 43.8 % of WT slices. Exposure of slices to 4-AP plus the KCC2 inhibitor VU0463271 induced rapid entry in status-like activity in both WT and KCC2-T906A/T1007A slices.

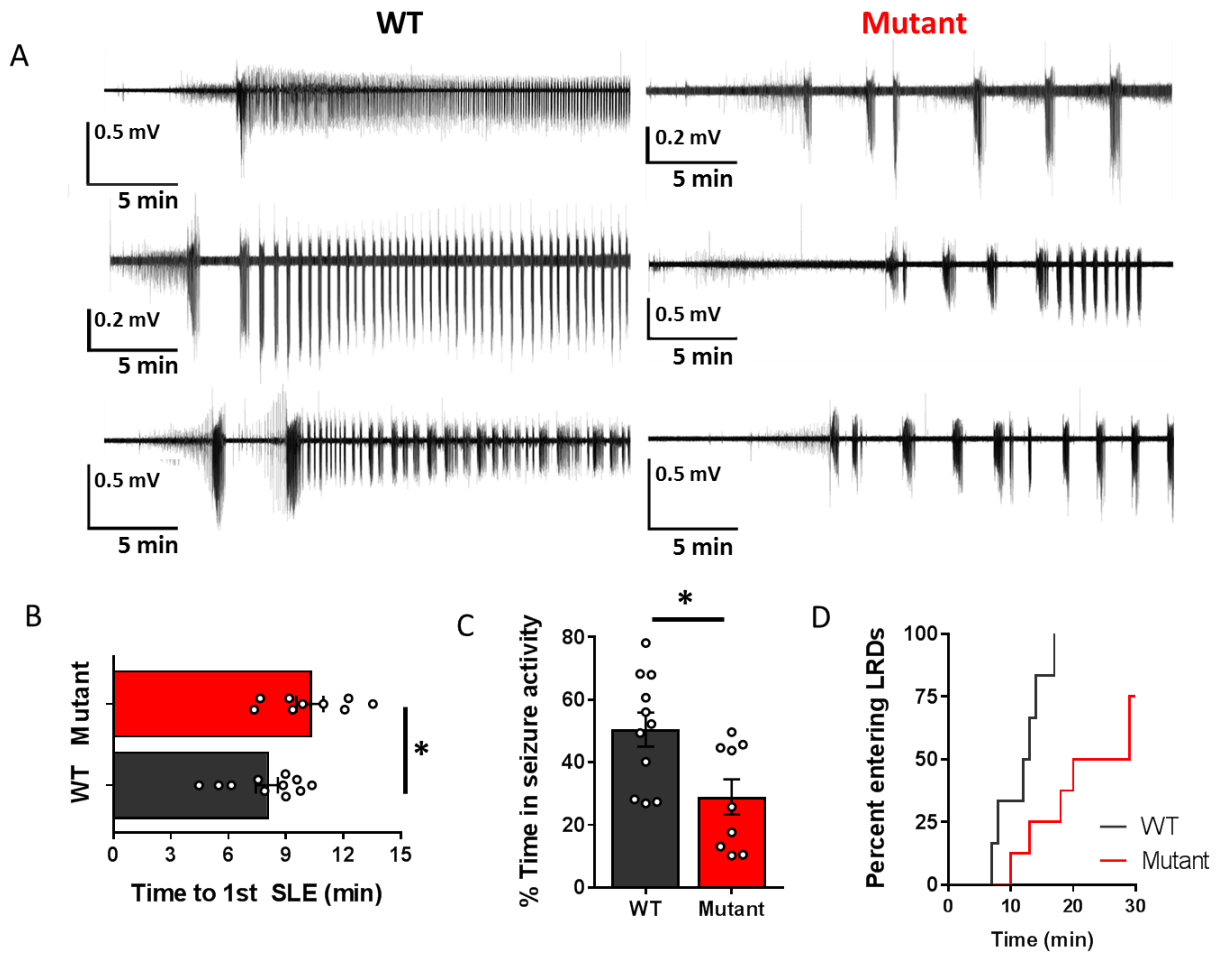
To ensure that the reduction in the seizure-like activity seen in the modified 4-AP model was not specific to seizure activity induced by blockade of voltage gated potassium channels, I assessed seizure activity in a second *in vitro* model, in which all Mg^{2+} is removed from the ACSF (0- Mg^{2+}). All WT and KCC2-T906A/T1007A slices exhibited SLEs (**Fig. 4.4 A**), however the onset to the 1st SLE was delayed in the KCC2-T906A/T1007A slices (WT: 8.007 ± 0.5735 min, n=11; T906A/T1007A: 10.25 ± 0.7067 min, n=9; p=0.0228) (**Fig. 4.4 B**). The KCC2-T906A/T1007A slices also spent less time in seizure activity than WT slices (WT: 50.47 ± 5.408 %, n=11; T906A/T1007A: 28.99 ± 5.591 %, n=9; p=0.0134) (**Fig. 4.4 C**).

Interestingly, seizure activity progressed into late-recurrent discharges in 100% of WT slices, but in only 75% of KCC2-T906A/T1007A slices (**Fig. 4.4D**). Power spectral density plots were created to examine the power of the 1st SLE across a range of frequency bands: delta (1-4 Hz), theta (4-8 Hz), alpha (8-13 Hz), beta (13-30 Hz) and low gamma (30-50 Hz). I detected lower levels of beta (WT: 1.16 ± 0.23 μV^2 , n=11; T906A/T1007A: 0.44 ± 0.09 μV^2 , n=9; p=0.0154) and low gamma (WT: 0.33 ± 0.07 μV^2 , n=11; T906A/T1007A: 0.10 ± 0.03 μV^2 , n=9; p=0.0143) power during the KCC2-T906A/T1007A SLEs compared to WT SLEs (**Fig. 4.5 A, B**).

KCC2-T906A/T1007A mice have reduced seizure-like activity in the *in vivo* kainate model

I then examined seizure activity *in vivo*. I recorded EEG activity from mice injected with the chemoconvulsant kainate, which induces epileptiform activity and

Figure 4:4: Seizure-like activity induced by 0-Mg²⁺ was reduced in the KCC2-T906A/T1007A mice compared to WT mice

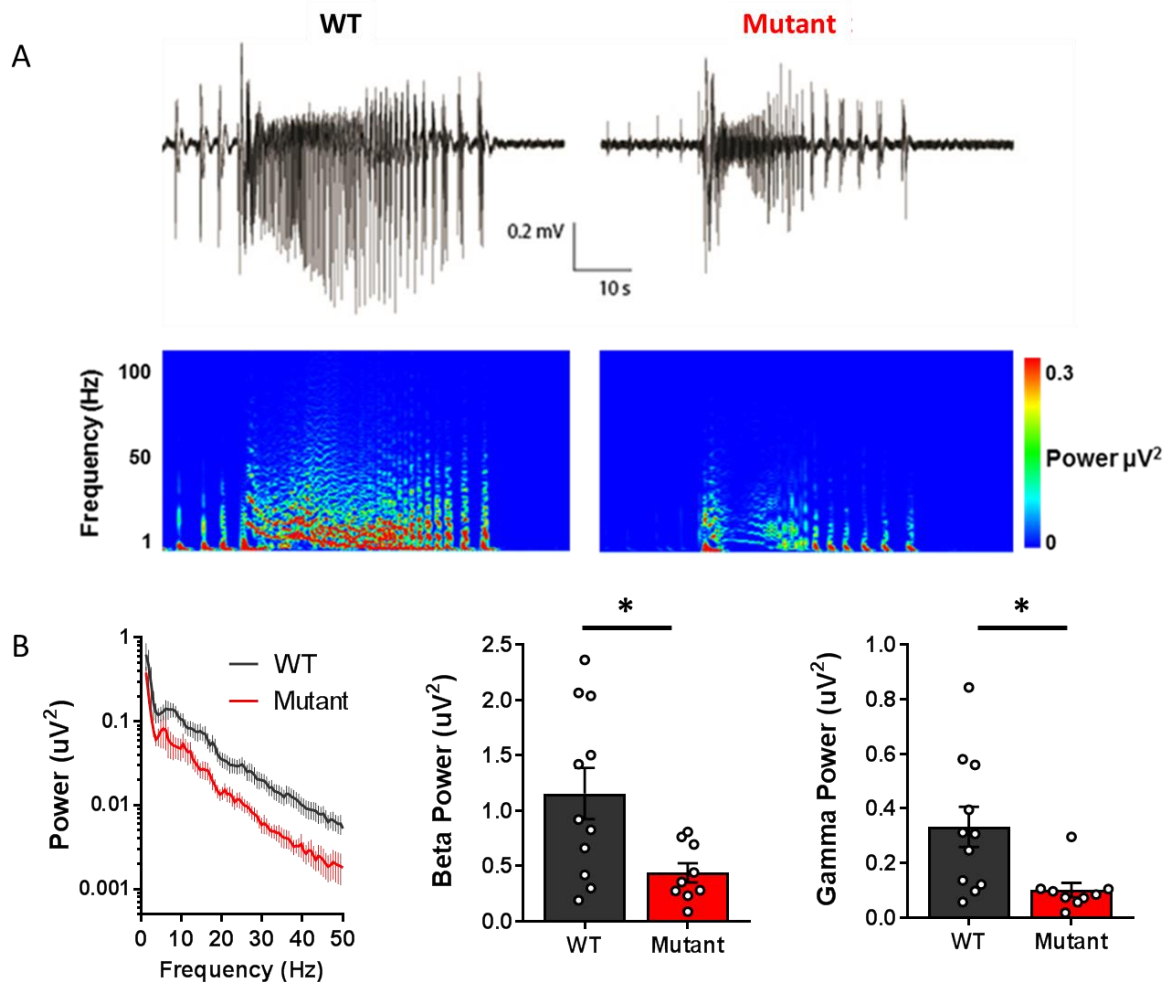


A. Example traces from 30 min local field potential recordings from layer III/IV of the entorhinal cortex of horizontal brain slices from WT and KCC2-T906A/T1007A mice exposed to artificial cerebrospinal fluid with complete removal of Mg²⁺ (0-Mg²⁺) to induce seizure-like activity. **B.** Onset to 1st SLE is delayed in KCC2-T906A/T1007A slices. **C.** The % time spent in seizure activity is reduced in the KCC2-T906A/T1007A slices. **D.** 100% of WT slices entered a state of late recurrent discharges (LRDs) representative of an *in vitro* form of status epilepticus) compared to only 75% of KCC2-T906A/T1007A slices.

discrete tonic seizures (**see Fig. 4.6, 4.7A**) which often degenerate into SE, where seizures fail to self-terminate. Through analysis of the electrographic activity I found that the onset of the 1st tonic seizure was delayed in the KCC2-T906A/T1007A mice compared to WT littermates ($137 \pm 16\%$ of WT littermates, $n = 9$; $p = 0.0376$) (**Fig. 4.7B**). As kainate is such a severe model, many mice died from SE, however the percentage of KCC2-T906A/T1007A mice that died was reduced compared to WT (WT: 42.1%, $n = 19$; T906A/T1007A: 23.5%, $n = 17$) (**Fig. 4.7C**).

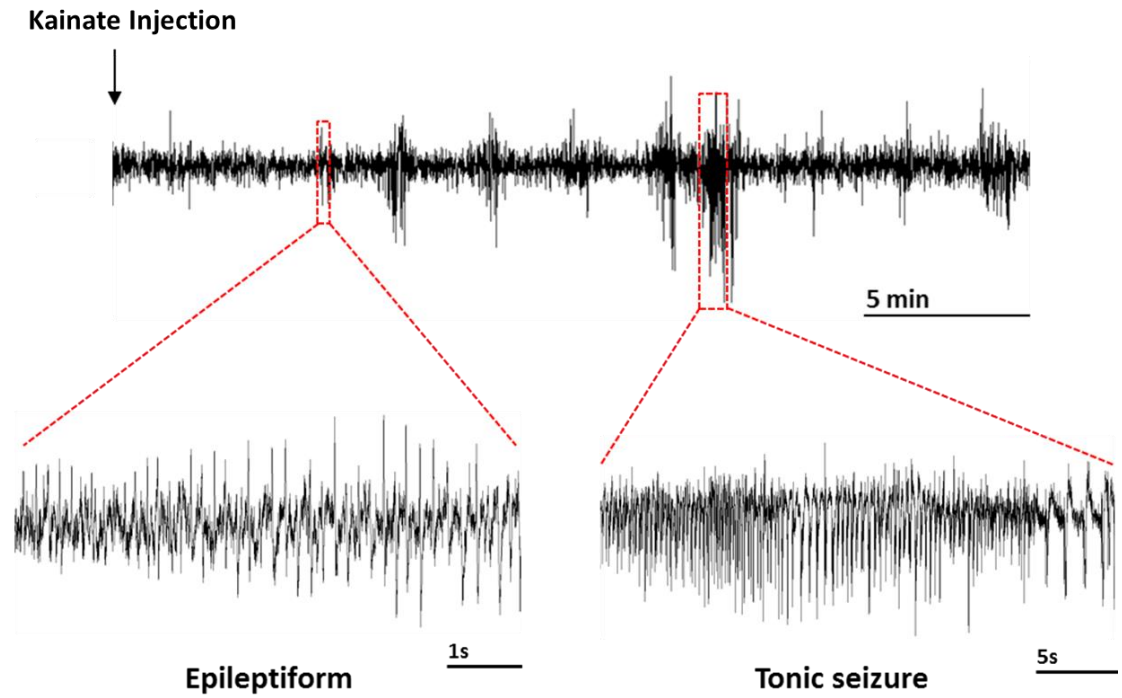
Power spectral density analysis of the first 1 hour after kainate injection revealed that the relative gamma power (50-100 Hz) was lower in the KCC2-T906A/T1007A mice (WT: $11 \pm 2\%$ total power, $n = 10$; T906A/T1007A: $5 \pm 1\%$ total power, $n = 7$; $p = 0.0140$) (**Fig. 4.7D**), further suggesting that there is a reduction in seizure severity in the KCC2-T906A/T1007A mice.

Figure 4:5: KCC2-T906A/T1007A mutations reduced high frequency neuronal synchronization during 0-Mg²⁺-induced SLEs.



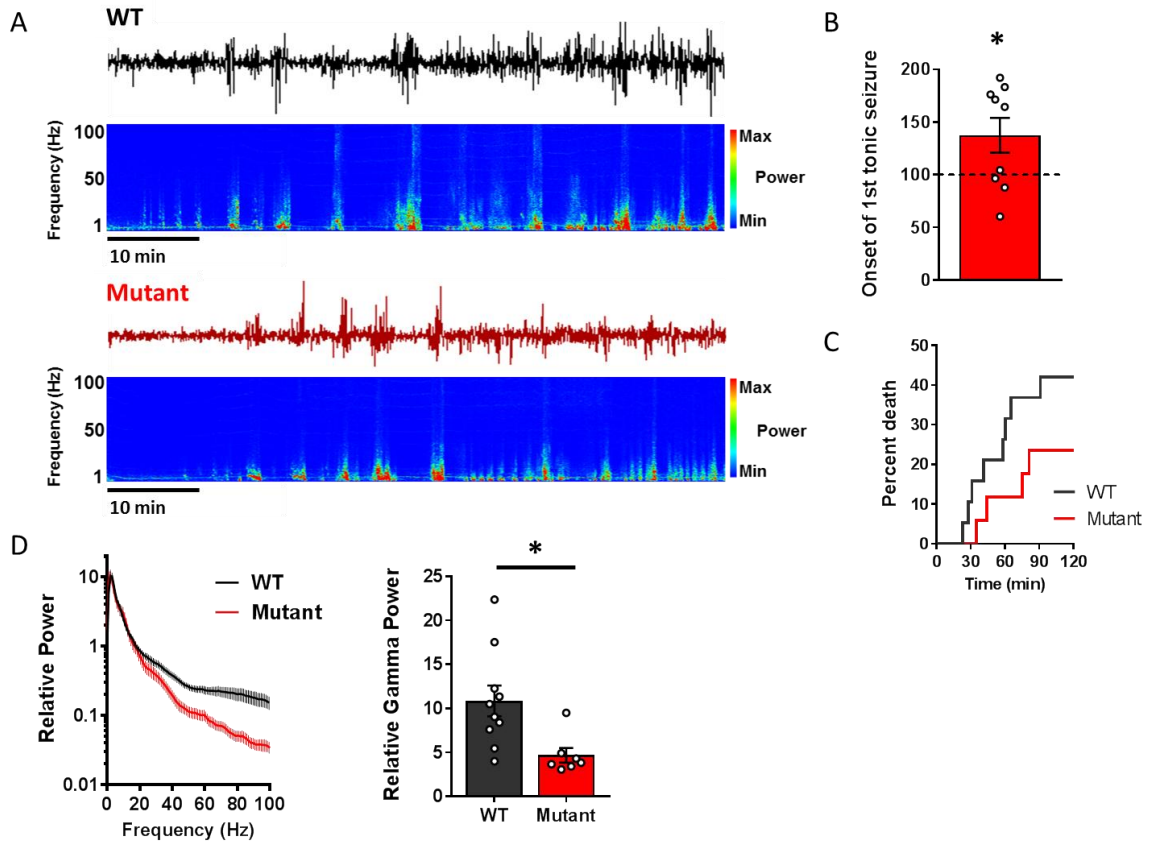
A. Traces depict individual SLEs induced by exposure to artificial cerebrospinal fluid with complete removal of Mg²⁺ (0-Mg²⁺). The corresponding spectrograms visualizing the power distribution across the frequency range between 1 and 100Hz are also displayed, where the color represents the signal power with red indicating the highest power. **B.** Power spectral density plot of the 1st SLE from WT and KCC2-T906A/T1007A slices. The power of 13-30Hz beta frequency activity and 30-50Hz gamma frequency activity during the 1st SLE was lower in KCC2-T906A/T1007A SLEs compared to WT.

Figure 4:6: Kainate induces epileptiform activity and tonic seizures



EEG trace from a WT mouse injected intraperitoneally with kainate. Epileptiform activity is detected as abnormal spiking activity on the EEG, which is not associated with any obvious seizure activity. Tonic seizures are detected on the EEG as high frequency activity which occurs in conjunction with a clear behavioral seizure.

Figure 4:7: The development and severity of kainate-induced seizures was reduced in KCC2-T906A/T1007A mice



A. EEG recordings from WT and KCC2-T906A/T1007A mice injected with kainate. The beginning of the trace represents 30 s after the time of injection. The corresponding spectrograms visualizing the power distribution across the frequency range between 1 and 100 Hz are displayed, with warmer colors representing higher power and cooler colors representing lower power. **B.** The onset to the 1st tonic seizure is delayed in the KCC2-T906A/T1007A mice. Time of onset is expressed as a % of WT littermate control. **C.** Kainate-induced lethality was reduced in KCC2-T906A/T1007A mice. The survival plot displays the % death of WT and KCC2-T906A/T1007A mice at the corresponding time of death after kainate injection. **D.** Power spectral density plot of the 1st hour of EEG activity after kainate injection in WT and KCC2-T906A/T1007A mice. The relative gamma power (50-100 Hz) over this period was lower in the KCC2-T906A/T1007A mice.

Discussion

KCC2 function impacts seizure initiation

This work reveals a role for KCC2 function and thus $[Cl^-]_i$ in several specific aspects of seizure activity. In all seizure models tested, the KCC2-T906A/T1007A mice exhibit delayed onset to first seizure/SLE, highlighting a role for KCC2 and GABAergic activity in seizure initiation (ictogenesis). This is supported by several studies implicating aberrant inhibitory interneuron activity at seizure onset as a key event in the process of seizure initiation. Excessive GABAergic inhibition at seizure onset precedes pyramidal cell firing, initially dampening pyramidal cell activity, demonstrated through patch clamp experiments (Gnatkovsky et al 2008, Lillis et al 2012). This is supported by the detection of high frequency electrographic activity within the beta–gamma range at seizure onset in human epileptic patients, a frequency range thought to result predominantly from inhibitory interneuron activity (Allen et al 1992, de Curtis & Gnatkovsky 2009, Fisher et al 1992). Excessive interneuron activity is thought to contribute to ictogenesis by prolonging GABA_A conductance, which when concurrent with membrane depolarization, can itself degrade synaptic inhibition by enhancing the driving force for Cl^- and increasing Cl^- flux into the cell. KCC2 likely cannot extrude this excess Cl^- at a sufficient rate to maintain hyperpolarizing fast synaptic inhibition, which effectively renders GABA_A synaptic currents excitatory (Deeb et al 2013, Thompson & Gahwiler 1989).

Further work has supported a role for Cl^- loading in pyramidal cells in ictogenesis. Artificially loading pyramidal neurons with Cl^- raises network excitability and triggers full ictal activity in the presence of sub-ictal 4-AP concentrations, highlighting Cl^- dysregulation as a major factor in triggering seizures (Alfonsa et al 2015). Chloride gradients are likely particularly labile in epilepsy patients that have reduced KCC2 function, thus the normal $[\text{Cl}^-]_i$ perturbations that occur in healthy individuals due to fluctuations in GABA_A conductance may be ictogenic in epileptic patients.

My work furthers our understanding of Cl^- dysregulation in seizure initiation; enhancing KCC2-mediated Cl^- extrusion is sufficient to reduce seizure initiation, likely by limiting activity-dependent Cl^- loading (**explored in aim 3**). This work counters a contrasting hypothesis proposed by several groups relating to a pro-convulsant role for KCC2; it is hypothesized that rises in extracellular K^+ during seizures would result in a reflexive rise in intracellular Cl^- mediated by a reversal in the direction of K^+/Cl^- flux through KCC2 (DeFazio et al 2000, Gonzalez et al 2018, Hamidi & Avoli 2015, Jarolimek et al 1999, Payne 1997, Staley & Proctor 1999, Viitanen et al 2010). This would raise intracellular Cl^- levels, collapse the Cl^- gradient and abolish fast synaptic inhibition (Kaila et al 2014). A role for KCC2 as either pro-convulsant or anti-convulsant therefore remains controversial. However, my work disagrees with this argument, and suggests that KCC2 function is indeed anti-convulsant.

A role for KCC2 in seizure termination

I also detected a lower incidence of SE development in KCC2-T906A/T1007A mice. Slices from KCC2-T906A/T1007A mice did not develop SE-like activity in the 4-AP model, and were more resistant to SE entry in the 0-Mg²⁺ model. This supports a role for Cl⁻ loading in the degeneration of seizure activity into uncontrolled seizures that fail to terminate and suggests that removal of intracellular Cl⁻ facilitates seizure termination. This compliments previous work demonstrating that reduced KCC2 function, either through pharmacological inhibition of KCC2 (Kelley et al 2016, Sivakumaran et al 2015) or by the KCC2 S940A mutation that reduces KCC2 function (Silayeva et al 2015), interferes with the termination of SLEs, leading to *in vitro* SE. My observation that pharmacological inhibition of KCC2 in both WT and KCC2-T906A/T1007A slices in the 4-AP model leads to rapid entry into SE supports this conclusion.

Despite a reduction in SE in the *in vitro* seizure models, all WT and KCC2-T906A/T1007A mice exhibited SE after kainate injection. This may be due to the severe nature of the kainate seizure model, with increased KCC2-mediated Cl⁻ extrusion potentially representing an insufficient mechanism to prevent SE. Furthermore, KCC2 surface expression is rapidly degraded after kainate injection (Silayeva et al 2015). This may explain why KCC2-T906A/T1007A mice are not resistant to developing SE in this model; removal of KCC2 from the cell surface would limit any benefit that the KCC2-T906A/T1007A mutations have on enhancing KCC2 function. However, experiments analyzing the surface expression of KCC2 in KCC2-T906A/T1007A mice after kainate would be needed to compare

the extent of this degradation between WT and KCC2-T906A/T1007A mice. Kainate-mediated reductions in KCC2 surface expression may explain the modest effect that the KCC2-T906A/T1007A mutations had on seizures in the kainate model. The greatest impact of the KCC2-T906A/T1007A mutations on reducing seizure activity was detected in the 4-AP model where KCC2 is clearly still present at the cell surface as demonstrated by rapid SE entry after application of the pharmacological inhibitor of KCC2. This suggests that increasing KCC2 function through dephosphorylation of KCC2-T906/T1007 will be most efficacious when sufficient levels of KCC2 protein are still present.

Increasing KCC2 function limits high frequency neuronal synchronization during seizures

The seizure activity was qualitatively less severe in the KCC2-T906A/T1007A mice. I detected lower raw power within the beta and low gamma frequency ranges during the 1st SLE in the 4-AP and 0-Mg²⁺ model in the KCC2-T906A/T1007A slices compared to WT. High frequency neuronal synchronization is associated with enhanced severity of seizures in human patients (Allen et al 1992, de Curtis & Gnatkovsky 2009, Fisher et al 1992), thus reductions in beta and gamma power suggest a reduction in seizure severity. In the kainate model, gamma power was also lower in the KCC2-T906A/T10076A mice relative to WT mice during seizures, even though the KCC2-T906A/T1007A mice entered SE. These data suggest that Cl⁻ loading facilitates synchronization of neurons at high frequency ranges, and

that increasing KCC2 function acts to resist this synchronization. Indeed, E_{GABA} depolarization is thought to contribute to high frequency oscillations in epileptic circuits (Alfonso et al 2015); reduced power of higher frequency activity during seizures in the KCC2-T906A/T1007A mice may therefore reflect a reduced susceptibility to E_{GABA} depolarization in these mutant neurons (**explored further in aim 3**). Importantly, the KCC2-T906A/T1007A mice are less susceptible to death from the severe behavioral seizures and SE that result from kainate injection, further indicating the reduced severity of the seizures/SE in these mutant mice. This observation nicely compliments previous work demonstrating that mice with reduced KCC2 function due to phosphomodulation of site serine 940 on KCC2 have more severe seizures after kainate injection and die rapidly from SE (Silayeva et al 2015). A prominent increase in the power of high frequency oscillations is detected immediately before death in both WT and KCC2-T906A/T1007A mice, which is readily apparent on the EEG spectrograms, thus the lower gamma power detected during seizure activity in the KCC2-T906A/T1007A mice compared to WT mice may be a contributory mechanism underlying the reduced seizure-induced lethality; indeed gamma power is indicative of enhanced severity of seizure activity (Tse et al 2014). Interestingly, decreased power in high frequency ranges is seen with anti-seizure drugs (Arzy et al 2010), further supporting reductions in gamma power as a measure of reduced seizure severity.

Collectively, this work identifies KCC2 as a seizure-limiting protein and highlights the potential of targeting this protein as a novel therapeutic strategy for treating seizures. Fortunately, some KCC2 protein is retained in patients with chronic

epilepsy, indicating an untapped potential for targeting KCC2 phosphorylation to restore KCC2 function to that of healthy individuals. The powerful chemoconvulsants used in this study rapidly remove KCC2 from the cell membrane (Silayeva et al 2015), thus it is possible that increasing KCC2 function in patients who retain sufficient levels of KCC2 protein will be even more efficacious in reducing seizures than the results described here. In summary, this work highlights KCC2 as a potential therapeutic target for the treatment of seizures and supports the search of pharmacological activators of KCC2.

Chapter 5 : Mechanisms underlying enhanced KCC2 function and reduced seizure activity in KCC2-T906A/T1007A mice

Summary

KCC2-T906A/T1007A mutations increase KCC2 function through a mechanism independent of its protein expression (**see aim 1**), suggesting that these mutations impact the kinetic properties of the transporter allowing for enhanced rate of Cl^- transport; here I present evidence supporting this hypothesis. I demonstrate that these mutations enhance the rate of Cl^- extrusion when neurons are loaded with high concentrations of Cl^- . I have determined that this increased rate of Cl^- extrusion limits activity-dependent E_{GABA} depolarization under pathological hyperexcitable conditions, providing insight into the potential mechanism through which the KCC2-T906A/T1007A mutations reduced seizure

activity in chemoconvulsant seizure models (**aim 2**). This supports a role for enhanced $[Cl^-]_i$ in the underlying pathophysiology of seizures.

Moreover, given a known impact of chemoconvulsants on KCC2-S940 phosphorylation, I investigated the impact of kainate on KCC2-T1007 phosphorylation and detected an increase in phosphorylation 1 hour after kainate administration. This suggests that preventing phosphoinhibition of KCC2 may be a further mechanism underlying the reduced seizure phenotype conferred by the KCC2-T906A/T1007A mutations.

Introduction

Impact of KCC2-T906A/T1007A mutations on the kinetic properties of KCC2

The mechanism through which phosphomodulation of KCC2 at sites T906 and T1007 mediates changes in KCC2 function is unknown. The KCC2-T906A/T1007A mutations do not impact the surface expression of KCC2 (**see aim 1**), indicating the enhanced Cl^- extrusion cannot simply be explained by more KCC2 protein on the cell surface. These mutations are therefore likely to be altering the Cl^- transport capacity of KCC2 through direct alteration of its kinetic properties. To investigate this, a whole cell patch clamp assay can be used to load neurons with high levels of Cl^- , which enables comparative rates of Cl^- extrusion to be measured. The ability of neurons to extrude this high $[\text{Cl}^-]_i$ results from the relatively slow diffusion of Cl^- from the patch pipette down through the dendrites. This enables KCC2 within the dendrites to “keep up” with the imposing Cl^- load to an extent proportional to the levels of functional KCC2 present in the dendrites (Jarolimek et al 1999, Khirug et al 2005). Levels of KCC2 function can be assessed by measuring E_{GABA} under these conditions, with more negative values representing increased rates of Cl^- extrusion. Use of this assay has enabled me to assess the impact of KCC2-T906A/T1007A mutations on the rate of Cl^- transport, and subsequently gain information about the mechanisms through which the KCC2-T906A/T1007A mutations increase KCC2 function.

Activity-dependent Cl⁻ loading occurs under hyperexcitable conditions

Despite current experimental limitations in understanding the role of KCC2 dysfunction in seizure induction, many studies have demonstrated a clear increase in intracellular Cl⁻ levels and an erosion of synaptic inhibition during seizures. It is possible that enhanced KCC2 function would increase the rate of Cl⁻ extrusion, potentially limiting Cl⁻ loading under hyperexcitable conditions. In support of this, mutation of T906/T1007 on KCC2 to alanine to prevent their phosphorylation is sufficient to maintain hyperpolarizing GABA responses when neurons are exposed to high K⁺ conditions which would normally depolarize E_{GABA} (Titz et al 2015). This suggests that enhanced KCC2 function would indeed limit excitation-induced E_{GABA} depolarization.

This activity-dependent Cl⁻ loading can be simulated *in vitro* using a series of short duration glutamate applications which depolarize E_{GABA} (Deeb et al 2013). Glutamate is particularly relevant to seizure disorders as the extracellular level of glutamate is known to increase within the human brain during a seizure (During & Spencer 1993). In this chapter, I use this glutamate challenge assay to explore the impact of KCC2-T906A/T1007A mutations on the susceptibility of neurons to undergo activity-dependent degradation of synaptic inhibition, providing insight into the potential mechanism underlying the reduction in seizure activity detected in the KCC2-T906A/T1007A mice (**aim 2**).

A pathological relevance of KCC2 phosphorylation for seizures

Phosphomodulation of KCC2 occurs as a result of seizures. Excessive glutamate dephosphorylates S940 on KCC2 which decreases its surface expression, reducing the neuronal chloride extrusion capacity, causing E_{GABA} depolarization (Lee et al 2011). Glutamate levels increase within the brain during a seizure (During & Spencer 1993), which may dephosphorylate KCC2-S940. In support of this, kainate-induced seizures dephosphorylate KCC2-S940 and reduce KCC2 surface expression in mice (Silayeva et al 2015). A glutamate-mediated reduction in KCC2-S940 phosphorylation may therefore contribute to the decrease in KCC2 surface expression detected in epileptic patients. No information is available on the pathological relevance of KCC2-T906/T1007 phosphorylation for seizure disorders. A seizure-induced increase in KCC2-T906/T1007 phosphorylation would be consistent with a phosphorylation-dependent decrease of KCC2 function and could be a further mechanism responsible reduced seizure activity in the KCC2-T906A/T1007A mice due to the inability of these mice to undergo KCC2-T906/T1007 mediated phospho-inactivation. Generation (by Prof. Stephen Moss) of an antibody specific to phosphorylated KCC2-T1007 (characterized by (Conway et al 2017)) has enabled me to address the impact of seizures on the phosphorylation of this site (lack of a KCC2-T906 phospho-antibody precluded assessment of this site), and subsequently provide insight into the pathological relevance of KCC2-T1007 phosphorylation for loss of KCC2 function in seizure-disorders.

Results

KCC2-T906A/T1007A mutations enhance rate of Cl⁻ transport

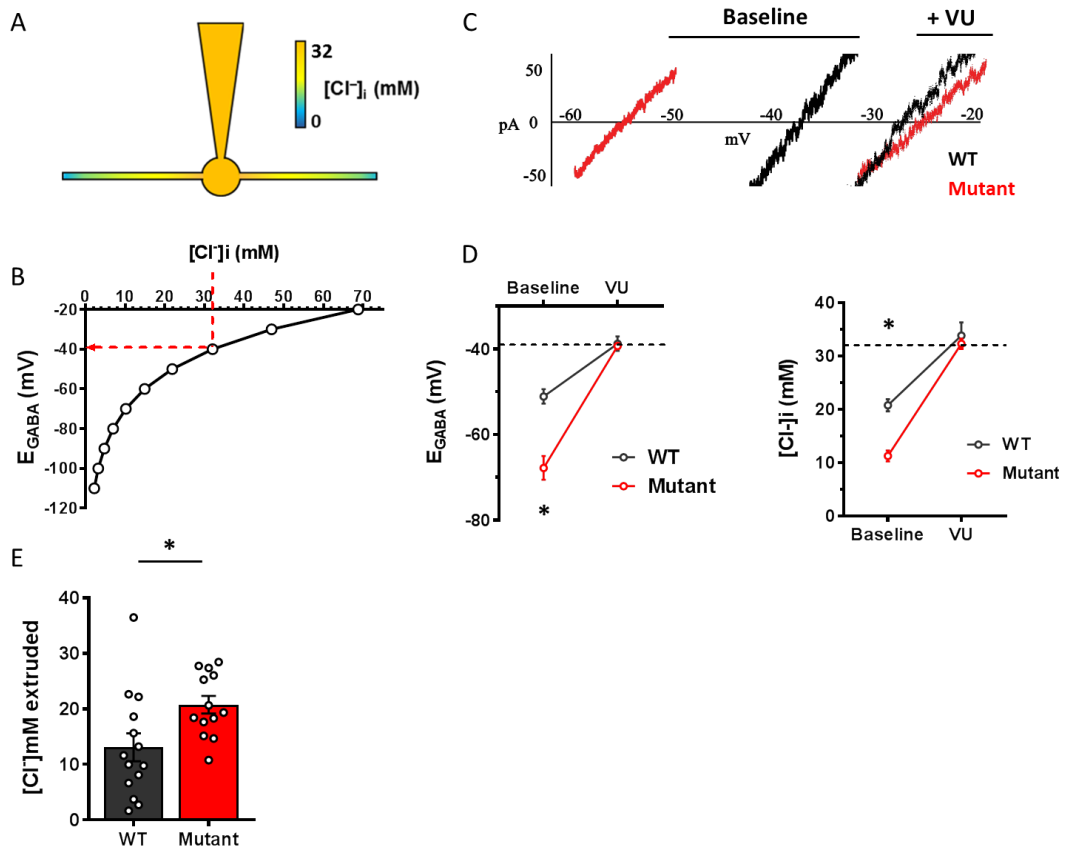
To directly compare the rate of Cl⁻ extrusion between WT and KCC2-T906A/T1007A neurons, I employed a whole-cell patch clamp Cl⁻ loading assay. By imposing a fixed concentration of Cl⁻ (32 mM) into the cell through the patch pipette (**Fig. 5.1A**), the subsequent measurement of E_{GABA} reported the degree to which these neurons were able to extrude these imposed Cl⁻ loads. Without KCC2 activity, the Nernst equation dictates that neurons should have an E_{GABA} value of -39 mV when loaded with 32 mM [Cl⁻]_i (**Fig. 5.1B**). Both WT and KCC2-T906A/T1007A neurons displayed resting E_{GABA} values that were more negative than this predicted value, indicating the presence of functional KCC2. The E_{GABA} values were more negative in KCC2-T906A/T1007A neurons compared to WT (WT: -51.1 ± 1.7 mV, n = 14; T906A/T1007A: -67.8 ± 2.8 mV, n = 14; p < 0.0001), which were equivalent to 20.8 ± 1.1 mM for WT neurons and 11.3 ± 1.0 mM for KCC2-T906A/T1007A neurons (p < 0.0001), indicating that the rate of Cl⁻ extrusion was increased by the KCC2-T906A/T1007A mutations (**Fig. 5.1 C, D**). I then exposed cells to the specific KCC2 inhibitor VU0463271 to confirm that these deviations from the predicted Nernst potentials and imposed Cl⁻ loads from the pipette were specifically due to KCC2 function. The E_{GABA} values shifted to equivalent values between WT and KCC2-T906A/T1007A neurons in the presence of VU0463271 (WT: -38.8 ± 1.7 mV, n = 14; T906A/T1007A: -39.3 ± 0.7 mV, n = 13; p = 0.7669) (**Fig. 5.1 C, D**). Conversion of these values to [Cl⁻]_i revealed the

validity of this assay: the Cl^- values of WT (33.8 ± 2.5 mM) and KCC2-T906A/T1007A (32.3 ± 1.0 mM) neurons were statistically similar to each other ($p = 0.5741$) and neither deviated from the pipette-imposed Cl^- load of 32 mM (WT $p = 0.47$; T906A/T1007A $p = 0.78$) (**Fig. 5.1 C, D**). Moreover, the Cl^- shift induced by exposure to VU0463271 indicated that the concentration of Cl^- that was extruded under baseline conditions was greater in the KCC2-T906A/T1007A neurons than in WT neurons (WT: 13.1 ± 2.5 mM, $n=14$; T906A/T1007A: 20.8 ± 1.6 mM, $n = 13$; $p = 0.018$, paired T-test) (**Fig. 5.1 E**).

KCC2-T906A/T1007A mutations confer resistance to E_{GABA} depolarization under hyperexcitable conditions

Seizure activity causes rapid accumulation of $[\text{Cl}^-]_i$ thus I wanted to simulate neuronal hyperexcitability and assess the impact of these conditions on GABA_A currents. WT and KCC2-T906A/T1007A hippocampal neurons were exposed to three consecutive pulses of glutamate (10s per pulse, 20 μM), which induces membrane depolarization and increases neuronal firing (Deeb et al 2013, Silayeva et al 2015). IPSPs occurring in conjunction with membrane depolarization drive Cl^- into the cell, leading to a rapid loss of hyperpolarizing GABA_A signaling (**Fig. 5.2A**). Baseline E_{GABA} measurements again revealed increased KCC2 activity in the KCC2-T906A/T1007A neurons (WT: -86 ± 3 mV, $n = 15$; T906A/T1007A: -112 ± 1 mV, $n = 14$; $p < 0.0001$), which were equivalent to $[\text{Cl}^-]_i$ values of 6.7 ± 0.8 mM for

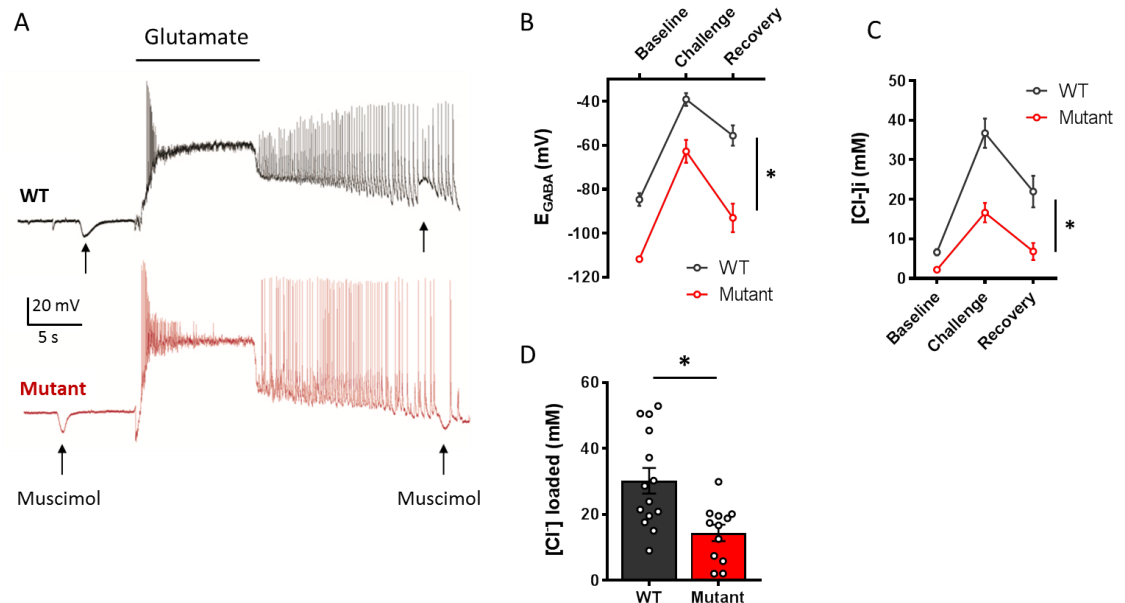
Figure 5:1: KCC2-T906A/T1007A mutations enhance the rate of KCC2-mediated Cl^- extrusion



A. Cartoon of whole cell patch clamp Cl^- loading assay that creates a somatic-dendritic Cl^- gradient. **B.** Predicted $[\text{Cl}^-]_i$ at a range of E_{GABA} values calculated using the Nernst equation. **C.** I-V plot of leak-subtracted muscimol currents depicting the E_{GABA} values, both before and after exposure to the KCC2 inhibitor VU0463271 (VU) (I-V plots depict results before correction for liquid junction potentials – see methods). **D.** E_{GABA} values were more negative in KCC2-T906A/T1007A neurons compared to WT indicating that the rate of Cl^- extrusion is increased by the KCC2-T906A/T1007A mutations. The E_{GABA} values were shifted to the expected value of approximately -39 mV (dashed line) when VU was applied. The corresponding $[\text{Cl}^-]_i$ values are also shown, with the 32mM $[\text{Cl}^-]_i$ indicated by the dashed line. **E.** The concentration of Cl^- that was extruded under baseline conditions was greater in the KCC2-T906A/T1007A neurons, calculated as the difference between $[\text{Cl}^-]_i$ under baseline and VU conditions.

WT and 2.2 ± 0.1 mM for the KCC2-T906A/T1007A neurons ($p < 0.0001$). Immediately after the glutamate exposure, E_{GABA} values shifted to -39 ± 2.9 mV ($n = 14$) for WT neurons and -63 ± 5.2 mV for KCC2-T906A/T1007A neurons ($n = 12$), ($p = 0.0004$). These E_{GABA} values were calculated as 37 ± 3.7 mM for WT neurons and 17 ± 2.5 mM for KCC2-T906A/T1007A neurons, indicating that glutamate induced a significantly smaller Cl^- load in the mutants ($p = 0.0002$). I then assessed the ability of these neurons to extrude this glutamate-mediated Cl^- load in the presence of TTX in order to minimize activity-dependent Cl^- shifts (Thompson & Gahwiler 1989). Over a three-minute period, WT neurons returned E_{GABA} values to -56 ± 4.6 mV ($n = 13$), equivalent to Cl^- values of 22 ± 4.0 mM, which were both significantly greater than the basal WT values (E_{GABA} $p < 0.0001$, paired T-test; Cl^- $p = 0.0004$, paired T-test). The KCC2-T906A/T1007A neurons returned E_{GABA} values to -93 ± 6.5 mV ($n = 13$), and Cl^- values to 6.8 ± 2.1 mM, both of which were significantly lower than the WT values (E_{GABA} $p < 0.0001$; Cl^- $p = 0.0032$), but still greater than basal KCC2-T906A/T1007A values (E_{GABA} $p = 0.007$, paired T-test; Cl^- $p = 0.03$, paired T-test) (**Fig. 5.2 B,C**). Importantly, the glutamate-induced Cl^- shift was reduced in KCC2-T906A/T1007A neurons compared to WT (WT: 30 ± 3.9 mM, $n = 14$; 14 ± 2.5 mM, $n = 12$; $p = 0.003$, paired T-test), demonstrating the KCC2-T906A/T1007A neurons were more resistant to Cl^- loading under hyperexcitable conditions than WT neurons (**Fig. 5.2D**).

Figure 5:2: KCC2-T906A/T1007A mutations limited E_{GABA} depolarization under hyperexcitable conditions



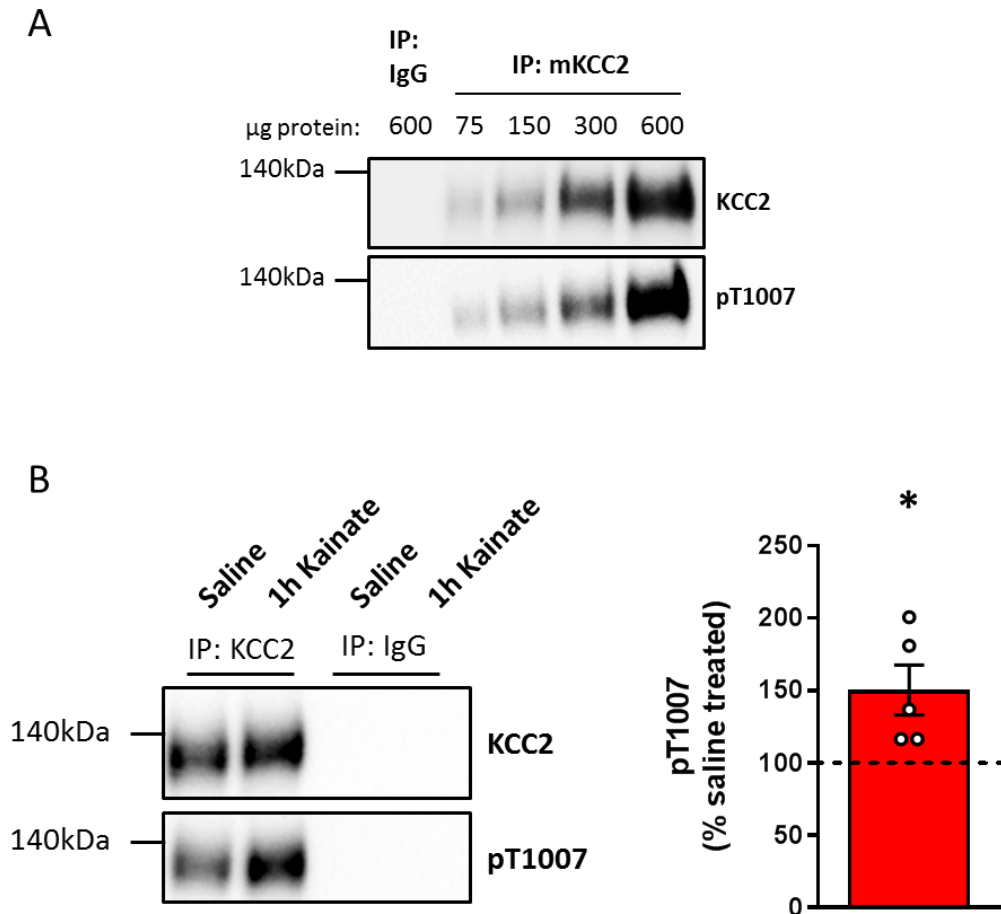
A. Example traces of the glutamate challenge performed on WT and KCC2-T906A/T1007A hippocampal neurons. Application of muscimol (arrows) to activate $GABA_A$ receptors was applied before and after glutamate exposure. A reversal in the polarity of $GABA_A$ currents in a WT neuron, and maintenance of hyperpolarizing current in a KCC2-T906A/T1007A neuron is evident. **B.** E_{GABA} measurements were taken before glutamate exposure, immediately after glutamate exposure, and after a 3 min recovery period in which TTX was used to block neuronal activity. E_{GABA} was more negative in KCC2-T906A/T1007A neurons at all 3 of these time points. The corresponding $[Cl^-]_i$ are shown in **C**. **D.** The concentration of Cl^- loaded into the neurons during the glutamate challenge is reduced in KCC2-T906A/T1007A neurons compared to WT.

Kainate-induced seizures increase KCC2-T1007 phosphorylation

No information is available on the pathological relevance of KCC2-T906/T1007 phosphorylation to seizure disorders; generation (by Prof. Stephen Moss) of an antibody specific to phosphorylated T1007 within KCC2 (characterized by (Conway et al 2017)) has enabled me to address this. To determine the ideal protein concentrations needed to visualize immunoprecipitated KCC2 and KCC2-T1007 phosphorylation, I performed immunoprecipitation and western blotting of various protein concentrations from WT hippocampal lysates. Protein concentrations ranging from 0-600 μ g were used. 300 μ g of protein provided adequate signal for visualization of KCC2 and KCC2-T1007 phosphorylation, while enabling increases/decreases in their expression to be detected. Thus, 300 μ g of protein was used for immunoprecipitation experiments to assess KCC2-T1007 phosphorylation (**Fig. 5.3A**).

Critically, one hour of kainate-induced seizures led to an increase in T1007 phosphorylation in WT mice (150 ± 17 % of WT littermates, $n = 5$; $p = 0.0193$) (**Fig. 5.3B**), which would be consistent with a phosphorylation-dependent decrease of KCC2 function (Conway et al 2017).

Figure 5:3: Kainate-induced seizures increase KCC2-T1007 phosphorylation in WT mice.



A. Characterizing protein concentration needed to visualize KCC2 and KCC2-T1007 phosphorylation in WT hippocampal lysate. 300ug of protein provided adequate signal for visualization of KCC2 and KCC2-T1007 phosphorylation, while enabling the detected of increases/decreases in their expression and was thus the selected concentration for all experiments **B.** Western blot visualizing immunoprecipitated KCC2 and the corresponding KCC2-T1007 phosphorylation in the hippocampus of WT mice dissected 1 hour after either saline or kainate injection. KCC2-T1007 phosphorylation was normalized to the immunoprecipitated KCC2 and expressed as a % of saline injected mice. 1 hour of kainate increased KCC2-T1007 phosphorylation.

Discussion

KCC2-T906A/T1007A mutations impact the kinetic properties of KCC2

Within this chapter I have examined the underlying mechanisms through which KCC2-T906A/T1007A mutations enhance KCC2 function. The KCC2-T906A/T1007A mutations did not impact KCC2 surface expression (**aim 1**), indicating the enhanced Cl^- extrusion cannot simply be explained by more KCC2 protein on the cell surface. These mutations appear to be altering the functional capacity of KCC2 through direct alteration of its kinetic properties, as I detected an enhanced rate of Cl^- extrusion when neurons were loaded with high levels of Cl^- . These changes in the rate of Cl^- extrusion may be due to alterations in the unit rate of Cl^- transport in a manner similar to phosphorylation-initiated crosslinking of NKCC1 transmembrane domains that ultimately lock it in active/inactive states (Monette et al 2014). On the other hand, these KCC2 mutations could increase its affinity for Cl^- . Given that KCC2-T906A/T1007A neurons equilibrate at more negative E_{GABA} values than WT neurons under basal conditions (assessed using gramicidin perforated patch clamp – see aim 1) when Cl^- entry is limited (due to the presence of TTX), an increased affinity for Cl^- is a more likely mechanism as this would enable Cl^- detection and extrusion beyond the threshold for WT. This “dual-affinity” state of KCC2 may be similar to nitrate transporters, which exhibit phosphorylation-dependent switching between high and low affinity states (Liu & Tsay 2003, Sun & Zheng 2015). However, enhanced Cl^- extrusion was detected even when neurons were loaded with high levels of Cl^- , which I anticipate would

reduce the importance of Cl^- affinity given the high availability of Cl^- within the cell. This would support the enhanced unit velocity hypothesis described above. It is quite possible that both mechanisms are involved, and more intricate examination of Cl^- extrusion in the KCC2-T906A/T1007A neurons is required to tease apart these two intimately linked factors. Furthermore, how (de)phosphorylation of the C-terminus of KCC2 can translate to the transmembrane domain to modulate KCC2 activity remains to be determined. Structure-function studies could clarify this process which may lead to a rational chemical strategy that exploits this mechanism to directly activate KCC2.

KCC2-T906A/T1007A mutations limit activity-dependent deficits in GABAergic inhibition

The importance of appropriate levels of KCC2-mediated Cl^- extrusion for maintaining a healthy nervous system becomes clear when we consider that fast synaptic inhibition is depolarizing and even excitatory during seizures due to a collapse in the Cl^- gradient. An ability to resist E_{GABA} depolarization and maintain effective inhibition may therefore be therapeutically beneficial. Interestingly, the KCC2-T906A/T1007A mutations conferred a resistance to glutamate induced Cl^- loading, limiting activity dependent deficits in synaptic inhibition. This protection against E_{GABA} depolarization is likely due to the capability to extrude Cl^- more rapidly in the KCC2-T906A/T1007A neurons as described above. It is possible that maintenance of hyperpolarizing GABAergic inhibition may be occurring in the

KCC2-T906A/T1007A neurons when exposed to chemoconvulsants. This provides a possible mechanistic explanation for why the KCC2-T906A/T1007A mice have a reduced seizure phenotype.

Pathological relevance of KCC2-T1007 phosphorylation

I have detected an increase in KCC2-T1007 phosphorylation after kainate-induced seizures. Given that increases in KCC2-T1007 phosphorylation correlate with KCC2 inhibition, this seizure-induced increase in KCC2-T1007 phosphorylation likely phospho-inhibits KCC2 function. As reductions in KCC2 function enhance seizure severity (Sivakumaran et al 2015), this likely enhances the severity of kainate-induced seizures. Preventing phospho-inactivation of KCC2 by mutating KCC2-T1007 to alanine may therefore be a contributory mechanism in the reduction of seizure activity detected in the KCC2-T906A/T1007A mice (**see aim 2**).

Understanding the pathological mechanisms underlying this enhanced T1007 phosphorylation may enable pharmacological intervention to prevent such phosphomodulation. The most well established pathological inhibitors of KCC2 function are excessive glutamate (Lee et al 2011) and high levels of BDNF (Rivera et al 2002). Kainate-induced seizures dephosphorylates KCC2-S940 which decreases its surface expression, reducing the chloride extrusion capacity of a neuron and depolarizing E_{GABA} (Silayeva et al 2015), possibly through glutamate-mediated NMDA receptor activation (Lee et al 2011). The increase in KCC2-T1007 phosphorylation after kainate-induced seizure could also be due to an impact of

enhanced glutamate exposure similar to KCC2-S940 phosphorylation as described above, although I did not assess the impact of glutamate on the phosphorylation state of KCC2-T1007.

BDNF signaling through tyrosine receptor kinase B (TrkB) activation also decreases KCC2 expression and function, although less is known about the mechanisms underlying this process. Rivera et al. first demonstrated KCC2 mRNA and protein is reduced in hippocampal slice cultures and in acute slices upon exposure to BDNF, and determined the effects to be mediated through TrkB (Rivera et al 2002). They also detected a consequent impairment of neuronal Cl^- extrusion capacity. Following this initial demonstration that BDNF downregulates KCC2 and depolarizes E_{GABA} in hippocampal neurons, similar observations were subsequently reported for different regions across the CNS, including the spinal dorsal horn (Coull et al 2005), the cortex (Molinaro et al 2009) ventral horn (Boulenguez et al 2010), ventral tegmental area (Vargas-Perez et al 2009), and in the cerebellum (Huang et al 2013). TrkB signaling triggers three downstream signaling pathways: phospholipase C γ (PLC γ), mitogen activated protein kinases (MAPK) and phosphoinositide 3-kinase-AKT (PI3K-AKT). BDNF mediated downregulation of KCC2 in hippocampal neurons is prevented when either Shc/FRS-2 (src homology 2 domain containing transforming protein/FGF receptor substrate), an adaptor protein that mediates downstream PI3K and MAPK signaling, or PLC γ are genetically uncoupled from TrkB (Rivera et al 2004), suggesting activation of both these signaling pathways is required for BDNF-mediated downregulation of KCC2. Interestingly, PI3K-AKT activation increases

SPAK activity (Sengupta et al 2013), which we would expect to result in enhanced KCC2-T1007 phosphorylation although this has never been assessed. It is possible that BDNF inhibits KCC2 through activation of TrkB and the downstream PI3K-AKT signaling pathway, resulting in WNK-SPAK activation and subsequent T1007 phosphorylation. Interrogation of this pathway could lead to novel targets to reduce KCC2-T1007 phosphorylation in the brain and subsequently activate KCC2.

It must be stated however that the phosphorylation state of KCC2-T1007 in patients with epilepsy has never been investigated; this limits our understanding of the pathological relevance of T1007 phosphorylation. However, even in the absence of any increase in T1007 phosphorylation in patients, reducing KCC2-T1007 phosphorylation should still potentiate KCC2 function above basal levels. This is important as we do not yet know if KCC2 is dysfunctional in all patients with epilepsy; the ability to reduce seizures even when KCC2 function is intact would have more widespread therapeutic potential, as targeting KCC2 could be attempted in both patients with and without KCC2 deficits. As I have determined that increasing KCC2 function beyond baseline levels enables neurons to resist excess Cl^- loading and E_{GABA} depolarization that accompanies hyperexcitation, targeting KCC2 to enable more rapid extrusion of seizure-induced neuronal Cl^- loading would likely be effective in patients with and without prior KCC2 dysfunction.

Chapter 6 : General Discussion

A novel mechanism of potentiating GABAergic inhibition

This thesis has centered on a novel mechanism of enhancing GABAergic inhibition in the brain: phospho-potential of KCC2 function. KCC2-mediated Cl^- extrusion was increased by genetically modifying KCC2 phosphorylation at sites T906 and T1007 to alanine residues *in vivo*, a strategy employed due to previous studies demonstrating KCC2-T906A/T1007A mutations enhance KCC2 function *in vitro* (Rinehart et al 2009, Titz et al 2015, Weber et al 2014) and when overexpressed *in vivo* through *in utero* electroporation (Inoue et al 2012). I have demonstrated that phosphomodulation of KCC2 at sites T906 and T1007 has a powerful impact on KCC2 function *in vivo*. Not only did preventing phosphorylation of these sites enhance E_{GABA} hyperpolarization at rest, it enhanced the rate of Cl^- extrusion when neurons were challenged with increased $[\text{Cl}^-]_i$. Furthermore, preventing phosphorylation of these sites induced a substantial acceleration of the developmental hyperpolarizing E_{GABA} shift.

A potential therapeutic strategy for seizure-associated disorders

One of the most important goals in epilepsy research is to identify the underlying mechanisms that contribute to seizures. Interneuron firing increases at the onset of ictal events *in vitro*, indicating a paradoxical role of excess GABAergic activity underlying ictogenesis. Prolonged GABA_A conductance, particularly when concurrent with membrane depolarization, degrades the efficacy of synaptic inhibition due to Cl⁻ loading, which abolishes hyperpolarizing GABA_A currents (Deeb et al 2013, Thompson & Gahwiler 1989). Epileptic patients who have reduced KCC2 function are predicted to have particularly labile chloride gradients due to a reduced ability to effectively regulate [Cl⁻]_i. Thus, the normal [Cl⁻]_i fluctuations that occur in healthy individuals due to dynamic changes in GABA_A conductance may be sufficient to initiate seizures in patients with epilepsy.

Despite a clear role for KCC2 dysfunction and depolarizing GABAergic inhibition in epilepsy, there were not yet any studies demonstrating that potentiating KCC2 function would reduce seizure activity. My thesis work has provided initial evidence to suggest that increased KCC2 function does indeed have a therapeutic benefit.

The KCC2-T906A/T1007A mutations limited loss of synaptic inhibition during hyperexcitable conditions by enhancing the rate of KCC2-mediated Cl⁻ extrusion. This was sufficient to delay the onset and severity of chemoconvulsant-induced seizure activity *in vitro* and *in vivo*, suggesting a key role for elevated neuronal [Cl⁻]_i and E_{GABA} depolarization in the initiation and progression of seizures.

Fortunately, some KCC2 protein is retained in patients with chronic epilepsy, indicating an untapped potential for targeting KCC2-T906/T1007 phosphorylation to restore KCC2 function. The powerful chemoconvulsants used in this study rapidly remove KCC2 from the cell membrane, far more than what is observed in human epileptic tissue, thus it is possible that increasing KCC2 function in patients that retain adequate levels of KCC2 protein will be efficacious in reducing seizures.

KCC2 dysfunction has also been linked to several other epilepsy-associated disorders including neurodevelopmental disorders and neuropathic pain (Deidda et al 2015, He et al 2014, Tang et al 2016). Given its critical role in supporting GABAergic inhibition, such deficits in KCC2 activity are likely to contribute to the enhanced seizure susceptibility seen in patients with these disorders. The use of the KCC2-T906A/T1007A mice would enable the potential therapeutic benefit of increasing KCC2 function in these disorders to be addressed.

Moreover, from a therapeutic perspective, it is encouraging that no overt phenotype was detected in the KCC2-T906A/T1007A mice, as this suggests targeting KCC2 pharmacologically to reduce seizure activity would avoid motor co-ordination and sedation side effects associated with known GABA_A modulators like benzodiazepines (Perucca & Gilliam 2012).

Physiological mechanisms underlying KCC2-T906/T1007 (de)phosphorylation

STE20/SPS1-related proline-alanine-rich protein kinase (SPAK) and the related kinase, oxidative stress-responsive 1 protein (OSR1), phosphorylate T1007 on KCC2. This process is thought to be regulated by the upstream 'with-no-lysine kinase' (WNK). The neuron-specific processes that mediate levels of WNK-SPAK/OSR1 activity must therefore be tightly regulated, although the mechanisms responsible for this regulation remain unclear. Several studies have begun to address this question. A study by Piali et al. found that Cl^- can directly bind to the catalytic site of WNK1, which prevents WNK1 auto-phosphorylation and activation (Piali et al 2014). Since this finding, the current leading theory of WNK1 regulation suggests WNK1 can detect increases in intraneuronal Cl^- , causing WNK1 inactivation, and subsequent inhibition of SPAK/OSR1 and activation of KCC2. It is suggested that this mechanism enables neurons to maintain $[\text{Cl}^-]_i$ at a stable level by detecting increases in $[\text{Cl}^-]_i$. However, using autoradiography, this study also demonstrates that increasing the Cl^- concentration has little effect on WNK1-mediated phosphorylation of OSR1, with an IC_{50} of 530mM. Physiological $[\text{Cl}^-]_i$ spans the range of approximately 2-60mM, thus the ability of $[\text{Cl}^-]_i$ to inhibit WNK1 is not relevant to KCC2 regulation, as high $[\text{Cl}^-]_i$ -mediated WNK1 auto-phosphorylation would not alter the ability of WNK1 to activate OSR1 in neurons. Additionally, under the current leading theory, if $[\text{Cl}^-]_i$ is high in immature neurons, then WNK-SPAK/OSR1 would be inactive, T1007 phosphorylation would be low and KCC2 would be more functional; we know this is not the case. Thus,

the cellular mechanisms responsible for regulating WNK/SPAK activity, and thus T1007 phosphorylation, remain unclear.

Therapeutic perspective of targeting KCC2 T906/T1007 phosphorylation

The findings from this study suggest that dephosphorylation of KCC2 at sites T906/T1007 potentiates KCC2 function and reduces seizure activity. However, this work has relied on alanine mutations at these sites to prevent phosphoinhibition. Of course, this cannot be reproduced in humans, thus targeting these sites pharmacologically would be necessary to recapitulate this effect on KCC2 function. This could be achieved either by activating phosphatases that regulate KCC2-T906/T1007 phosphorylation, or by inhibiting the responsible kinases. We do not know which phosphatases mediate KCC2-T906/T1007 dephosphorylation, but the specificity of phosphatases is very low. It would be reasonable to assume that inhibiting the kinase pathways that regulate KCC2-T906/T1007 phosphorylation would be a more specific method of potentiating KCC2 activity; unfortunately, this is likely to be similarly problematic. This is due to the presence of the major kinases that regulate T1007, WNK and SPAK/OSR1, in most non-neuronal cells; inhibition of these kinases would lead to an undesirable inactivation of NKCC1 in non-neuronal cells as NKCC1 is inactivated by inhibition of these kinases. The consequence of this is evident from studies on patients treated with the NKCC1 inhibitor bumetanide. Bumetanide has numerous side-effects including alkalosis, hypokalemia and diuresis (Puskarjov et al 2014a).

Moreover, bumetanide caused deafness in 27% of infants administered the drug (Pressler et al 2015). WNK-SPAK/OSR1 inhibition reduces NKCC1 function, so inhibition of these kinases would likely result in side-effects similar to those of bumetanide. Development of prodrugs that can more effectively target the brain, and limit extra-neuronal exposure, may enable circumvention of these side-effects although such drugs have yet to be developed.

We do not yet know if KCC2 is dysfunctional in all patients with epilepsy; the ability to reduce seizures even when KCC2 function is intact would have more widespread therapeutic potential, as targeting KCC2 could be attempted in both patients with and without KCC2 deficits. I have determined that increasing KCC2 function beyond baseline levels enables neurons to resist excess Cl^- loading and depolarizing GABA_A currents that accompanies hyperexcitation. As neuronal Cl^- loading occurs during a seizure, targeting KCC2 to enable more rapid extrusion of this Cl^- would likely be effective in both patients with and without prior KCC2 dysfunction.

Collectively, this work identifies KCC2 as a seizure-limiting protein and highlights the potential of targeting the phosphorylation state of this protein as a novel therapeutic strategy for treating seizures.

References

- Agez M, Schultz P, Medina I, Baker DJ, Burnham MP, et al. 2017. Molecular architecture of potassium chloride co-transporter KCC2. *Scientific reports* 7: 16452
- Alfonsa H, Lakey JH, Lightowlers RN, Trevelyan AJ. 2016. Cl-out is a novel cooperative optogenetic tool for extruding chloride from neurons. *Nature communications* 7: 13495
- Alfonsa H, Merricks EM, Codadu NK, Cunningham MO, Deisseroth K, et al. 2015. The contribution of raised intraneuronal chloride to epileptic network activity. *The Journal of neuroscience : the official journal of the Society for Neuroscience* 35: 7715-26
- Allen PJ, Fish DR, Smith SJ. 1992. Very high-frequency rhythmic activity during SEEG suppression in frontal lobe epilepsy. *Electroencephalography and clinical neurophysiology* 82: 155-9
- Anderson WW, Lewis DV, Swartzwelder HS, Wilson WA. 1986. Magnesium-free medium activates seizure-like events in the rat hippocampal slice. *Brain research* 398: 215-9
- Arzy S, Allali G, Brunet D, Michel CM, Kaplan PW, Seeck M. 2010. Antiepileptic drugs modify power of high EEG frequencies and their neural generators. *European journal of neurology* 17: 1308-12
- Awapara J, Landua AJ, Fuerst R, Seale B. 1950. Free gamma-aminobutyric acid in brain. *The Journal of biological chemistry* 187: 35-9
- Banerjee A, Rikhye RV, Breton-Provencher V, Tang X, Li C, et al. 2016. Jointly reduced inhibition and excitation underlies circuit-wide changes in cortical processing in

References

- Rett syndrome. *Proceedings of the National Academy of Sciences of the United States of America* 113: E7287-E96
- Barmashenko G, Hefft S, Aertsen A, Kirschstein T, Kohling R. 2011. Positive shifts of the GABA(A) receptor reversal potential due to altered chloride homeostasis is widespread after status epilepticus. *Epilepsia* 52: 1570-78
- Ben-Ari Y, Cherubini E, Corradetti R, Gaiarsa JL. 1989. Giant synaptic potentials in immature rat CA3 hippocampal neurones. *The Journal of physiology* 416: 303-25
- Blaesse P, Schmidt T. 2015. K-Cl cotransporter KCC2--a moonlighting protein in excitatory and inhibitory synapse development and function. *Pflugers Archiv : European journal of physiology* 467: 615-24
- Boistel J, Fatt P. 1958. Membrane permeability change during inhibitory transmitter action in crustacean muscle. *The Journal of physiology* 144: 176-91
- Bonislawski DP, Schwarzbach EP, Cohen AS. 2007. Brain injury impairs dentate gyrus inhibitory efficacy. *Neurobiology of disease* 25: 163-9
- Bormann J, Hamill OP, Sakmann B. 1987. Mechanism of anion permeation through channels gated by glycine and gamma-aminobutyric acid in mouse cultured spinal neurones. *The Journal of physiology* 385: 243-86
- Boulenguez P, Liabeuf S, Bos R, Bras H, Jean-Xavier C, et al. 2010. Down-regulation of the potassium-chloride cotransporter KCC2 contributes to spasticity after spinal cord injury. *Nat Med* 16: 302-7
- Bragin DE, Sanderson JL, Peterson S, Connor JA, Muller WS. 2009. Development of epileptiform excitability in the deep entorhinal cortex after status epilepticus. *The European journal of neuroscience* 30: 611-24
- Brock LG, Coombs JS, Eccles JC. 1952. The Recording of Potentials from Motoneurons with an Intracellular Electrode. *J Physiol-London* 117: 431-60

References

- Buckmaster PS. 2004. Laboratory animal models of temporal lobe epilepsy. *Comparative medicine* 54: 473-85
- Buzsaki G, Kaila K, Raichle M. 2007. Inhibition and brain work. *Neuron* 56: 771-83
- Campbell SL, Robel S, Cuddapah VA, Robert S, Buckingham SC, et al. 2015. GABAergic disinhibition and impaired KCC2 cotransporter activity underlie tumor-associated epilepsy. *Glia* 63: 23-36
- Cancedda L, Fiumelli H, Chen K, Poo MM. 2007. Excitatory GABA action is essential for morphological maturation of cortical neurons in vivo. *The Journal of neuroscience : the official journal of the Society for Neuroscience* 27: 5224-35
- Chevy Q, Heubl M, Goutierre M, Backer S, Moutkine I, et al. 2015. KCC2 Gates Activity-Driven AMPA Receptor Traffic through Cofilin Phosphorylation. *The Journal of neuroscience : the official journal of the Society for Neuroscience* 35: 15772-86
- Cohen I, Navarro V, Clemenceau S, Baulac M, Miles R. 2002. On the origin of interictal activity in human temporal lobe epilepsy in vitro. *Science* 298: 1418-21
- Conway LC, Cardarelli RA, Moore YE, Jones K, McWilliams LJ, et al. 2017. N-ethylmaleimide increases KCC2 activity by modulating transporter phosphorylation. *The Journal of biological chemistry*
- Coull JA, Beggs S, Boudreau D, Boivin D, Tsuda M, et al. 2005. BDNF from microglia causes the shift in neuronal anion gradient underlying neuropathic pain. *Nature* 438: 1017-21
- de Curtis M, Gnatkovsky V. 2009. Reevaluating the mechanisms of focal ictogenesis: The role of low-voltage fast activity. *Epilepsia* 50: 2514-25
- de Los Heros P, Alessi DR, Gourlay R, Campbell DG, Deak M, et al. 2014. The WNK-regulated SPAK/OSR1 kinases directly phosphorylate and inhibit the K⁺-Cl⁻ cotransporters. *The Biochemical journal* 458: 559-73

References

- Deeb TZ, Nakamura Y, Frost GD, Davies PA, Moss SJ. 2013. Disrupted Cl⁻ homeostasis contributes to reductions in the inhibitory efficacy of diazepam during hyperexcited states. *The European journal of neuroscience* 38: 2453-67
- DeFazio RA, Keros S, Quick MW, Hablitz JJ. 2000. Potassium-coupled chloride cotransport controls intracellular chloride in rat neocortical pyramidal neurons. *The Journal of neuroscience : the official journal of the Society for Neuroscience* 20: 8069-76
- Deidda G, Parrini M, Naskar S, Bozarth IF, Contestabile A, Cancedda L. 2015. Reversing excitatory GABAAR signaling restores synaptic plasticity and memory in a mouse model of Down syndrome. *Nature medicine* 21: 318-26
- Delpire E, Days E, Lewis LM, Mi D, Kim K, et al. 2009. Small-molecule screen identifies inhibitors of the neuronal K-Cl cotransporter KCC2. *Proceedings of the National Academy of Sciences of the United States of America* 106: 5383-8
- Delpire E, Lauf PK. 1991. Kinetics of Cl⁻-dependent K fluxes in hyposmotically swollen low K sheep erythrocytes. *The Journal of general physiology* 97: 173-93
- Doding A, Hartmann AM, Beyer T, Nothwang HG. 2012. KCC2 transport activity requires the highly conserved L(6)(7)(5) in the C-terminal beta1 strand. *Biochemical and biophysical research communications* 420: 492-7
- Doyon N, Vinay L, Prescott SA, De Koninck Y. 2016. Chloride Regulation: A Dynamic Equilibrium Crucial for Synaptic Inhibition. *Neuron* 89: 1157-72
- Dreier JP, Heinemann U. 1991. Regional and time dependent variations of low Mg²⁺ induced epileptiform activity in rat temporal cortex slices. *Experimental brain research* 87: 581-96
- Dunham PB, Ellory JC. 1981. Passive potassium transport in low potassium sheep red cells: dependence upon cell volume and chloride. *The Journal of physiology* 318: 511-30

References

- Dunham PB, Stewart GW, Ellory JC. 1980. Chloride-activated passive potassium transport in human erythrocytes. *Proceedings of the National Academy of Sciences of the United States of America* 77: 1711-5
- During MJ, Spencer DD. 1993. Extracellular hippocampal glutamate and spontaneous seizure in the conscious human brain. *Lancet* 341: 1607-10
- Dzhala VI, Brumback AC, Staley KJ. 2008. Bumetanide enhances phenobarbital efficacy in a neonatal seizure model. *Ann Neurol* 63: 222-35
- Ellender TJ, Raimondo JV, Irkle A, Lamsa KP, Akerman CJ. 2014. Excitatory effects of parvalbumin-expressing interneurons maintain hippocampal epileptiform activity via synchronous afterdischarges. *The Journal of neuroscience : the official journal of the Society for Neuroscience* 34: 15208-22
- Elliott KA, Van Gelder NM. 1958. Occlusion and metabolism of gamma-aminobutyric acid by brain tissue. *Journal of neurochemistry* 3: 28-40
- Fisher RS, Acevedo C, Arzimanoglou A, Bogacz A, Cross JH, et al. 2014. ILAE official report: a practical clinical definition of epilepsy. *Epilepsia* 55: 475-82
- Fisher RS, Webber WR, Lesser RP, Arroyo S, Uematsu S. 1992. High-frequency EEG activity at the start of seizures. *Journal of clinical neurophysiology : official publication of the American Electroencephalographic Society* 9: 441-8
- Fiumelli H, Briner A, Puskarjov M, Blaesse P, Belem BJ, et al. 2013. An ion transport-independent role for the cation-chloride cotransporter KCC2 in dendritic spinogenesis in vivo. *Cerebral cortex* 23: 378-88
- Florey E. 1954. An inhibitory and an excitatory factor of mammalian central nervous system, and their action of a single sensory neuron. *Archives internationales de physiologie* 62: 33-53

References

- Florey E, Mc LH. 1959. The effects of factor I and of gamma-aminobutyric acid on smooth muscle preparations. *The Journal of physiology* 145: 66-76
- Friedel P, Kahle KT, Zhang J, Hertz N, Pisella LI, et al. 2015. WNK1-regulated inhibitory phosphorylation of the KCC2 cotransporter maintains the depolarizing action of GABA in immature neurons. *Science signaling* 8: ra65
- Fujiwara-Tsukamoto Y, Isomura Y, Imanishi M, Ninomiya T, Tsukada M, et al. 2010. Prototypic Seizure Activity Driven by Mature Hippocampal Fast-Spiking Interneurons. *Journal of Neuroscience* 30: 13679-89
- Fujiwara-Tsukamoto Y, Isomura Y, Nambu A, Takada M. 2003. Excitatory GABA input directly drives seizure-like rhythmic synchronization in mature hippocampal CA1 pyramidal cells. *Neuroscience* 119: 265-75
- Fulton JF. 1939. Physiology of the Nervous System. *Science* 90: 110
- Gastaut H, Naquet R, Poire R, Tassinari CA. 1965. Treatment of Status Epilepticus with Diazepam (Valium). *Epilepsia* 6: 167-82
- Gauvain G, Chamma I, Chevy Q, Cabezas C, Irinopoulou T, et al. 2011. The neuronal K-Cl cotransporter KCC2 influences postsynaptic AMPA receptor content and lateral diffusion in dendritic spines. *Proceedings of the National Academy of Sciences of the United States of America* 108: 15474-9
- Ge S, Goh EL, Sailor KA, Kitabatake Y, Ming GL, Song H. 2006. GABA regulates synaptic integration of newly generated neurons in the adult brain. *Nature* 439: 589-93
- Gnatkovsky V, Librizzi L, Trombin F, de Curtis M. 2008. Fast activity at seizure onset is mediated by inhibitory circuits in the entorhinal cortex in vitro. *Annals of neurology* 64: 674-86

References

- Gonzalez OC, Shiri Z, Krishnan GP, Myers TL, Williams S, et al. 2018. Role of KCC2-dependent potassium efflux in 4-Aminopyridine-induced Epileptiform synchronization. *Neurobiology of disease* 109: 137-47
- Gulyas AI, Sik A, Payne JA, Kaila K, Freund TF. 2001. The KCl cotransporter, KCC2, is highly expressed in the vicinity of excitatory synapses in the rat hippocampus. *The European journal of neuroscience* 13: 2205-17
- Haas M, McManus TJ. 1983. Bumetanide inhibits (Na + K + 2Cl) co-transport at a chloride site. *The American journal of physiology* 245: C235-40
- Hamidi S, Avoli M. 2015. KCC2 function modulates in vitro ictogenesis. *Neurobiology of disease* 79: 51-8
- Hartmann AM, Wenz M, Mercado A, Storger C, Mount DB, et al. 2010. Differences in the large extracellular loop between the K(+)-Cl(-) cotransporters KCC2 and KCC4. *The Journal of biological chemistry* 285: 23994-4002
- He Q, Nomura T, Xu J, Contractor A. 2014. The developmental switch in GABA polarity is delayed in fragile X mice. *The Journal of neuroscience : the official journal of the Society for Neuroscience* 34: 446-50
- Hekmat-Safe DS, Lundy MY, Ranga R, Tanouye MA. 2006. Mutations in the K+/Cl- cotransporter gene *kazachoc* (*kcc*) increase seizure susceptibility in *Drosophila*. *The Journal of neuroscience : the official journal of the Society for Neuroscience* 26: 8943-54
- Hewitt SA, Wamsteeker JI, Kurz EU, Bains JS. 2009. Altered chloride homeostasis removes synaptic inhibitory constraint of the stress axis. *Nature neuroscience* 12: 438-43
- Huang Y, Wang JJ, Yung WH. 2013. Coupling between GABA-A receptor and chloride transporter underlies ionic plasticity in cerebellar Purkinje neurons. *Cerebellum* 12: 328-30

References

- Huberfeld G, Wittner L, Clemenceau S, Baulac M, Kaila K, et al. 2007. Perturbed chloride homeostasis and GABAergic signaling in human temporal lobe epilepsy. *The Journal of neuroscience : the official journal of the Society for Neuroscience* 27: 9866-73
- Hubner CA, Stein V, Hermans-Borgmeyer I, Meyer T, Ballanyi K, Jentsch TJ. 2001. Disruption of KCC2 reveals an essential role of K-Cl cotransport already in early synaptic inhibition. *Neuron* 30: 515-24
- Ilie A, Raimondo JV, Akerman CJ. 2012. Adenosine release during seizures attenuates GABAA receptor-mediated depolarization. *J Neurosci* 32: 5321-32
- Inoue K, Furukawa T, Kumada T, Yamada J, Wang T, et al. 2012. Taurine inhibits K⁺-Cl⁻ cotransporter KCC2 to regulate embryonic Cl⁻ homeostasis via with-no-lysine (WNK) protein kinase signaling pathway. *The Journal of biological chemistry* 287: 20839-50
- Isaacson JS, Scanziani M. 2011. How inhibition shapes cortical activity. *Neuron* 72: 231-43
- Ivakine EA, Acton BA, Mahadevan V, Ormond J, Tang M, et al. 2013. Neto2 is a KCC2 interacting protein required for neuronal Cl⁻ regulation in hippocampal neurons. *Proceedings of the National Academy of Sciences of the United States of America* 110: 3561-6
- Jarolimek W, Lewen A, Misgeld U. 1999. A furosemide-sensitive K⁺-Cl⁻ cotransporter counteracts intracellular Cl⁻ accumulation and depletion in cultured rat midbrain neurons. *The Journal of neuroscience : the official journal of the Society for Neuroscience* 19: 4695-704
- Jennings ML, Alrohil N. 1990. Kinetics of Activation and Inactivation of Swelling-Stimulated K⁺/Cl⁻ Transport - the Volume-Sensitive Parameter Is the Rate-Constant for Inactivation. *Journal of General Physiology* 95: 1021-40

References

- Jennings ML, Schulz RK. 1991. Okadaic acid inhibition of KCl cotransport. Evidence that protein dephosphorylation is necessary for activation of transport by either cell swelling or N-ethylmaleimide. *The Journal of general physiology* 97: 799-817
- Kahle KT, Barnett SM, Sassower KC, Staley KJ. 2009. Decreased seizure activity in a human neonate treated with bumetanide, an inhibitor of the Na(+)-K(+)-2Cl(-) cotransporter NKCC1. *Journal of child neurology* 24: 572-6
- Kahle KT, Merner ND, Friedel P, Silayeva L, Liang B, et al. 2014. Genetically encoded impairment of neuronal KCC2 cotransporter function in human idiopathic generalized epilepsy. *EMBO reports* 15: 766-74
- Kaila K. 1994. Ionic basis of GABAA receptor channel function in the nervous system. *Progress in neurobiology* 42: 489-537
- Kaila K, Price TJ, Payne JA, Puskarjov M, Voipio J. 2014. Cation-chloride cotransporters in neuronal development, plasticity and disease. *Nature reviews. Neuroscience* 15: 637-54
- Kaila K, Voipio J. 1987. Postsynaptic fall in intracellular pH induced by GABA-activated bicarbonate conductance. *Nature* 330: 163-5
- Kapur J, Coulter DA. 1995. Experimental status epilepticus alters gamma-aminobutyric acid type A receptor function in CA1 pyramidal neurons. *Annals of neurology* 38: 893-900
- Karlocai MR, Wittner L, Toth K, Magloczky Z, Katarova Z, et al. 2016. Enhanced expression of potassium-chloride cotransporter KCC2 in human temporal lobe epilepsy. *Brain structure & function* 221: 3601-15
- Kelley MR, Cardarelli RA, Smalley JL, Ollerhead TA, Andrew PM, et al. 2018. Locally Reducing KCC2 Activity in the Hippocampus is Sufficient to Induce Temporal Lobe Epilepsy. *EBioMedicine* 32: 62-71

References

- Kelley MR, Deeb TZ, Brandon NJ, Dunlop J, Davies PA, Moss SJ. 2016. Compromising KCC2 transporter activity enhances the development of continuous seizure activity. *Neuropharmacology* 108: 103-110
- Khirug S, Huttu K, Ludwig A, Smirnov S, Voipio J, et al. 2005. Distinct properties of functional KCC2 expression in immature mouse hippocampal neurons in culture and in acute slices. *The European journal of neuroscience* 21: 899-904
- Klausberger T, Somogyi P. 2008. Neuronal diversity and temporal dynamics: the unity of hippocampal circuit operations. *Science* 321: 53-7
- Kravitz EA, Kuffler SW, Potter DD. 1963. Gamma-Aminobutyric Acid and Other Blocking Compounds in Crustacea. Iii. Their Relative Concentrations in Separated Motor and Inhibitory Axons. *Journal of neurophysiology* 26: 739-51
- Krnjevic K, Phillis JW. 1963. Ionophoretic Studies of Neurones in Mammalian Cerebral Cortex. *J Physiol-London* 165: 274-&
- Krnjevic K, Schwartz S. 1967. The action of gamma-aminobutyric acid on cortical neurones. *Experimental brain research* 3: 320-36
- Kuffler SW. 1954. Mechanisms of activation and motor control of stretch receptors in lobster and crayfish. *Journal of neurophysiology* 17: 558-74
- Kuffler SW, Edwards C. 1958. Mechanism of gamma aminobutyric acid (GABA) action and its relation to synaptic inhibition. *Journal of neurophysiology* 21: 589-610
- Lauf PK. 1985. Passive K⁺-Cl⁻ fluxes in low-K⁺ sheep erythrocytes: modulation by A23187 and bivalent cations. *The American journal of physiology* 249: C271-8
- Lee HH, Deeb TZ, Walker JA, Davies PA, Moss SJ. 2011. NMDA receptor activity downregulates KCC2 resulting in depolarizing GABA_A receptor-mediated currents. *Nature neuroscience* 14: 736-43

References

- Lee HH, Jurd R, Moss SJ. 2010. Tyrosine phosphorylation regulates the membrane trafficking of the potassium chloride co-transporter KCC2. *Molecular and cellular neurosciences* 45: 173-9
- Lee HH, Walker JA, Williams JR, Goodier RJ, Payne JA, Moss SJ. 2007. Direct protein kinase C-dependent phosphorylation regulates the cell surface stability and activity of the potassium chloride cotransporter KCC2. *The Journal of biological chemistry* 282: 29777-84
- Li H, Khirug S, Cai C, Ludwig A, Blaesse P, et al. 2007. KCC2 interacts with the dendritic cytoskeleton to promote spine development. *Neuron* 56: 1019-33
- Li H, Tornberg J, Kaila K, Airaksinen MS, Rivera C. 2002. Patterns of cation-chloride cotransporter expression during embryonic rodent CNS development. *The European journal of neuroscience* 16: 2358-70
- Li X, Zhou J, Chen Z, Chen S, Zhu F, Zhou L. 2008. Long-term expressional changes of Na⁺ - K⁺ -Cl⁻ co-transporter 1 (NKCC1) and K⁺ -Cl⁻ co-transporter 2 (KCC2) in CA1 region of hippocampus following lithium-pilocarpine induced status epilepticus (PISE). *Brain research* 1221: 141-6
- Lillis KP, Kramer MA, Mertz J, Staley KJ, White JA. 2012. Pyramidal cells accumulate chloride at seizure onset. *Neurobiology of disease* 47: 358-66
- Liu KH, Tsay YF. 2003. Switching between the two action modes of the dual-affinity nitrate transporter CHL1 by phosphorylation. *The EMBO journal* 22: 1005-13
- Llano O, Smirnov S, Soni S, Golubtsov A, Guillemin I, et al. 2015. KCC2 regulates actin dynamics in dendritic spines via interaction with beta-PIX. *The Journal of cell biology* 209: 671-86

References

- Lothman EW, Collins RC. 1981. Kainic acid induced limbic seizures: metabolic, behavioral, electroencephalographic and neuropathological correlates. *Brain research* 218: 299-318
- Ludwig A, Uvarov P, Soni S, Thomas-Crusells J, Airaksinen MS, Rivera C. 2011. Early growth response 4 mediates BDNF induction of potassium chloride cotransporter 2 transcription. *The Journal of neuroscience : the official journal of the Society for Neuroscience* 31: 644-9
- Maguire J, Salpekar JA. 2013. Stress, seizures, and hypothalamic-pituitary-adrenal axis targets for the treatment of epilepsy. *Epilepsy & behavior : E&B* 26: 352-62
- Mahadevan V, Dargaei Z, Ivakine EA, Hartmann AM, Ng D, et al. 2015. Neto2-null mice have impaired GABAergic inhibition and are susceptible to seizures. *Frontiers in cellular neuroscience* 9: 368
- Mahadevan V, Khademullah CS, Dargaei Z, Chevrier J, Uvarov P, et al. 2017. Native KCC2 interactome reveals PACSIN1 as a critical regulator of synaptic inhibition. *eLife* 6
- Mahadevan V, Pressey JC, Acton BA, Uvarov P, Huang MY, et al. 2014. Kainate receptors coexist in a functional complex with KCC2 and regulate chloride homeostasis in hippocampal neurons. *Cell reports* 7: 1762-70
- Marin O. 2012. Interneuron dysfunction in psychiatric disorders. *Nature reviews. Neuroscience* 13: 107-20
- Markkanen M, Karhunen T, Llano O, Ludwig A, Rivera C, et al. 2014. Distribution of neuronal KCC2a and KCC2b isoforms in mouse CNS. *The Journal of comparative neurology* 522: 1897-914
- Markkanen M, Ludwig A, Khirug S, Pryazhnikov E, Soni S, et al. 2017. Implications of the N-terminal heterogeneity for the neuronal K-Cl cotransporter KCC2 function. *Brain research* 1675: 87-101

References

- Markkanen M, Uvarov P, Airaksinen MS. 2008. Role of upstream stimulating factors in the transcriptional regulation of the neuron-specific K-Cl cotransporter KCC2. *Brain research* 1236: 8-15
- Mayer SA, Claassen J, Lokin J, Mendelsohn F, Dennis LJ, Fitzsimmons BF. 2002. Refractory status epilepticus: frequency, risk factors, and impact on outcome. *Archives of neurology* 59: 205-10
- Mazarati A, Shin D, Sankar R. 2009. Bumetanide inhibits rapid kindling in neonatal rats. *Epilepsia* 50: 2117-22
- Mercado A, Broumand V, Zandi-Nejad K, Enck AH, Mount DB. 2006. A C-terminal domain in KCC2 confers constitutive K⁺-Cl⁻ cotransport. *The Journal of biological chemistry* 281: 1016-26
- Molinaro G, Battaglia G, Riozzi B, Di Menna L, Rampello L, et al. 2009. Memantine treatment reduces the expression of the K⁽⁺⁾/Cl⁽⁻⁾ cotransporter KCC2 in the hippocampus and cerebral cortex, and attenuates behavioural responses mediated by GABA(A) receptor activation in mice. *Brain Res* 1265: 75-9
- Monette MY, Somasekharan S, Forbush B. 2014. Molecular motions involved in Na-K-Cl cotransporter-mediated ion transport and transporter activation revealed by internal cross-linking between transmembrane domains 10 and 11/12. *The Journal of biological chemistry* 289: 7569-79
- Moore YE, Kelley MR, Brandon NJ, Deeb TZ, Moss SJ. 2017. Seizing Control of KCC2: A New Therapeutic Target for Epilepsy. *Trends in neurosciences* 40: 555-71
- Munoz A, Mendez P, DeFelipe J, Alvarez-Leefmans FJ. 2007. Cation-chloride cotransporters and GABA-ergic innervation in the human epileptic hippocampus. *Epilepsia* 48: 663-73

References

- Pallud J, Le Van Quyen M, Bielle F, Pellegrino C, Varlet P, et al. 2014. Cortical GABAergic excitation contributes to epileptic activities around human glioma. *Science translational medicine* 6: 244ra89
- Palma E, Amici M, Sobrero F, Spinelli G, Di Angelantonio S, et al. 2006. Anomalous levels of Cl⁻ transporters in the hippocampal subiculum from temporal lobe epilepsy patients make GABA excitatory. *Proceedings of the National Academy of Sciences of the United States of America* 103: 8465-8
- Pathak HR, Weissinger F, Terunuma M, Carlson GC, Hsu FC, et al. 2007. Disrupted dentate granule cell chloride regulation enhances synaptic excitability during development of temporal lobe epilepsy. *The Journal of neuroscience : the official journal of the Society for Neuroscience* 27: 14012-22
- Payne JA. 1997. Functional characterization of the neuronal-specific K-Cl cotransporter: implications for [K⁺]_o regulation. *The American journal of physiology* 273: C1516-25
- Payne JA, Stevenson TJ, Donaldson LF. 1996. Molecular characterization of a putative K-Cl cotransporter in rat brain. A neuronal-specific isoform. *The Journal of biological chemistry* 271: 16245-52
- Peng Z, Huang CS, Stell BM, Mody I, Houser CR. 2004. Altered expression of the delta subunit of the GABA_A receptor in a mouse model of temporal lobe epilepsy. *The Journal of neuroscience : the official journal of the Society for Neuroscience* 24: 8629-39
- Perreault P, Avoli M. 1991. Physiology and pharmacology of epileptiform activity induced by 4-aminopyridine in rat hippocampal slices. *Journal of neurophysiology* 65: 771-85

References

- Perucca P, Gilliam FG. 2012. Adverse effects of antiepileptic drugs. *The Lancet. Neurology* 11: 792-802
- Petilla Interneuron Nomenclature G, Ascoli GA, Alonso-Nanclares L, Anderson SA, Barrionuevo G, et al. 2008. Petilla terminology: nomenclature of features of GABAergic interneurons of the cerebral cortex. *Nature reviews. Neuroscience* 9: 557-68
- Piala AT, Moon TM, Akella R, He H, Cobb MH, Goldsmith EJ. 2014. Chloride sensing by WNK1 involves inhibition of autophosphorylation. *Science signaling* 7: ra41
- Piechotta K, Lu J, Delpire E. 2002. Cation chloride cotransporters interact with the stress-related kinases Ste20-related proline-alanine-rich kinase (SPAK) and oxidative stress response 1 (OSR1). *The Journal of biological chemistry* 277: 50812-9
- Plotkin MD, Snyder EY, Hebert SC, Delpire E. 1997. Expression of the Na-K-2Cl cotransporter is developmentally regulated in postnatal rat brains: a possible mechanism underlying GABA's excitatory role in immature brain. *Journal of neurobiology* 33: 781-95
- Pressey JC, Mahadevan V, Khademullah CS, Dargaei Z, Chevrier J, et al. 2017. A kainate receptor subunit promotes the recycling of the neuron-specific K(+)-Cl(-) cotransporter KCC2 in hippocampal neurons. *The Journal of biological chemistry* 292: 6190-201
- Pressler RM, Boylan GB, Marlow N, Blennow M, Chiron C, et al. 2015. Bumetanide for the treatment of seizures in newborn babies with hypoxic ischaemic encephalopathy (NEMO): an open-label, dose finding, and feasibility phase 1/2 trial. *The Lancet. Neurology* 14: 469-77

References

- Puskarjov M, Ahmad F, Kaila K, Blaesse P. 2012. Activity-dependent cleavage of the K-Cl cotransporter KCC2 mediated by calcium-activated protease calpain. *The Journal of neuroscience : the official journal of the Society for Neuroscience* 32: 11356-64
- Puskarjov M, Kahle KT, Ruusuvuori E, Kaila K. 2014a. Pharmacotherapeutic targeting of cation-chloride cotransporters in neonatal seizures. *Epilepsia* 55: 806-18
- Puskarjov M, Seja P, Heron SE, Williams TC, Ahmad F, et al. 2014b. A variant of KCC2 from patients with febrile seizures impairs neuronal Cl⁻ extrusion and dendritic spine formation. *EMBO reports* 15: 723-9
- Reddy DS, Kuruba R. 2013. Experimental models of status epilepticus and neuronal injury for evaluation of therapeutic interventions. *International journal of molecular sciences* 14: 18284-318
- Rinehart J, Maksimova YD, Tanis JE, Stone KL, Hodson CA, et al. 2009. Sites of regulated phosphorylation that control K-Cl cotransporter activity. *Cell* 138: 525-36
- Rivera C, Li H, Thomas-Crusells J, Lahtinen H, Viitanen T, et al. 2002. BDNF-induced TrkB activation down-regulates the K⁺-Cl⁻ cotransporter KCC2 and impairs neuronal Cl⁻ extrusion. *The Journal of cell biology* 159: 747-52
- Rivera C, Voipio J, Payne JA, Ruusuvuori E, Lahtinen H, et al. 1999. The K⁺/Cl⁻ cotransporter KCC2 renders GABA hyperpolarizing during neuronal maturation. *Nature* 397: 251-5
- Rivera C, Voipio J, Thomas-Crusells J, Li H, Emri Z, et al. 2004. Mechanism of activity-dependent downregulation of the neuron-specific K-Cl cotransporter KCC2. *The Journal of neuroscience : the official journal of the Society for Neuroscience* 24: 4683-91
- Roberts E, Frankel S. 1950. gamma-Aminobutyric acid in brain: its formation from glutamic acid. *The Journal of biological chemistry* 187: 55-63

References

- Romermann K, Fedrowitz M, Hampel P, Kaczmarek E, Tollner K, et al. 2017. Multiple blood-brain barrier transport mechanisms limit bumetanide accumulation, and therapeutic potential, in the mammalian brain. *Neuropharmacology* 117: 182-94
- Rudolph U, Knoflach F. 2011. Beyond classical benzodiazepines: novel therapeutic potential of GABAA receptor subtypes. *Nature reviews. Drug discovery* 10: 685-97
- Saito H, Watanabe M, Akita T, Ohba C, Sugai K, et al. 2016. Impaired neuronal KCC2 function by biallelic SLC12A5 mutations in migrating focal seizures and severe developmental delay. *Scientific reports* 6: 30072
- Schofield PR, Darlison MG, Fujita N, Burt DR, Stephenson FA, et al. 1987. Sequence and functional expression of the GABA A receptor shows a ligand-gated receptor super-family. *Nature* 328: 221-7
- Sengupta S, Lorente-Rodriguez A, Earnest S, Stippec S, Guo X, et al. 2013. Regulation of OSR1 and the sodium, potassium, two chloride cotransporter by convergent signals. *Proceedings of the National Academy of Sciences of the United States of America* 110: 18826-31
- Sharma AK, Reams RY, Jordan WH, Miller MA, Thacker HL, Snyder PW. 2007. Mesial temporal lobe epilepsy: pathogenesis, induced rodent models and lesions. *Toxicologic pathology* 35: 984-99
- Shen L, Liang F, Walensky LD, Huganir RL. 2000. Regulation of AMPA receptor GluR1 subunit surface expression by a 4. 1N-linked actin cytoskeletal association. *The Journal of neuroscience : the official journal of the Society for Neuroscience* 20: 7932-40
- Silayeva L, Deeb TZ, Hines RM, Kelley MR, Munoz MB, et al. 2015. KCC2 activity is critical in limiting the onset and severity of status epilepticus. *Proceedings of the National Academy of Sciences of the United States of America* 112: 3523-8

References

- Sivakumaran S, Cardarelli RA, Maguire J, Kelley MR, Silayeva L, et al. 2015. Selective inhibition of KCC2 leads to hyperexcitability and epileptiform discharges in hippocampal slices and in vivo. *The Journal of neuroscience : the official journal of the Society for Neuroscience* 35: 8291-6
- Sivakumaran S, Maguire J. 2016. Bumetanide reduces seizure progression and the development of pharmaco-resistant status epilepticus. *Epilepsia* 57: 222-32
- Staley K. 1992. Enhancement of the excitatory actions of GABA by barbiturates and benzodiazepines. *Neuroscience letters* 146: 105-7
- Staley KJ, Proctor WR. 1999. Modulation of mammalian dendritic GABA(A) receptor function by the kinetics of Cl⁻ and HCO₃⁻ transport. *The Journal of physiology* 519 Pt 3: 693-712
- Stein V, Hermans-Borgmeyer I, Jentsch TJ, Hubner CA. 2004. Expression of the KCl cotransporter KCC2 parallels neuronal maturation and the emergence of low intracellular chloride. *The Journal of comparative neurology* 468: 57-64
- Stodberg T, McTague A, Ruiz AJ, Hirata H, Zhen J, et al. 2015. Mutations in SLC12A5 in epilepsy of infancy with migrating focal seizures. *Nature communications* 6: 8038
- Strange K, Singer TD, Morrison R, Delpire E. 2000. Dependence of KCC2 K-Cl cotransporter activity on a conserved carboxy terminus tyrosine residue. *American journal of physiology. Cell physiology* 279: C860-7
- Sun J, Zheng N. 2015. Molecular Mechanism Underlying the Plant NRT1.1 Dual-Affinity Nitrate Transporter. *Frontiers in physiology* 6: 386
- Tang X, Kim J, Zhou L, Wengert E, Zhang L, et al. 2016. KCC2 rescues functional deficits in human neurons derived from patients with Rett syndrome. *Proceedings of the National Academy of Sciences of the United States of America* 113: 751-6

References

- Terunuma M, Xu J, Vithlani M, Sieghart W, Kittler J, et al. 2008. Deficits in phosphorylation of GABA(A) receptors by intimately associated protein kinase C activity underlie compromised synaptic inhibition during status epilepticus. *The Journal of neuroscience : the official journal of the Society for Neuroscience* 28: 376-84
- Thompson SM, Gahwiler BH. 1989. Activity-dependent disinhibition. I. Repetitive stimulation reduces IPSP driving force and conductance in the hippocampus in vitro. *Journal of neurophysiology* 61: 501-11
- Timofeev I, Grenier F, Steriade M. 2002. The role of chloride-dependent inhibition and the activity of fast-spiking neurons during cortical spike-wave electrographic seizures. *Neuroscience* 114: 1115-32
- Titz S, Sammler EM, Hormuzdi SG. 2015. Could tuning of the inhibitory tone involve graded changes in neuronal chloride transport? *Neuropharmacology* 95: 321-31
- Tollner K, Brandt C, Topfer M, Brunhofer G, Erker T, et al. 2014. A novel prodrug-based strategy to increase effects of bumetanide in epilepsy. *Annals of neurology* 75: 550-62
- Tornberg J, Voikar V, Savilahti H, Rauvala H, Airaksinen MS. 2005. Behavioural phenotypes of hypomorphic KCC2-deficient mice. *The European journal of neuroscience* 21: 1327-37
- Treiman DM, Meyers PD, Walton NY, Collins JF, Colling C, et al. 1998. A comparison of four treatments for generalized convulsive status epilepticus. Veterans Affairs Status Epilepticus Cooperative Study Group. *The New England journal of medicine* 339: 792-8
- Tremblay R, Lee S, Rudy B. 2016. GABAergic Interneurons in the Neocortex: From Cellular Properties to Circuits. *Neuron* 91: 260-92

References

- Tse K, Puttachary S, Beamer E, Sills GJ, Thippeswamy T. 2014. Advantages of repeated low dose against single high dose of kainate in C57BL/6J mouse model of status epilepticus: behavioral and electroencephalographic studies. *PLoS one* 9: e96622
- Turski WA, Cavalheiro EA, Schwarz M, Czuczwar SJ, Kleinrok Z, Turski L. 1983. Limbic seizures produced by pilocarpine in rats: behavioural, electroencephalographic and neuropathological study. *Behavioural brain research* 9: 315-35
- Uvarov P, Ludwig A, Markkanen M, Pruunsild P, Kaila K, et al. 2007. A novel N-terminal isoform of the neuron-specific K-Cl cotransporter KCC2. *The Journal of biological chemistry* 282: 30570-6
- Uvarov P, Ludwig A, Markkanen M, Rivera C, Airaksinen MS. 2006. Upregulation of the neuron-specific K⁺/Cl⁻ cotransporter expression by transcription factor early growth response 4. *The Journal of neuroscience : the official journal of the Society for Neuroscience* 26: 13463-73
- Uvarov P, Pruunsild P, Timmusk T, Airaksinen MS. 2005. Neuronal K⁺/Cl⁻ co-transporter (KCC2) transgenes lacking neurone restrictive silencer element recapitulate CNS neurone-specific expression and developmental up-regulation of endogenous KCC2 gene. *Journal of neurochemistry* 95: 1144-55
- Vargas-Perez H, Ting AKR, Walton CH, Hansen DM, Razavi R, et al. 2009. Ventral tegmental area BDNF induces an opiate-dependent-like reward state in naive rats. *Science* 324: 1732-4
- Viitanen T, Ruusuvoori E, Kaila K, Voipio J. 2010. The K⁺-Cl cotransporter KCC2 promotes GABAergic excitation in the mature rat hippocampus. *The Journal of physiology* 588: 1527-40
- Wamsley B, Fishell G. 2017. Genetic and activity-dependent mechanisms underlying interneuron diversity. *Nature reviews. Neuroscience* 18: 299-309

References

- Weber M, Hartmann AM, Beyer T, Ripperger A, Nothwang HG. 2014. A novel regulatory locus of phosphorylation in the C terminus of the potassium chloride cotransporter KCC2 that interferes with N-ethylmaleimide or staurosporine-mediated activation. *The Journal of biological chemistry* 289: 18668-79
- Woo NS, Lu J, England R, McClellan R, Dufour S, et al. 2002. Hyperexcitability and epilepsy associated with disruption of the mouse neuronal-specific K-Cl cotransporter gene. *Hippocampus* 12: 258-68
- Wu H, Che X, Tang J, Ma F, Pan K, et al. 2016. The K(+)-Cl(-) Cotransporter KCC2 and Chloride Homeostasis: Potential Therapeutic Target in Acute Central Nervous System Injury. *Molecular neurobiology* 53: 2141-51
- Yamada J, Okabe A, Toyoda H, Kilb W, Luhmann HJ, Fukuda A. 2004. Cl⁻ uptake promoting depolarizing GABA actions in immature rat neocortical neurones is mediated by NKCC1. *The Journal of physiology* 557: 829-41
- Yeo M, Berglund K, Augustine G, Liedtke W. 2009. Novel repression of Kcc2 transcription by REST-RE-1 controls developmental switch in neuronal chloride. *The Journal of neuroscience : the official journal of the Society for Neuroscience* 29: 14652-62
- Yu J, Proddutur A, Elgammal FS, Ito T, Santhakumar V. 2013. Status epilepticus enhances tonic GABA currents and depolarizes GABA reversal potential in dentate fast-spiking basket cells. *Journal of neurophysiology* 109: 1746-63
- Zayachivsky A, Lehmkuhle MJ, Dudek FE. 2015. Long-term Continuous EEG Monitoring in Small Rodent Models of Human Disease Using the Epoch Wireless Transmitter System. *Journal of visualized experiments : JoVE*: e52554
- Zhao B, Wong AY, Murshid A, Bowie D, Presley JF, Bedford FK. 2008. Identification of a novel di-leucine motif mediating K(+)/Cl(-) cotransporter KCC2 constitutive endocytosis. *Cellular signalling* 20: 1769-79

References

Ziburkus J, Cressman JR, Barreto E, Schiff SJ. 2006. Interneuron and pyramidal cell interplay during in vitro seizure-like events. *Journal of neurophysiology* 95: 3948-

54